NATIONAL TECHNICAL UNIVERSITY OF ATHENS

SCHOOL OF NAVAL ARCHITECTURE AND MARINE ENGINEERING

LABORATORY OF MARINE ENGINEERING

Diploma's Thesis

Smoke Emission Reduction of Marine Diesel Engines by Leading Part of the Exhaust Gas into Diesel Particulate Filter During Transient Loading

Papoulias Fotis

Professor Supervisor: N.P. Kyrtatos

Athens, October 2014

Abstract

Potential reduction of smoke emission of marine diesel engines is investigated through the installation of an exhaust bypass system featuring two diesel particulate filters in the Laboratory of Marine Engineering of the National Technical University of Athens. This system differs from the ones already in use in the automotive industry because it charges only during engine transient loading in order to avoid early filter contamination. The exhaust flow is controlled by the operation of two butterfly valves. When the engine is idle or operating in steady state the first valve is fully open and the exhaust gas flows through the main duct unfiltered. In case of engine transient loading, during which there is high smoke emission, the second valve gradually opens leading part of the exhaust gas into the filters. When it is almost fully open, the first one closes and the exhaust gas is being fully filtered until the engine operates in steadier conditions. Then, the valves are moved to their initial positions. The efficiency of the method, in terms of smoke emission reduction, is assessed by measuring the exhaust gas opacity after the filters. Furthermore, the differential pressure across the filters is measured, as well as the system back pressure, in order to estimate the soot load in the filters and its impact on the engine operation.

The project includes the supervision of the construction and proper installation of the exhaust bypass system in the exhaust processing unit of the laboratory, the acquisition and mounting of all sensors, the installation of the necessary subsystems and the conduction of the experiments. In the context of this project, opacity measurements on a high speed passenger vessel are also carried out in order to evaluate the opacity sensor performance, as well as to observe the smoke emission from an engine operating in real conditions. In addition, a brief description of the radio – frequency soot sensing technology is performed in order to decide whether to use this or the state of the art differential pressure in order to estimate the soot load in the filters.

The main objective is to develop a system that will reduce efficiently and in a safe way the smoke emission of diesel engines without interfering in their overall operation. Furthermore, additional issues must be considered so that the system will be suitable for retrofit in marine engines.

Acknowledgements

Contents

List of Figures

Abbreviations

A/D   Analogue to Digital

Al   Aluminum

ASL   Aegean Speed Lines

ATDC Angle from Top Dead Centre

CO   Carbon Monoxide

CO_2 Carbon Dioxide

CPT   Closed Pulse Turbocharging

Cr   Chrome

CRT   Continuously Regenerating Trap

Cu   Copper

D/A   Digital to Analogue

DA   Double Acting

DAQ   Data Acquisition

DIP   Dual In-line Package

DPF   Diesel Particulate Filter

EBS   Exhaust Bypass System

EC   Elemental Carbon

EGR   Exhaust Gas Recirculation

H_2O Water

HC   Hydrocarbons

HDD   Heavy-Duty Diesel

HFO   Heavy Fuel Oil

I/O   Input/output

ISF   Insoluble Solid Fraction

JA   Jet Air

LME   Laboratory of Marine Engineering

MCR   Maximum Continuous Rating

MDO   Marine Diesel Oil

Mn   Manganese

NI   National Instruments

Ni   Nickel

NO   Nitrogen Monoxide

NO_2 Nitrogen Dioxide

NO_X Nitrogen Oxide

NTUA   National Technical University of Athens

O   Atomic Oxygen

O_2 Oxygen

O_3 Ozone

OC   Organic Compound

OH   Hydroxide

PAH   Polycyclic Aromatic Hydrocarbon

PM   Particulate Matter

RF   Radio Frequency

RTD   Resistance Temperature Detector

SC   Spring to Close

SDM   Smoke Density Monitor

Si   Silicon

SiC   Silicon Carbide

SO   Spring to Open

SO_2 Sulphur Dioxide

SO_3 Sulphur Trioxide

SO$_4$ Sulphate

SOF   Soluble Organic Fraction

Δp   Differential Pressure

Introduction

This thesis is investigating the possibilities of obtaining lower smoke emissions in the exhaust gas of a marine diesel engine, by installing a bypass duct in the existing exhaust system of the Laboratory of Marine Engineering of the National Technical University of Athens which will lead whole or part of the exhaust gas into diesel particulate filters during engine transient loading. This project was elaborated as part of a research program which is conducted this period in the laboratory and includes the supervision of the construction and installation of the exhaust bypass system and all necessary sub-systems, the acquisition and mounting of all sensors and the experimental procedure which will decide the overall efficiency of the system and its suitability for retrofit in marine engines.

The first chapter of the thesis provides the project overview, offering a concise view of the general background and the existing problem as well as a brief description of emission abatement methods including the exhaust bypass system.

The second chapter provides information on the diesel particulate filter technology. It includes some interesting facts about the particulate filter, a short description of its operation and problems, as well as the reasoning of the DPF selection for the exhaust bypass system.

The third chapter reviews the exhaust bypass system and describes in a detailed way every part of the system as well as its operation. In fact, this chapter is the description of the system as it was initially conceived.

The fourth chapter describes the installation of the exhaust bypass system, including its construction and assembly in the laboratory, the mounting of the sensors and all the additional tasks that had to be carried out for its proper operation.

The fifth chapter includes the opacity measurements that were carried out on a high speed passenger vessel in order to investigate the opacity sensor behaviour operating in real conditions. Apart from the description of the tasks that had to be done in order to take these measurements, it also includes results analysis and discussion.

The sixth chapter covers the experimental procedure and all of its aspects such as the preparation for the experiments and the results analysis.

The seventh and final chapter provides general conclusions, evaluates the system's overall efficiency, mentions all the problems that were encountered and offers recommendations for future work.

Chapter 1: Project Overview

1.1 General Background

Close to a century after the entry into service of the first oceangoing motor vessel, the diesel engine enjoys almost total dominance in merchant and passenger ship propulsion markets as well as in the heavy duty sector of the automotive industry. The most important step in strengthening the status of diesel engine, especially in marine propulsion, is its ability to burn cheaper, heavier fuel oils with high efficiency (1). In addition, progressive advantages in the efficiency of turbochargers has led to an increase of the overall efficiency of the marine propulsion systems by exploiting the heat of the exhaust gas and supplement the main engine effort or drive a generator (2). However, its high thermal efficiency, which in simple terms means high fuel economy, is opposed by tightening international controls and environmental pressures that impose the continuing effort to reduce exhaust gas pollutants.

Exhaust gas emissions from marine diesel engines largely comprise nitrogen, oxygen, carbon dioxide, and water vapour, with smaller quantities of carbon monoxide, oxides of sulphur and nitrogen, partially reacted and non-combusted hydrocarbons and particulate matter (1). The majority of these emissions are considered pollutants due to their adverse effect on the environment and on human health. Thus, several regulatory bodies have addressed the issue and enforcement of legislation aimed to reduce marine emissions is in progress (3). In the wake of this development the maritime industries are continuously seeking and implementing emission abatement strategies such as the selective catalytic reduction system for reducing NO_X emissions or the diesel particulate filter technology for reducing PM emissions.

Besides environmental considerations, however, other factors influence the growth and development in the maritime industry. This can be illustrated by the marked increase in the number of passenger ferry services operating with high-speed vessels over the past decade. This trend is likely to continue with the increasing demands for shorter travel and delivery times (3). These vessels usually operate in environmental sensitive areas such as island harbours where the emission control is urgent. As a consequence, smokeless main and auxiliary engines operation is requested because the smoke emissions are prominent due to the clean environment and the bright background found in these areas.

In general, legislation imposes that marine diesel engines operating in environmental sensitive areas should burn light fuel oils – the so-called MDO, in order to reduce the pollutants emitted. Marine medium and high speed diesel engines can burn such a fuel, with typical properties as shown in table 1, very efficiently. Heavy fuel oils, which are very popular as typical fuels of big low speed diesel engines operating in big oceangoing merchant ships, produce smoke density almost two times that of MDO (figure 1), due to the fact that HFO contain a lot of residues which are impinged and adhered onto the piston crown during the ignition delay, their evaporation is delayed and the combustion is deteriorated (4). Although this is not so obvious when the engines work around the service load, it becomes prominent when the ships are in ports or narrow channels and the engines work at low loads.

Density at 15°C, g cm^{-3}	0.849
Net calorific value, MJ/kg	42.52
Viscosity at 50°C, cSt	3.05
Carbon, wt%	87.2
Hydrogen, wt%	13.9
Nitrogen, wt%	0.006
Oxygen, wt%	0.2
Sulphur, wt%	0.09

Table 1: Properties of a typical MDO (3)
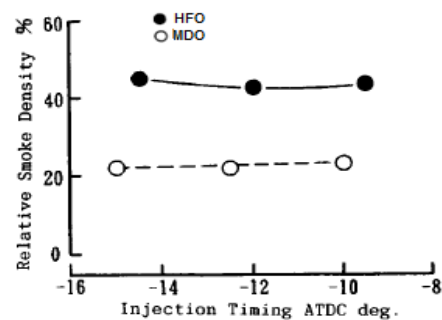
Figure 1: Relationship between fuel injection timing and smoke density as a function of fuel quality (4)

For the time being, the majority of the emissions of marine diesel engines are controlled with standards already in force (Tier I, II, III), except for the PM emissions for which no emission standard has been adopted yet. However, manufacturers are required to measure and report them (5). Nevertheless, this does not apply to on-road light or heavy-duty, railway and stationary diesel engines, whose PM emissions are already regulated. From 2007 the PM emissions of heavy-duty highway engines operating in USA are limited to 0.01 g/bhp-hr, while for the non-road diesel engines the limits range from 0.3 g/bhp-hr to 0.03 g/bhp-hr (depending on engine power) (5). Moreover, the European Union has adopted the new Euro 6 standard which limits the PM emissions of HDD engines to 0.01 g/kW-hr and that of non-road diesel engines to 0.025 g/kW-hr (5). Similar standards have already been adopted in the rest of the world (e.g. Japan) (6) . In addition, in USA from 2014 PM emissions of medium power (2750 bhp ≤ P < 6000 bhp) marine diesel engines will be controlled and limited to 0.09 g/bhp-hr, posing more pressure on the engine manufacturers to promote "green" technologies (5).

1.2   Problem Description

Marine engine designers in recent years have had to address the challenge of tightening controls on noxious exhaust gas emissions imposed by national, regional and international authorities responding to concern over atmospheric pollution and its impact on human health and climate change. One of the most characteristic, yet hazardous, emissions of diesel engines is PM, which is a complex mixture of inorganic and organic compounds resulting from incomplete combustion, partly unburned lube oil, thermal splitting of HC from the fuel and lube oil, ash in the fuel and lube oil, sulphates and water. More than half of the total particulate mass is soot (inorganic carbonaceous particles), whose visible evidence is smoke. Soot particles (unburned elemental carbon) are not themselves toxic, but they can cause the build-up of aqueous HC, and some of them are believed to be carcinogens (1). Fortunately, particulates constitute no more than around 0.003 percent of the engine exhaust gases, but this number tends to increase sharply during engine transient loadings when poor combustion conditions prevail.

The primary cause for soot (PM) formation is that regardless of the flame type (diesel cycle is characterised by diffusion flames), if the combustion conditions are poor, (elevated temperature, poor mixing of fuel and oxidant etc) the fuel undergoes either pure or oxidative pyrolysis. Some precursors of the fuel pyrolysis undergo cyclization and create an aromatic ring. The ring structure is thought to add alkyl groups, developing into polynuclear aromatic (PAH) structure that grows owing to the presence of acetylene and other vapour-phase soot precursors. These precursors arise as free radicals from the breaking of the bonds of the hydrocarbon molecules due to the elevated temperature in the combustion chamber. Eventually, the aromatic structures reach a large enough size to develop into particle nuclei. Such condensed-phase carbon particles contain large amounts of hydrogen. The particles dehydrogenate in high-temperature combustion field while physically and chemically absorbing other gaseous hydrocarbon species that dehydrogenate. As a result the soot mass increases rapidly and the growing particles agglomerate and conglomerate. The absorbed species undergo to a large degree chemical reformation, which results in a carbonaceous soot structure. However, while these events are occurring, oxidative attack on the particles continues to form gaseous products (7). Consequently, the fuel properties and the conditions in which the combustion takes place, determine the level of soot formation.

The PM emissions exhausted from diesel engines can be divided into soluble (SOF) and insoluble (ISF) organic fractions and sulphates (figure 2). Elemental carbon and ash constitutes the ISF of PM and is not considered as hazardous as the SOF which is formed mainly by

hydrocarbons, deriving from the lube oil, and other harmful components such as PAH that are contained in the fuel (8). The sulphur particles (sulphates) are formed by the interaction between sulphur acid and water so their emission depends on the humidity and temperature of the exhaust gas as well as on the sulphur content of the fuel.

As far as the particle form is concerned, PM emissions are primarily formed in two separate modes:

- Nuclei mode particles which consist mainly of condensed hydrocarbons and sulphates. The gaseous precursors condense as temperature decreases in the exhaust system and after mixing with cold air in the atmosphere. They constitute part of the SOF and sulphates.

- Accumulation mode particulates which are formed during combustion by agglomeration of primary carbonaceous particles and other solid materials as described above. The majority of the accumulation mode particulates form in the core of the burning fuel spray and they constitute the ISF. Further, gases and condensed hydrocarbon vapours, also part of the SOF, are absorbed into the surface of the particles (9).

Particulate Emissions are considered a contributory factor in causing asthma, allergies and various other human health problems. Smaller particulates are thought more likely to penetrate deep in human lungs, the most minute of them perhaps even moving into blood stream (1). In addition, the condensed hydrocarbons in the nuclei mode particles and on the surface of the accumulation mode particles contain toxic and carcinogenic hydrocarbons (9). That's why there is a strong correlation between ambient PM concentrations and human health.

As mentioned before the most dangerous part of the PM emissions of diesel engines is the so-called SOF which consists of highly toxic and carcinogenic hydrocarbons. However, the ratio of the SOF to the total PM emissions depends on the engine load as it is shown in figures 3 and 4, rendering the need for reducing these emissions in the areas where the engines operate at low loads (e.g. island ports), urgent.
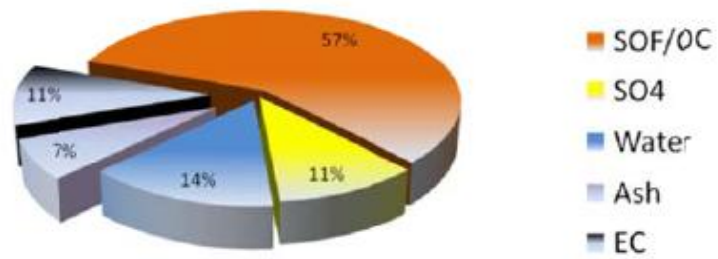
Figure 2: Particulate emission composition of a large 4-stroke medium speed diesel engine running on MDO at steady state high load (8)
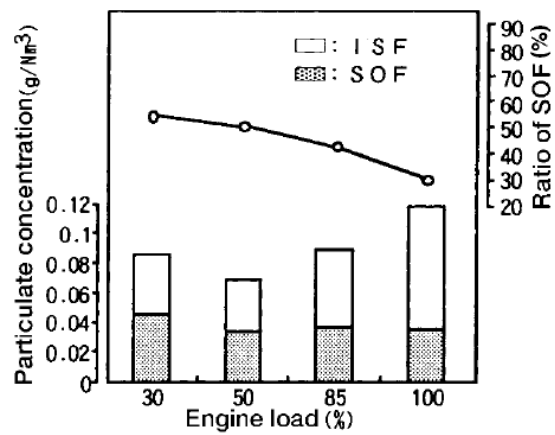
Figure 3: Relation between engine load and PM concentration (4-stroke marine diesel engine with propeller load operation) (8)
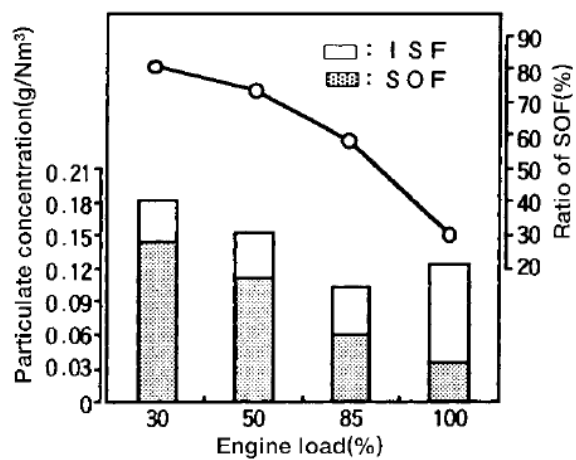
Figure 4: Relation between engine load and PM concentration (4-stroke marine diesel engine with constant engine speed) (8)

1.3   Smoke Emission Abatement Methods

The biggest challenge concerning the emissions reduction of diesel engines is that pollutants are formed under different conditions, rendering a reduction method often suitable for one particular emission but inappropriate for another. For example, while NO_X are generated thermally from nitrogen and oxygen at high combustion temperatures in the cylinder, as well as for small fuel to air ratio (lean burn combustion), PM is formed at intermediate temperatures and for high fuel to air ratio, where the soot precursors cannot be oxidised, thus forming species that transform into soot (figure 5) (10). Therefore, special caution must be given and all necessary parameters have to be taken into account for optimizing the potential abatement method in order to achieve efficient engine operation with reduced emissions. In order to accomplish this, there must be either an improvement of the combustion process or the use of external devices. The first one is called prevention method as it deals with the problem at its origin, whilst the other is called mitigation method because it transposes the problem to a next level of confrontation (11).
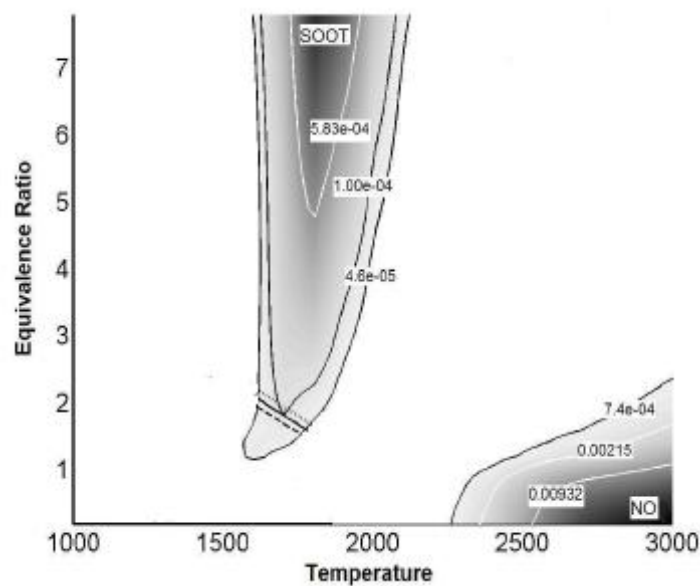
Figure 5: Soot and NO concentrations as a function of fuel to air equivalence ratio and temperature. Soot in g/m3, NO in mole fractions and temperature in degrees Kelvin (10)

As regards the combustion process improvement, for engine manufacturers it has been one of the most important sales arguments for decades. Consequently, focus has been for long on improving the combustion process and reducing unburned compounds (e.g. HC, PM), so there is no large leap to be expected from further improvements (12). This is proved by the fact that at

7

very high engine loads, combustion in a state of the art medium speed diesel engine can be modelled to give invisible smoke.

However, this does not apply at low service loads and especially during rapid start-up manoeuvres and load changes, when the turbochargers deliver less intake air than the engine needs for complete fuel combustion, so the engine 'smokes' (1). Many systems for improving combustion during transient loading have been proposed with sometimes ambiguous results. Such systems are:

- Turbocharger optimization for part load, with a waste gate
- Charge air bypass below a certain engine load
- Smaller Injection bores
- Nozzles with short sac holes
- Auxiliary blower for operation below a certain engine load
- Fuel-water emulsification
- Retarded fuel injection below a certain engine load
- Common rail fuel system

From the systems cited above, the later provides the most promising results because it offers the freedom to choose the fuel injection pressure and timing completely independent of the engine load, whereas computerised control allows several key engine parameters to be considered. The ability to maintain fuel injection pressures sufficiently, high at all engines loads and speeds (even at the lowest levels and during starting and transient load changes) contributes to clean combustion with no visible smoke emissions (1). In addition new ideas are currently investigated for eliminating the air to fuel mismatch in the combustion chamber during transient loading. For example a smoke abatement method, which comprises a compressed air injection system (JA) and a closed pulse turbocharging system (CPT), has been developed in the Laboratory of Marine Engineering of the National Technical University of Athens. The system is activated during engine transient loading, when compressed air is injected on the compressor impeller to increase its rotational speed as well as the air pressure and quantity in the intake manifold, while the constant pressure turbocharging system turns to pulse (figure 6) and exploits the high kinetic energy of the exhaust gas (in form of high pressure tuned pulses) to further improve the compressors response to the load change (13). The results are very promising as the opacity is reduced almost 80-85% (figure 7). In addition, the response time of the turbocharger to the transient loading is extremely fast. As a result the compressor

reaches steady state condition very quickly indicating that the required amount of air is supplied to the engine at the right time (14).

Although there is a limited scope to significantly reduce particulate emissions by improving the combustion, methods of removing particulates from the exhaust gas are available as well (1). Moreover, in contrast to the prevention methods, the use of exhaust after-treatment devices, offer the possibility to be installed in older or out-of-date engines where no modifications for improving engine performance can be made. In other words they are suitable for retrofit as the prerequisites for their installation are few.
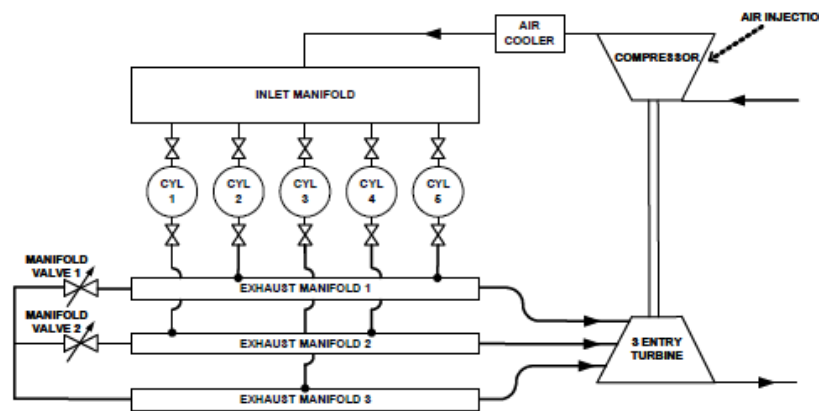
Figure 6: The overall system set-up with the air injection and the variable path exhaust manifold configuration (13)
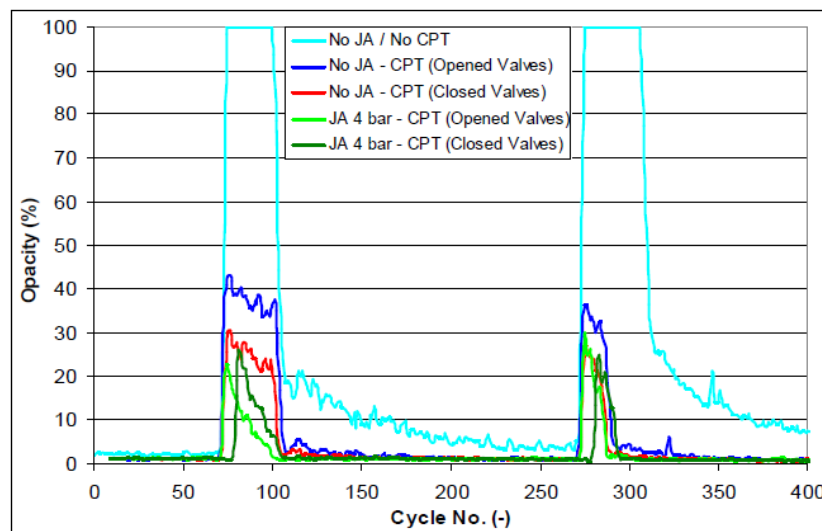
Figure 7: Opacity for combination of JA and CPT systems for two steps loading at constant engine speed (14)

The most widely found after-treatment devices for reducing PM emissions are:

- Diesel Particulate Filters (DPF)
- Bag Filters
- Electrostatic Precipitators
- Scrubbers

In Diesel Particulate filters the exhaust flow is forced through very small channels (μm range) where solid particulate matter is collected (figure 8). However, a large pressure difference is needed for forcing the exhaust flow through the small channels. Therefore, the engine may experience high backpressure, which will result in high thermal loading. Despite the fact that this technology is used in some truck and rail engines, there is no demonstrated DPF technology available for large marine and stationary engines operating on typical ''non-automotive'' fuel quality. Additional challenges for its use in large scale applications are the big dimensions needed, its mechanical strength and its early clogging due to ash presence in the exhaust gas. As a consequence, for the time being DPF is considered as a not feasible solution for marine applications (12).

Bag filters or dust collectors are systems designed to enhance the quality of gases by collecting dust (even for high volume dust loads) and other impurities that they may contain. They consist of a blower, dust filter, a filter-cleaning system and a dust receptacle or dust removal system. Dust enters the bag-house compartment through inlet on the hoppers (figure 9). Larger particles drop out while smaller dust particles collect on filter bags. When the dust layer thickness reaches a level where flow through the system is sufficiently restricted, bag cleaning is initiated. Cleaning can be done while the bag-house is still online (filtering) or in isolation (offline). Once cleaned, the compartment is placed back in service and the filtering process starts over (15). This system is able to achieve relatively good particulate reduction, as long as it is sufficiently large. However, a ''protection reagent'' is needed in order to protect the filter from clogging. In addition the flue gas has to be cooled and a fan is needed due to high pressure drop. At last but not least, there must be room for waste disposal regarding the ''protection reagent'' and the removed particulate. For these reasons, bag filters are used almost exclusively in large-land based industrial sources and not in the marine or the automobile sector (12).

Precipitators function by electro-statically charging the dust particles in the gas stream. The charged particles are then attracted to and deposited on plates or other collection devices. When enough dust has accumulated, the collectors are shaken to dislodge the dust, causing it to

fall with the force of gravity to hoppers below. The dust is then removed by a conveyor system for disposal or recycling. Depending upon dust characteristics and the gas volume to be treated, there are many different sizes, types and designs of electrostatic precipitators (16). The particulate reduction achieved is good, the pressure drop is low and the high exhaust gas temperature does not pose additional problems. However, these systems are extremely bulky (figure 10) and too expensive. Moreover, the waste disposal problem remains and there are additional electrical risks due to high voltage, rendering them not viable systems for marine installations (12).

Scrubbers are special devices that are used to remove particulates from industrial exhaust streams. These systems work via the contact of the target compounds with the scrubbing solution which may simply be water (for dust) or solutions of reagents for targeting specific compounds. Removal efficiency of pollutants is improved by increasing residence time in the scrubber or by the increase of surface area of the scrubber solution (18). Although such systems are very efficient concerning SO_X reduction (figure 11), it remains unclear whether are appropriate for reducing PM emissions (12).

Figure 8: Diesel particulate filter
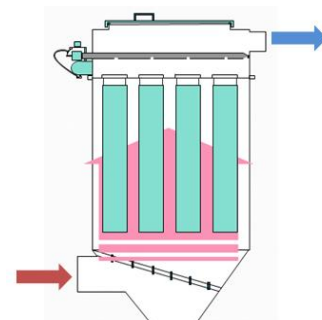
Figure 10: Bag filter (15)

Figure 9: Cylindrical electrostatic precipitator in waste incineration plant (17)

Figure 11: Desulphurisation scrubber (18)

1.4   Exhaust Bypass System

The Exhaust Bypass System or EBS has been developed in the Laboratory of Marine Engineering of the National Technical University of Athens as an emission control device for reducing smoke of marine diesel engines of high-speed vessels operating in environmental sensitive areas.

The EBS mainly takes advantage of the DPF technology as it features two diesel particulate filters. Therefore, it can be considered as an after-treatment emission abatement method. Although the reduction method is based on technology already-in-use, it's the first DPF system that is referring to marine applications. In addition, this system is designed to be easily applied to existing marine installations as a retrofit solution for emission control. As a consequence, apart from some necessary modifications that had to be made, the system functions in a quite different manner in relation to the usual DPF systems. Conventional DPF applications consist of a diesel particulate filter that collects PM emissions throughout the whole engine operation. Despite the fact that this method produces good results as the emissions reduction is concerned, the system suffers from early filter contamination, due to clogging, which leads to need for premature filter replacement. Filter manufacturers have developed many methods (some of them somewhat sophisticated) for addressing this problem. Nevertheless, these methods cannot be applied on vessels because of the stringent safety regulations. That's why a new system for achieving high smoke emission reduction and simultaneously avoiding early filter contamination needed to be developed.

The EBS satisfies these prerequisites as it consists of a bypass duct which leads the exhaust gas to two diesel particulate filters for as long as it is required. In contrast to diesel engines operating on-road, marine engines are more steadily loaded. Thus, the periods in which the engines work in transient loadings can be easily distinguished. The EBS activates only during these periods by opening the valve which leads the exhaust gas to the bypass duct and then to the filters, whilst the valve, which controls the exhaust gas flow through the main duct, closes (figure 12). The filters collect all unwanted products of incomplete combustion during the transition of the engine load from low to high levels, and when the engine reaches steady state conditions, EBS deactivates via the reposition of the valves to their initial positions. In this case, the exhaust gas remains unfiltered but without increasing the smoke emission as the engine works properly and the combustion is complete. In this way the filters are not burdened from unnecessary soot loading and are kept functional until their replacement which takes place during ship maintenance intervals.

EXHAUST BYPASS SYSTEM
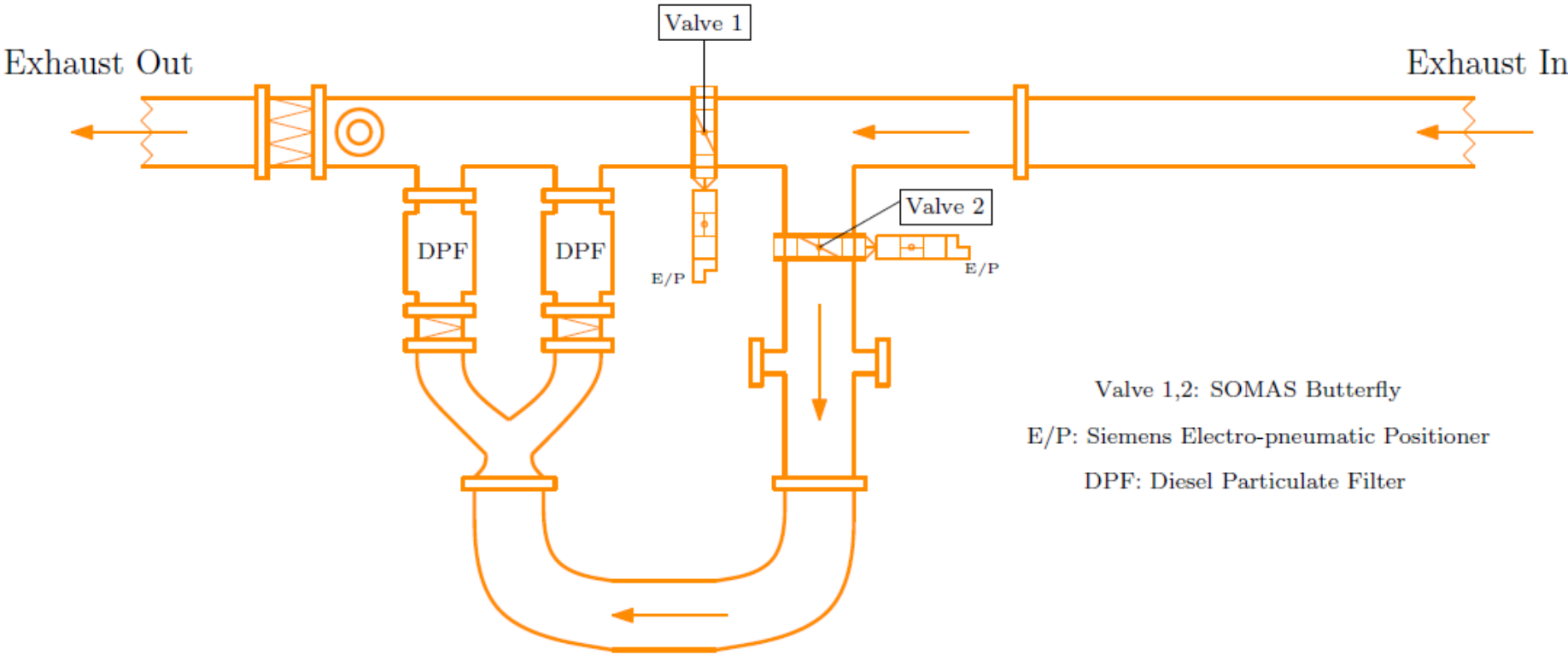
Figure 12: The exhaust bypass system (EBS) at LME/NTUA

Chapter 2: Diesel Particulate Filter Technology

2.1 The Particulate Filter

The particulate filter is today the most efficient device for reducing diesel soot emissions, attaining filtration efficiencies of the order of 90%, at nominal operation conditions. Soot filtering is especially important in the case of worn-out diesel engines with poorly controlled fuel combustion. However, specific application problems have limited the use of particulate filters, mainly on city buses, some delivery trucks and fork lift trucks (figure 13) (19). Due to the new emission standards (Euro VI, Tier II, etc) that impose further PM control, intensive research is being carried out aiming at developing diesel filter systems suitable for a wider application to commercial vehicles or passenger cars. In addition, future PM emission limits, introduced by United States Environmental Protection Agency (US-EPA), render DPF technologies necessary also for marine Diesel engines.

The particulate filter concept has focused research and development activities around the world, and a variety of systems is offered by various manufacturers. A trap oxidiser system is based on a durable temperature resistant filter, which removes particulate matter from the exhaust before it is emitted in the atmosphere. The accumulated particulate raises the filter backpressure, i.e. the pressure difference across the filter which is necessary to force the exhaust through it. The typical backpressure level depends on the filter type, and increases as the filter becomes loaded with particulate. High backpressure is undesirable because it raises the engine cycle pumping work and eventually the exhaust gas enthalpy. As a consequence, it reduces the available engine power and increases the thermal load and the fuel consumption of the engine. Therefore, minimizing mean backpressure levels while still maintaining acceptable filtration efficiency in a reliable, durable, compact and low cost system constitutes the major goals of particulate filter design (20).

The most proof-worthy trap oxidiser for controlling diesel particulate matter is the wall-flow ceramic monolith filter (figure 14) which is characterised by high trapping efficiency, temperature tolerance, high demonstrated durability and moderate cost (20). Ceramic monoliths are the most common type of diesel filter substrate. It is a honeycomb structure made from porous ceramic material. The adjacent channels of the honeycomb are alternatively plugged at each end in order to force the diesel aerosol through the porous substrate walls, which act as a mechanical filter. The particulates cannot flow through the wall and are deposited in the channel walls. To reflect this flow pattern, the substrates are referred to as the

wall-flow monoliths (figure 15). The main advantage of the wall flow particulate filter is the high surface area per unit volume, which combined with the high collection efficiencies, makes this technique very attractive. The filter walls have a porous structure that is carefully controlled during the manufacture process. Typical values of material porosity are between 45 and 50% while the medium pore size varies in the range between 10 and 20μm (21).

Figure 13: Particulate filter of HDD engine
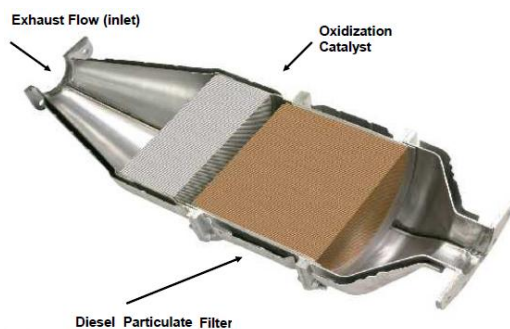
Figure 14: Trap oxidiser featuring an oxidization catalyst and a DPF (21)
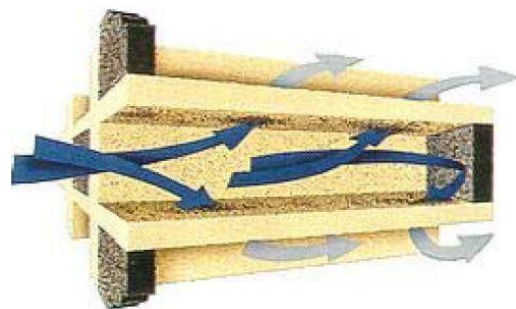
Figure 15: Schematic representation of flow pattern in a wall flow monolith (21)

The particulate collection mechanisms can be categorised as follows (21):

- Depth filtration where the particles with a mean diameter lower than the filter porosity are deposited inside the porous material due to a combination of mechanisms that are driven by various force fields
- Cake filtration where the particles are deposited on the channel wall through sieving

The depth filtration relies on three mechanisms of aerosol deposition (21):

- Diffusional deposition
- Inertial deposition
- Flow stream-line interception

These mechanisms are illustrated in figure 16 where the large circle in the middle represents a collecting body in the filter media; say a fibre of a filter. Diesel exhaust gas flows around the filter media, as indicated by the streamlines. The small black-red spheres represent diesel exhaust particles travelling with the gas stream.

(a)   (b)   (c)
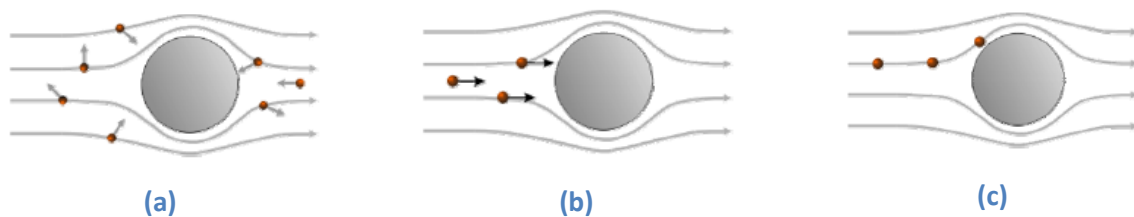
Figure 16: Depth filtration mechanisms: (a) Diffusional deposition, (b) Inertial deposition, (c) Flow stream-line interception (21)

Diffusional deposition (a) depends on the Brownian movement exhibited by smaller particles, particularly those below 0.3 µm in diameter. Those particles do not move uniformly along the gas streamlines. Rather they diffuse from the gas to the surface of the collecting body and are deposited there.

Inertial deposition (b), also called inertial interception, becomes more important with increasing particle size (mass). While these bigger particles are approaching the collecting body, because of their increased inertia, they cannot follow the stream-lines and they strike the obstruction.

Flow stream-line interception (c) occurs when a fluid stream-line passes within one particle radius of the collecting body. Then, a particle travelling along the streamline touches the body and is collected without the influence of Brownian diffusion or inertia (21).

As far as the filter material is concerned, two types are commonly established: *cordierite* and *silicon carbide*. Cordierite is a synthetic ceramic developed for flow-through catalyst substrates and subsequently adapted for the filter application. Silicon carbide or SiC has been used for a long time in a number of industries for such applications as semiconductors, abrasives, or high temperature/molten metal contact materials. More recently, it was successfully introduced as a diesel filter material. Cordierite substrates perform satisfactory in most heavy-duty applications with high exhaust temperature. However, cordierite is more

susceptible to thermal stresses. SiC has higher maximum operating temperature limits and better durability in high thermal stress applications, but it also has higher weight and it is more expensive (21).

Nowadays, in the automotive industry metallic monolith is being developed as the best material for trap oxidisers due its characteristics which induce some important advantages over the ceramic monolith. The construction of this type of filters resembles a streamer as it consists of two corrugated metallic sheets, which are wrapped and formed in layers and via a welding they compose the compact body of the monolith (figure 17). The most commonly used material is steel of high endurance to heat and corrosion and appropriate for welding and for ''accepting'' the catalytic coating. The placement of the metallic monolith is easier since there is almost no dilatation between the monolith and the shell of the filter and there is no need for the intermediate compensatory material which is necessary for the ceramic monolith. In addition, due to the fact that metallic substrates have sinusoidal channels, while the ceramic ones have square cells (figure 18), the metallic monolith exhibits smaller exhaust backpressure for the same catalytic effect. Furthermore, the risk for melting is smaller due to the metal's high thermal conductivity and the size is reduced because of the increased catalytic area. However, the material for the construction of the metallic monolith is more expensive, it is more vulnerable to high temperatures, especially those above 1100 ^{o}C, and there is always the risk of welding break which will lead to the separation of the two corrugated sheets (22). Therefore, for the time being this type of filter is inappropriate for large DPF applications where the more state of the art materials are dominant.

Figure 17: Monolithic substrates (23)
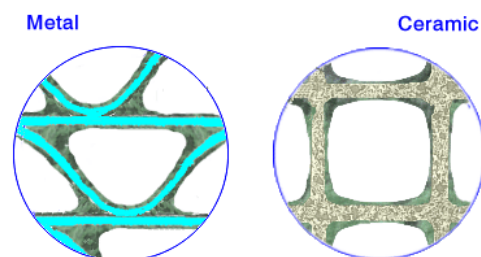
Figure 18: Monolithic cells (23)

2.2 DPF Regeneration Strategies

The biggest challenge that DPF systems face is their early-clogging due to accumulation of the collected PM inside the filters. The reduction of the exhaust flow through the filters is directly translated to an increase of the engine backpressure which is undesirable because it leads to worse engine performance. That is why it is necessary to clean the filter periodically by burning off (oxidizing) the collected particulate; this process is known as regeneration. Under the conditions met in diesel exhaust systems, regarding exhaust flow and oxygen concentration, the required reaction rates for complete regeneration are attained at temperatures above 550°C. Exhaust temperatures of that order are observed only at high load operation of the diesel engine. Thus, special regeneration techniques are employed, that fall into three broad categories (19):

- Thermal regeneration by use of engine measures or by the supply of external energy
- Catalytic regeneration (catalytically coated filter or fuel doping)
- Aerodynamic cleaning (using compressed air to remove the soot)

In the first category, a significant fuel consumption penalty must be foreseen to supply the additional energy (i.e. burners, electrical igniters, etc) required for regular thermal regeneration. This can be achieved with the incorporation of an air assisted burner or HC doser. The latter is a system where fuel is injected upstream of a special catalyst where the injected fuel is thermally converted. Nevertheless, there is also the possibility of implementing engine measures in order to raise the trap inlet temperature. For instance, the throttling of the engine exhaust results to a rise of the engine cycle pumping work, and eventually to a rise of the mean effective pressure and temperature of the high-pressure loop of the engine cycle. The energy balance of the exhaust throttled engine shows that an increased portion of the fuel energy per cycle is dissipated as exhaust gas enthalpy. This causes the onset of regeneration (20). However, the PM oxidization at elevated temperatures may lead to local thermal shocks or in a worse case to uncontrolled burning which can eventually destroy the filter.

Catalytic regeneration, on the other hand, is based on the use of catalysts to achieve the onset of regeneration at significantly lower temperatures. The catalyst may impregnate the porous ceramic wall or be used as a fuel additive, which is emitted and accumulated in the filter together with the particulate. The use of catalysts is critical to the design of a successful diesel filter system, because it ensures minimum backpressure, as well as filter regeneration at

temperatures below 350°C, although stochastic regenerations may be observed even down to 200°C (19).

The design of successful catalytic fuel additive assisted trap systems depends on the solution of problems related to filter durability and additive ash accumulation. The disadvantage of the additive currently being used is that it causes extra ash build up in the diesel particulate filter and therefore, with increasing mileage accumulation, makes it necessary to clean the filter or even to replace it (21).

The catalysed ceramic traps or wash-coated filters were developed in the early 80's. Their first applications included diesel powered cars and, later, underground mining machinery. The main component of the filter is the ceramic (cordierite, SiC) wall-flow monolith whose porous walls are coated with an active catalyst. Many materials, that are catalytically active in soot oxidation, have been studied in the last 20 years and have been tested as coating of a particulate filter. These materials are mainly oxides of base metals (Ba, Ca, Ce, Co, Cr, Cu, Fe, La, Mn and V) and noble metals (Pd, Pt) as well as mixtures of base and noble metals. The main drawback of these systems is that pure contact between the catalytic coating and the soot particles is indispensable. Therefore, if the distance is too high, catalytic action cannot take place. Only the particulates that are in direct contact with the catalytic coating are able to oxidise. Another problem of catalysed filters is the generation of sulphates by catalytic oxidation of the exhaust SO_2 to SO_3, at high exhaust temperatures. The gaseous SO_3 can penetrate the porous walls and freely leave the filter. Combining with water it forms sulphate particulates that increase the total PM output especially in case of fuels with high sulphur content (21).

Apart from the active regeneration systems described above, new systems for filter regeneration have been developed. These systems are called passive regeneration systems because filter cleaning is continuous and does not need activation. The CRT (Continuously Regenerating Trap) particulate filter is a patented emission control technology that is based on the presence of NO_X in the exhaust gases. The main parts of a CRT filter (figure 19) are a Platinum (Pt) catalyst and a particulate filter. It is modularly engineered as a totally passive emission control system, which does not require the use of supplemental heat. The CRT particulate filter functions on the basis that soot will oxidise in the presence of NO_2 at a lower temperature than with O_2. In fact, this lower temperature is compatible with the typical exhaust temperature from diesel engines. The device is made up of two chambers where the oxidation step is separate from the soot collection - combustion process. The first chamber contains a substrate coated with a proprietary, highly active Pt oxidation catalyst which is designed to oxidise a portion of the NO in the exhaust to NO_2, which is the key to the oxidation of soot

collected by the CRT filter. The catalyst also converts CO and HC into CO_2 and H_2O. In the second chamber, the exhaust flows through a particulate filter, where soot is trapped on the walls of the filter. The trapped soot then is destroyed by the NO_2 produced by the catalyst in the first chamber. This particulate filter may be uncoated or it may be coated with Pt to further enhance the reaction of soot with NO_2. The basic requirements for maximum PM reduction with the CRT particulate filter are ultra low sulphur fuel, an average exhaust temperature of 260^oC and a NOx/PM ratio of at least 25. For use on higher sulphur fuels the basic requirements are exhaust temperatures above 350^oC with NOx/PM ratio above 25 (21).

Except for the CRT, there is also a more advanced regeneration system capable to reduce diesel particulate matter attaining low oxidation temperatures. This system takes advantage of the sharp increase of soot oxidation rate in air that has been ionised by an electric arc (thermal plasma) at temperatures in the range of 200 to 450^oC. This is attributed to some reactive species generated in plasma, such as O and OH radicals or NO_2 that facilitate the oxidation of soot particles at low temperatures.

Two reactor configurations have been proposed to achieve this objective in a plasma device:

- Two-stage reactor, where a diesel particulate filter (DPF) is positioned downstream of a plasma generator. The role of plasma in the two-stage configuration is to generate NO_2 and, possibly, O_3, which can oxidise particulates in the filter. However the applicability of this kind of system is questionable, due to the production of NO_X.
- Single-stage reactor, where a packed bed plasma reactor acts as the PM trapping device (figure 20).
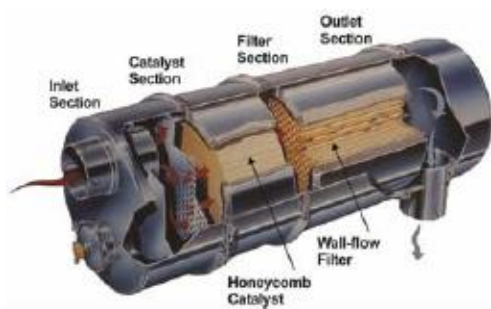
Figure 19: A CRT filter system (21)
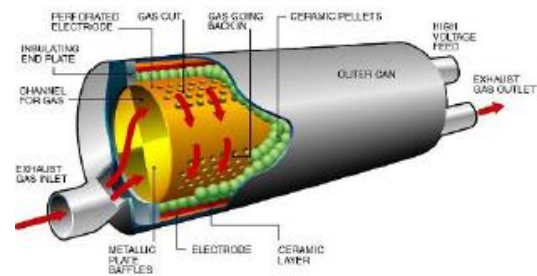
Figure 20: A plasma regeneration system (21)

In both configurations the plasma generator may be controlled and actuated by the engine management system in order to operate intermittently according to each engine operation condition, which is characterized by different soot emissions (21).

Finally, the filters can also be aerodynamically cleaned with compressed air, injected periodically and in different positions in order to sweep the whole surface of the filter. In this case, bag-houses to collect the dislodged soot particles are needed, as well as adequate compressed air supply. For the time being, such a system is only experimental and is considered as part of an emission control device which features DPF for soot emission reduction and EGR for reducing NO_x production. The particulate trap is rotated and cleaned with intermittent (pulsed) compressed air at specific time periods which allow low air consumption and lightly soot loaded filter. The cleaning air stream, after passing through the trap, is conducted to a fabric bag, enclosed in a sealed container (bag-house), where the particulates are finally collected, while part of the soot-free exhaust gas is led to the engine (EGR) to reduce the cylinders peak temperature and pressure. The collected soot is either discarded or burned in a separate incinerator (24).

Although with the techniques described above the filters can be kept clean for a relatively long period of operation, there is another factor that gradually downgrades the filters function and efficiency. This factor is the accumulation on the filter of non-oxidisable particulates, such as sulphates and ash, which results in a build-up of residual pressure drop. Sulphates production can be limited by adopting either desulphurisation strategies or by using fuels with low sulphur content. On the other hand, ash production and accumulation on the filter cannot be easily controlled. Nevertheless, recent studies have shed some light onto the ash mass balance puzzle, demonstrating that the amount of ash collected on filters might be less than 50% of the ash expected based on lube oil consumption. Moreover, the reason for the high ash accumulation on filters is due to their high trapping efficiency of ultrafine particles, typically more than 99%, in the size range of the fundamental ash particle. However, an initial ash layer is beneficial to the filter function as it prevents the penetration of ultrafine soot particles into the walls which may cause a marked increase in backpressure. As far as the ash removal is concerned, it can be achieved aerodynamically by injecting compressed air in the filter. In addition, for removing stubborn ash, water can be used although special caution must be given as it may impact mat materials (6).

2.3 DPF System Design for Marine Applications

In order to achieve high trapping efficiency as well as prolonged period of proper operation of a DPF system, several parameters have to be considered for optimizing the system design, especially if it is referring to marine applications where there is not such experience as in the automotive industry. These parameters include the DPF substrate material that is going to be used, the filter dimensions, the cell density and finally the regeneration strategy that is going to be followed.

As far as the DPF substrate selection is concerned, a general challenge is the limited ash storage capacity of certain DPF substrates. In some cases the DPF was blocked after less than 700 operating hours contrary to the expected design maintenance interval of 3,000 to 4,000 hours. For marine applications, an acceptable duration would be in the range of a maintenance interval, typical for marine Diesel engines after approximately 12,000 to 16,000 hours. In the ideal case it would be equivalent to approximately 24,000 to 36,000 hours before exchange of the substrates is required. As a consequence, based on the actual achieved operating hours of the filter mentioned above, a 17 to 51 times larger DPF would be required to reach the desired operating hours (25). In addition, ash amount deriving from not only the lube oil, but also from the fuel oil as well should always be considered due to the different ash content of the marine distillate oil. Therefore, the DPF should have an ash storage capacity of 300 to 400 liters depending on the desired operating hours (12,000 – 16,000 hours). Furthermore, as a rule of thumb from automotive, a filled DPF must not lose more than 20% of its free volume for ash storage due to the induced backpressure. Hence, the resulting free volume required is much bigger rendering the DPF system very bulky since it would be 8 times larger than a typical SCR system for the same engine. That is why, to circumvent such unrealistic DPF space requirements, DPF substrates with lower PM reduction efficiency but ash penetration capability need to be applied. This can be achieved by selecting a special substrate cell structure (figure 21) as well as a suitable cell density. For choosing the appropriate cell density, a compromise must be found between maximising the available substrate surface area within a fixed volume and the risk of blocking of the small cells. Due to the lower trapping efficiency of the special DPF substrate, a PM reduction of only 50% should be envisaged. Moreover, a resulting backpressure 2- 5 times above the currently allowed for serial marine Diesel engines should be considered depending on the DPF soot load (lower values for unloaded or respectively fresh regenerated state, while higher values for loaded state respectively before regeneration).
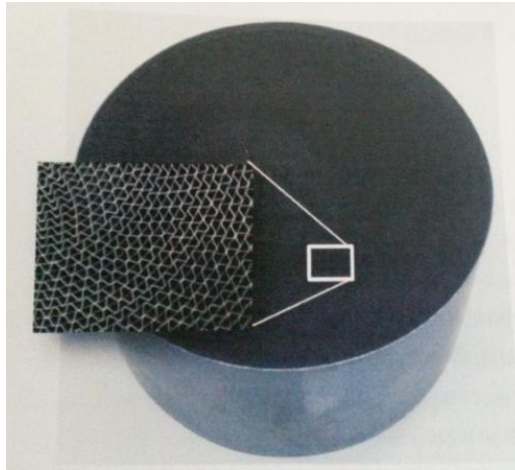
Figure 21: Special DPF substrate variant with zoom of the cell structure

As far as the DPF regeneration strategy is concerned, active regeneration by an exhaust gas burner upstream the filter is a trustworthy solution although noticeable increased fuel oil consumption has to be considered (25). However, according to automotive applications, passive regeneration is also possible with sulphur free fuels (the upper limit of the sulphur content of the fuel depends on the sulphur tolerance of the catalytic coating) and at exhaust gas temperatures above 230°C. A CRT system is of course the most desired option for this kind of application. In addition, the required exhaust gas temperature (above 230°C) can be provided by marine Diesel engines under normal operating conditions. Nevertheless, a device for an additional exhaust gas temperature rise above the normal operating conditions cannot be omitted completely due to the required elevated exhaust gas temperatures for the desulphurisation strategy of the catalytic coating. Moreover, a possibility for active regeneration needs to be considered as a backup solution for a fail-safe DPF operation on board ships. This requires a temperature rise up to 600-650°C, which is far beyond what is experienced today for medium speed marine Diesel engines. Furthermore, for the desulphurisation of a catalytic coating, a temperature rise to 500-550 ^{o}C is needed. For these reasons, the incorporation of an air assisted burner or a HC-doser is necessary with the latter being a more compact and probably less complex solution. However, the collected soot, respectively EC, as well as the injected fuel of the HC-doser poses a serious fire hazard onboard a ship. For the time being, strict safety regulations don't allow the installation of burners in the exhaust system due to the fire hazard, so there isn't any existing installation of this kind on a ship. In the future, the need for high PM reduction of marine diesel engines will impose the installation of DPF systems on ships. Therefore, a thoroughly monitoring of the DPF system behaviour and additional control measures are necessary before such a system can be operated safely on a vessel.

By using special DPF substrates with reduced PM trapping ability, EC reduction is expected to be almost on the same level of a conventional DPF substrate of 99% trapping efficiency. However, reduction of the organic fraction (SOF) is expected to be limited to 30-60% for sulphur tolerant but not precious metal catalytic coating. The biggest drawback of conventional precious metal catalytic coatings is that they deteriorate quickly due to the presence of catalyst poisons in the fuels. As a consequence innovative catalytic coatings have been developed recently in order to exploit their higher reduction capability of the SOF and at the same time to enable the application of passive regeneration strategies. This provides the possibility for minimizing the additional energy consumption for regeneration.

2.4 DPF Selection for the Exhaust Bypass System

The Exhaust Bypass System (EBS), that has been developed and installed in the LME/NTUA, takes advantage of the DPF technology as it features two particulate filters for reducing PM emissions. During the EBS design three solutions regarding the particulate filter were suggested. The first constructional solution was proposed from the company HUG Engineering and included one square DPF, made of SiC, with a diameter of 500 mm and volume of 175 liters. The cell density of the filter was 177 cells per inch with an average wall thickness of 12 mils (thousandths of an inch). Several computational simulations were carried out and produced some interesting results that are presented in figure 22. When the filter was cleaned, the pressure drop was 15 mbar while in the loaded state (100g of soot) it only rose to 30 mbar. Such a low pressure drop is undesirable since it leads to significant maldistribution of the flow inside the filter because the exhaust gas flows only through the central core of the filter and most of the soot is deposited there (26). For this reason the suggested filter from HUG Engineering was rejected because it was considered oversized.
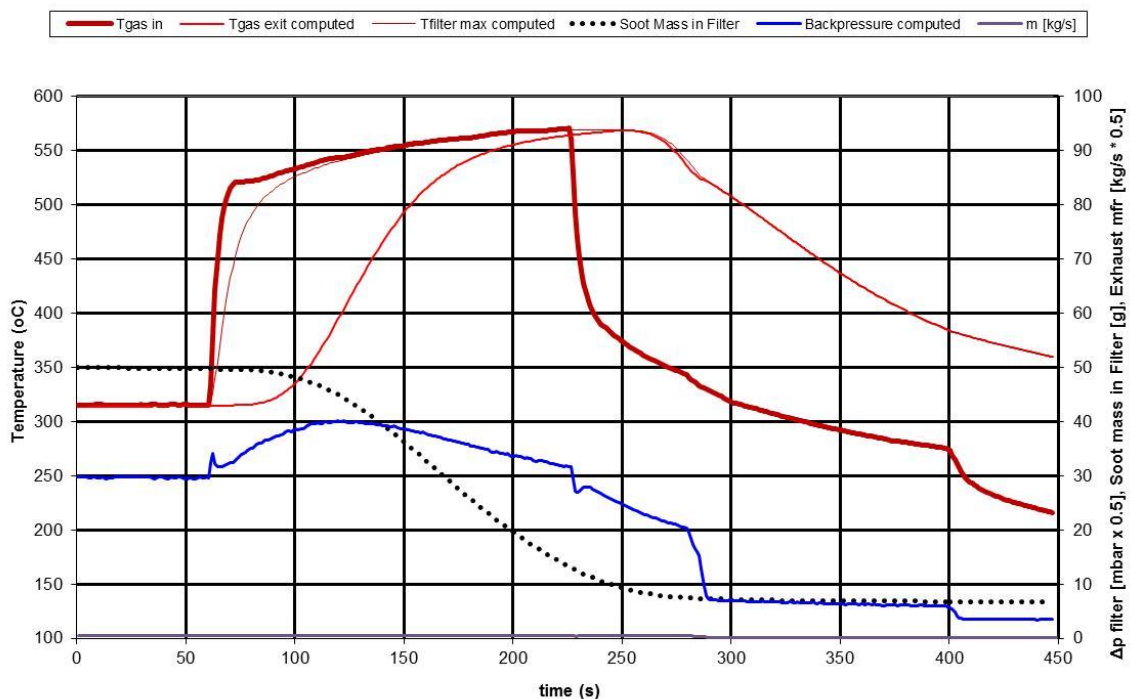
Figure 22: Calculation of pressure drop and regeneration temperatures of the HUG Engineering filter based on a certain regeneration scenario with 100g initial filter soot load (26).

25

The second constructional solution, which was proposed from the company Mine-X, included one cylindrical DPF made from cordierite, with a diameter of 350 mm and volume of 70 liters (much smaller from the first DPF proposed). The cell density of the filter was 100 cells per inch with an average wall thickness of 17 mils. The same computational simulations as in the first case were carried out and demonstrated that when the filter was cleaned, the pressure drop was higher (25 mbar) in relation to the oversized filter, while in the loaded state (100g of soot) it rose to 100 mbar (26). A pressure drop of this level is considered acceptable as it is below the limit (120 mbar) that manufacturers define for proper engine operation.

The third constructional solution was proposed from the company DCL and included two cylindrical DPFs made from cordierite. Each filter had a diameter of 267 mm and volume of 24.2 liters. The selected DPF substrate was the same as in the second case since the cell density was 100 cells per inch and the wall thickness was 17 mils. The computational simulations (figure 23) predicted an initial pressure drop of 40 mbar for clean filters and 140 mbar for the loaded state (26).
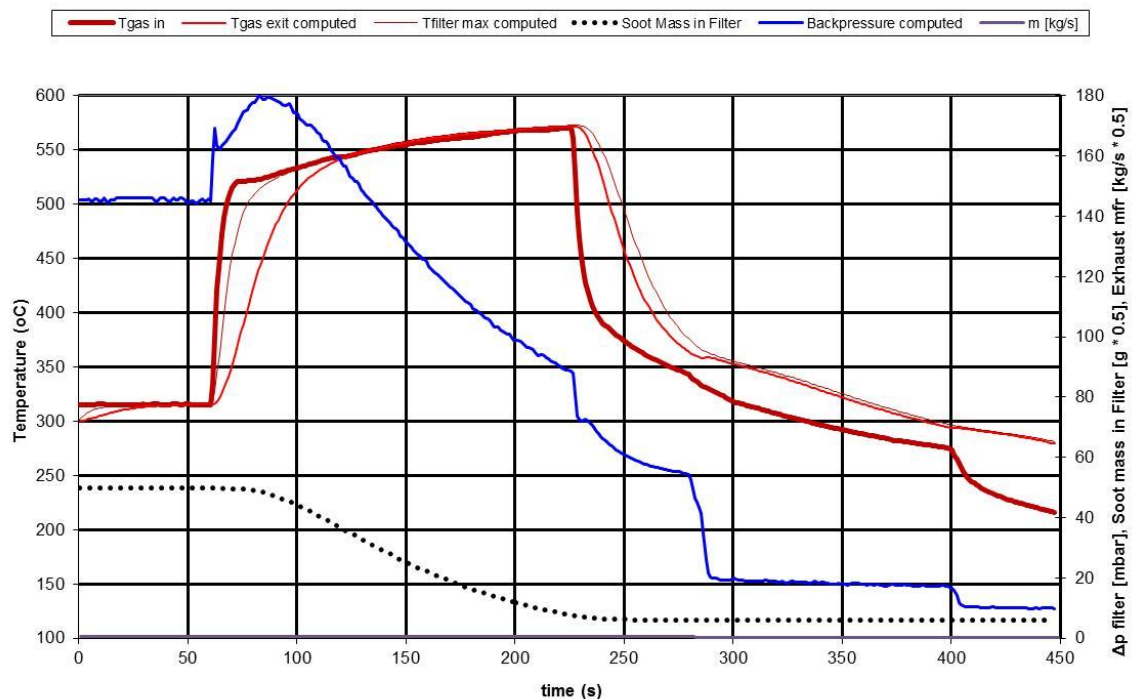
Figure 23: Calculation of pressure drop and regeneration temperatures of the DCL filter based on a certain regeneration scenario with 100g initial filter soot load (26).

In table 2 the three proposed constructional solutions regarding the DPF selection, are presented (26). Although the second solution from Mine-X was considered suitable for the specific application, difficulties regarding the filter supply, as well as the possibility for investigating the performance of two DPFs in the EBS led to the selection of the third solution, proposed from DCL. The two particulate filters were removed from trucks, then cleaned (regenerated) and delivered at the laboratory (figure 24). Despite the relatively high pressure drop that was predicted in the loaded condition (140 mbar for 100g of soot) the installation of two filters allows each time the removal of the more loaded filter so the system without interrupting the system operation. As far as the selected regeneration strategy is concerned, the EBS doesn't predict any active or passive regeneration system. If a filter is loaded at an undesirable level, it will be removed and placed in special furnaces where the soot will be oxidised. Then the clean filter will be re-installed on the system.

Constructional solution	1st	2nd	3rd
Manufacturer	HUG Engineering	Mine-X	DCL
Diameter (mm)	500 (square)	350 (cylindrical)	267 (cylindrical)
Length (mm)	700	570	432
Components	1	1	2
Overall volume	175	70	48.4
Cell density (cpsi)/Wall thick. (mils)	177/12	100/17	100/17
Substrate material	SiC	Cordierite	Cordierite
Δp clean filter (mbar)	15	25	40
Δp loaded filter (mbar)	30	100	140

Table 2: Suggested solutions regarding the DPF selection (26)

Figure 24: The two DCL particulate filters (26)

Chapter 3: Exhaust Bypass System Overview

3.1 System Description

The Exhaust Bypass System or EBS is an after-treatment emission control device which takes advantage of the DPF technology by featuring two particulate filters. However, it differs from the conventional DPF systems since its design enables the selective reduction of the prominent smoke (PM) emissions of marine diesel engines. The system is named EBS because it is characterised by the presence of a bypass duct connected to the main exhaust duct. The initially conceived idea comprises the activation of the EBS only during engine transient loadings, such as engine start-up or sharp increase in the engine load, when there is high PM (smoke) production. The eventual smoke reduction is achieved by leading the exhaust gas through this bypass duct and then to the particulate filters that collect the increased PM emissions of the engine[1]. When the engine operates in steady-state conditions and smoke emissions are less, the EBS deactivates by allowing the exhaust gas pass through the main duct and then to the atmosphere unfiltered. The selective exhaust filtering is far from being optional since it is the only way to avoid early filter-clogging due to the exhaust content in ash and PM that contaminates the filters[2]. The exhaust gas flow control, which is necessary for the EBS operation, is achieved by two butterfly valves which open and close alternately and determine the EBS activation – deactivation. The valves are positioned by pneumatic actuators which are electro-pneumatically controlled via the respective positioners.

The system efficiency is a measure of two dependent variables: the accomplished smoke emission reduction and the engine backpressure developed from the filters presence. Thus, the respective sensors that measure exhaust opacity and exhaust pressure across the filters are considered as an integral part of the EBS. Furthermore, additional sensors that measure the overall system backpressure and the exhaust temperature before the filters and the bypass duct are considered major parts of the EBS. The system parameters are limited only to the exhaust gas flow control since the amount of the exhaust gas to be filtered determines uniquely the system efficiency. Finally, the system provides the potential of leading part of the exhaust gas through the filters (by the simultaneous opening of the two valves) which can further increase the system efficiency. As a consequence, a possible sensor that measures the exhaust gas flow before and after the bypass duct has also been considered. The EBS is presented in figure 25.

---

[1] See section 1.4 p.13
[2] See section 2.3 p.22
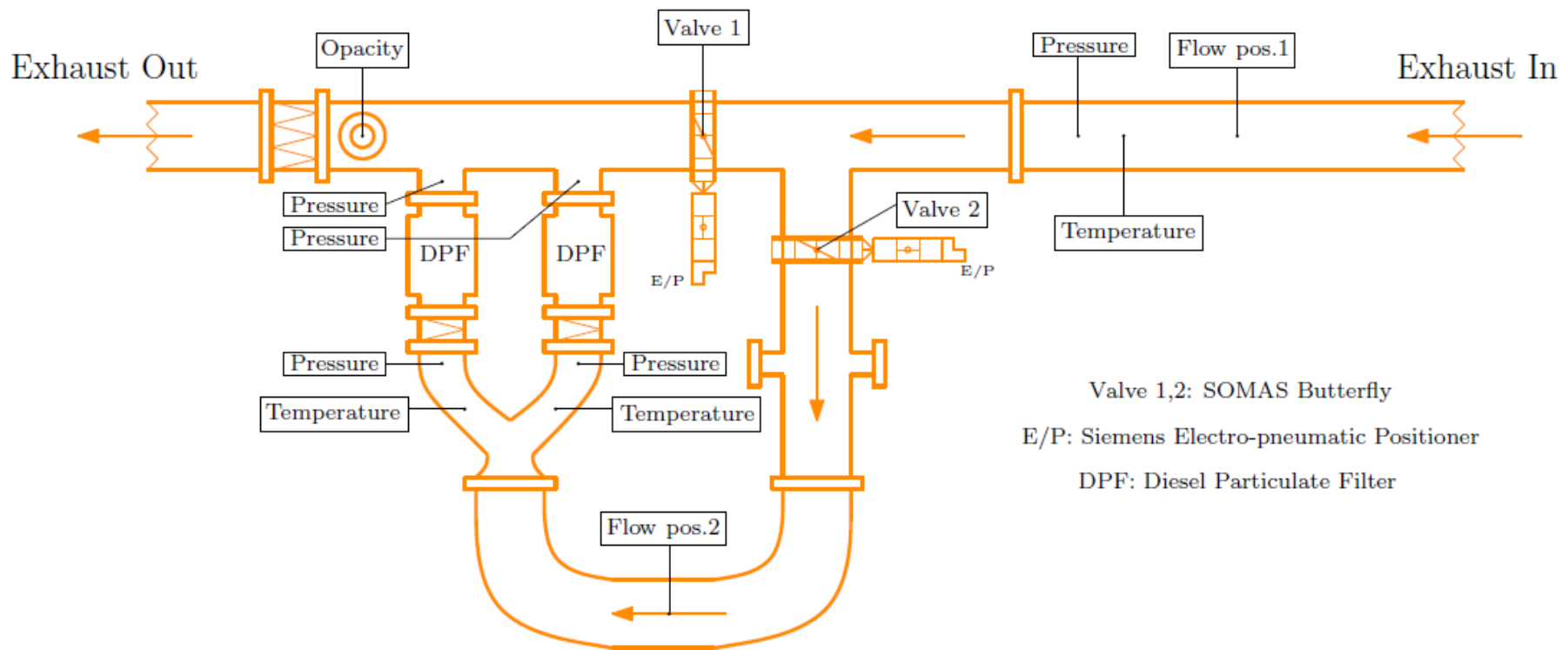
Figure 25: The exhaust bypass system overview at LME/NTUA with sensors and actuators

The EBS is to be installed in the exhaust gas processing unit (room I.13) of the LME of the NTUA. For the implementation of the necessary experiments the laboratory is equipped with a state of the art engine testing facility which features two diesels engines. The first one is an MAN-B&W Holeby L16/24 5-cylinder, 4-stroke turbocharged diesel engine of a maximum power of 500 kW and maximum speed of 1200 rpm (figure 26). The engine is mainly used for ship-board electric power generation and is coupled via a shaft and an elastic coupling with an AEG electric dynamometer which allows complex transient loadings. One of the main features of the MAN-B&W Holeby L16/24 engine is that it offers the possibility for optional fuelling with HFO as well as with MDO. The second engine is a Caterpillar 3176, 4-stroke turbocharged diesel engine with 6 cylinders in-line, having a maximum power of 448 kW and a maximum speed of 2300 rpm and mainly used for propulsion of small vessels or for electric power generation (figure 27). This engine is equipped with an electric starter and runs on diesel oil. It is coupled with a Zoellner hydraulic dynamometer via a cardan coupling and can simulate either stationary operation (gen-set) or a propeller curve operation. Both engines specifications are presented in table 3. The two engines have a common exhaust system that passes through the exhaust gas processing unit and then to the funnel (figure 28). The outer diameter of the exhaust system duct is 323.8 mm while the inner diameter is 313.5 mm which is somewhat oversized considering the latest exhaust gas flow measurements of the larger, especially in terms of volume, engine (MAN B&W L16/24) which at 90% engine load provides 0.955 kg/s of exhaust gas. However, the fact that the exhaust system is common and oversized for both engines offers the possibility for simultaneous engines operation.

Figure 26: MAN B&W Holeby L16/24

Figure 27: Caterpillar 3176B

Figure 28: Exhaust pipeline system

Engine	MAN B&W Holeby L16/24	Caterpillar 3176B
Operation cycle	4-stroke	4-stroke
Cylinders number	5	6
Cylinders configuration	In-line	In-line
Diameter	160 mm	125 mm
Stroke	240 mm	140 mm
Volume	24 liters	10.3 liters
Compression ratio	15.5 : 1	16 : 1
Maximum pressure	180 bar	-
Mean effective pressure	20.7 bar	22.7 bar
Maximum power	500 kW	449.3 kW
Nominal speed	1200 rpm	1900 rpm
Maximum speed	1200 rpm	2300 rpm

Table 3: Engines Specifications

The majority of the experiments are to be conducted with the Caterpillar 3176B engine so during the DPF selection[3] for the EBS a series of computanional simulations were conducted to investigate the selected DPF performance (figure 29).
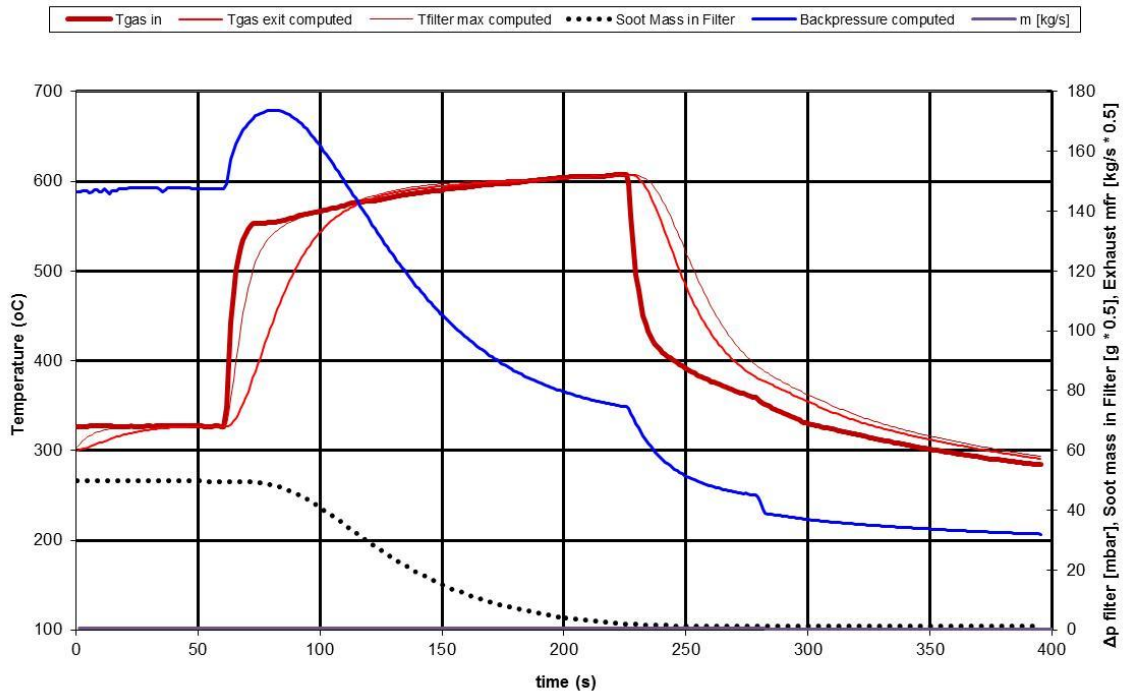
Figure 29: Calculation of pressure drop and regeneration temperatures of the DCL filter based on a certain regeneration scenario with the CAT 3176B engine and with 100g initial filter soot load (26).

---

[3] See section 2.4 p.25-26

3.2 System Efficiency Evaluation

The EBS efficiency is assessed by simultaneously measuring the smoke emission reduction achieved and the backpressure developed across the two particulate filters. The first variable is a measure of the system performance while the second variable is a direct indication of the system influence on the engine operation. Both depend on the amount of the exhaust gas being bypassed and led to the filters and are considered important since each one is proportional to the other; higher smoke emission reduction means more PM being collected on the filters which immediately increases the system backpressure and vice versa. High backpressure is considered undesirable since it increases the engine thermal load and the fuel consumption. For this reason sensors that can accurately estimate the smoke emission and the pressure drop across the filters are considered vital parts of the EBS.

3.2.1 Smoke Emission Measurement

In order to estimate the smoke emission of an engine several methods have been proposed which include either thermal processes (e.g. combustion) or optical ones. For the optimisation of the EBS a quick and accurate measurement of the smoke emission is necessary so a suitable method must be selected.

Thermal methods can provide information of the organic compounds (mainly EC) in the exhaust gas and several protocols have already been developed. However, special laboratory equipment is needed as the particulate sample is collected and heated in ovens in order to measure the produced CO_2. As a consequence, thermal methods are considered inappropriate for the specific application (EBS) as they cannot satisfy the need for quick and continuous smoke emission measurements during engine transient loadings.

As far as the optical methods are concerned, many standards have been developed since their applicability has rendered them very popular. These methods directly relate smoke emission to light absorption so measurements depend highly on light wavelength and sampling parameters. The most reliable instruments for measuring smoke, based on optical methods, are the aethalometers or filter smoke meters. These instruments measure light absorption changes due to filter paper blackening caused by a sample gas drawn through the filter (12). Although they are considered simple and robust instruments, they cannot measure smoke in transient conditions due to the extended sampling period. For this reason, they are unsuitable for the

EBS. Other optical instruments for measuring smoke are the opacity meters which measure the light attenuation caused by the sample gas. Although these instruments provide simple and quick measurements, their accuracy is disputed since some light attenuation may be a result of redirection (scattering) instead of absorption. However, opacity meters are suitable for measurements on engine transient loadings due to their small sampling period. Therefore, a sensor of this kind is to be installed on the EBS.

Several other methods for measuring smoke have also been proposed, such as the photoacoustic one, which includes firing the sample gas with intense laser light. The light absorptive particles, which are hit by the laser, heat up rapidly and make noise. Then, the noise is detected and the particulate concentration is evaluated. Although this method measures light absorption directly, it does not give complete information of light over different wavelengths, it requires dilution prior to measurements from diesel engines and has high maintenance requirements. Furthermore, it isn't a standardised method so its applicability is limited (12).

Recently, new methods for smoke identification have been developed although further experience is needed before such methods are widely applied. For example, instruments that measure PM (smoke) based on the triboelectric effect have been produced, featuring a protruding probe (figure 30) that is inserted into the exhaust flow and measures the electrical charge which the soot particles experience due to friction (27). Unfortunately, despite the simplicity of their operation, they require constant exhaust gas speed so they are not suitable in diesel engines applications. In addition, new compact sensors for PM measurement after DPF applications are under development (figure 31). Such sensors contain special configurations which due to PM deposition create conductive contact between two electrodes that are under constant voltage. The sensors measure the induced electric current which is directly related to the PM deposition. Then, the deposited PM is oxidised via regeneration processes so that new measurements can be obtained (28).

Figure 30: PM measurement instrument based on the triboelectric effect (27)

Figure 31: PM compact sensor (28)

3.2.2 The G1000 Smoke Density Monitor

For measuring the reduction of the smoke emission achieved by the EBS, an opacity meter capable of providing accurate and quick measurements has been chosen. The manufacturer is a Danish company named Green Instruments A/S and the selected model is the G1000 Smoke Density Monitor. It is designed to monitor optically smoke emission in uptakes after boilers, incinerators and engines and provides prompt and accurate response to the smoke density since it is positioned directly on the exhaust flow and it doesn't require collecting sample gas. As a result this smoke sensor is considered ideal for the EBS as its signal can be incorporated easily in a closed loop automatic system. Furthermore, it doesn't depend on weather conditions or ambient light and considering its limited dimensions, this monitor is suitable for applications where flexibility and easy sensor mounting – removal are required.

As a standard configuration, the G1000 Smoke Density Monitor (SDM) consists of the following main elements (29):

- Opposed optic heads with lenses (figure 32 and 33)
- Fiber optic cables (figure 33)
- Purge air system
- Monitoring unit with digital display (figure 34)

The SDM uses a high-power infrared light beam. It is single pass system where the beam of light is transmitted from the optical fiber of the transmitter across the exhaust gas stack to the optical fiber of the receiver. The transceiver is an optic beam module amplifier which is placed inside the monitoring unit. The beam is absorbed and scattered by smoke causing a reduction in the amount of light received by the transceiver. The monitoring unit, which displays the opacity, indicates 0% if there is no opacity and 100% if the light beam is totally blocked. Apart from the digital display, the monitoring unit provides analogue signals in the form of current and voltage outputs of 4-20mA and 0-10V respectively. Higher signal values (20mA and 10V) correspond to 0% opacity while the lower ones (4mA and 0V) indicate 100% opacity. The SDM overall specifications are presented in appendix I page 113.

American regulations are in most cases based on absorption and employ the Ringelmann method (published by Prof. Maximilien Ringelmann in 1898) in which a trained observer makes visual estimate of the smoke appearance. It has a 5 levels of density inferred from a grid of black lines on a white surface which, if viewed from a distance, merge into known shades of grey. There is no definitive chart, rather, Prof. Ringelmann provides a specification; where smoke level

'0' is represented by white, levels '1' to '4' by 10mm square grids drawn with 1mm, 2.3mm, 3.7mm and 5.5 mm wide lines and level '5' by all black (30). The Ringelmann chart serves for visual comparison of plume to the six levels of opacity as shown in figure 35. The alternative Bacharach scale compares the darkness of spots resulting on a filter paper after percolating a given amount of fumes (using a soot pump). Both methods are not directly convertible. The Bacharach scale is employed by IMO in its regulations on shipboard incinerators (MARPOL V) when limiting the emissions to Bacharach 3. Usually, this is interpreted to correspond to Ringelmann 1 (29).

Figure 32: Optic heads of SDM

Figure 33: Lenses with fibre optic cables

Figure 34: The SDM monitoring unit
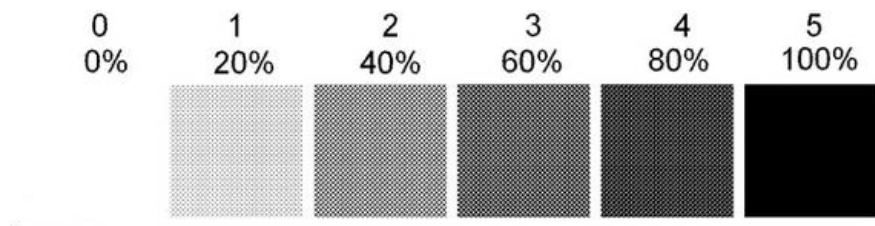
Figure 35: Ringelmann scale for smoke density (30)

For the SDM process connection, the optic heads are positioned on socket pipes (figure 36), made of ordinary mild steel, that are welded onto each side of the smoke channel. Furthermore, the SDM includes a purge air system which supplies clean and dry air (of 1-2 bar pressure) through a non return valve, an air distributor (figure 37) and two hoses (figure 38) to the head housings. The purge air supply is crucial to the SDM proper operation since it averts the lenses fouling from smoke. On the other hand, too much air velocity will affect the effective light path

length as it blows the exhaust gas out of the way. Therefore, for securing a sufficient, but not excessive air flow, an air supply filter regulator and a flow meter are optionally provided with the sensor. The volumetric air supply should be approximately 2×5 l/min and can be controlled using the flow control screw at the purge air connection of the head housing (29). An overall schematic representation of the G1000 SDM process installation is presented in figure 39.

Figure 36: Pipe sockets for process connection

Figure 37: Air distributor of purge air system

Figure 38: Air hoses of purge air system
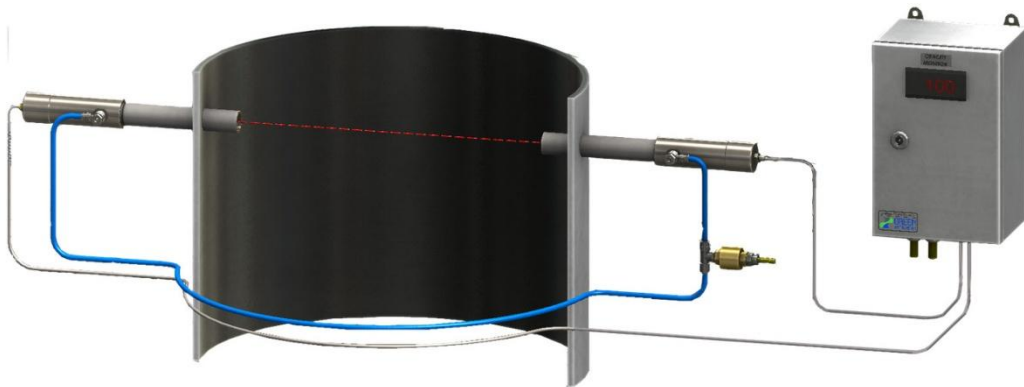
Figure 39: Schematic representation of the G1000 SDM process installation (31)

3.2.3　System Backpressure Measurement

In order to estimate the system backpressure that is developed due to the DPF soot loading, pressure sensors must be installed across the filters. Pressure sensors measure either absolute pressure (pressure related to perfect vacuum) or gauge pressure (pressure related to atmospheric pressure). There are also pressure sensors that measure the difference between two pressures, one connected to each side of the sensor. These are called differential pressure sensors and are suitable for measuring pressure drops across filters. As far as the sensing technology is concerned, the majority of pressure sensors are force collector types which generally use a force collector (such a diaphragm, piston, bourdon tube, or bellows) to measure strain (or deflection) due to applied force (pressure) over an area.

The most common force collector pressure sensors take advantage of the piezoresistive strain gauge technology. The applied – measured pressure deforms an elastic diaphragm onto the ends of which are located four strain gauges which are connected to form a Wheatstone bridge circuit. The bridge balances when the applied voltage is zero. The deformation of the elastic diaphragm is measured via the strain gauges. As a result, the voltage output of the Wheatstone bridge varies accordingly to the applied pressure. The elastic diaphragm is usually made of silicon (32).

Several other types of force collector pressure sensors exist such as (33):

- Capacitive which use a diaphragm and pressure cavity to create a variable capacitor to detect strain due to applied pressure.
- Electromagnetic which measure the displacement of a diaphragm by means of changes in inductance (reluctance).
- Piezoelectric which take advantage of the piezoelectric effect of some materials (e.g. quartz) to measure the strain caused by the applied pressure. This technology is commonly employed for the measurement of highly dynamic pressures.
- Optical which use the physical change of an optical fibre to detect strain due to applied pressure. This technology is employed in challenging applications where the measurement may be highly remote, under high temperature, or may benefit from technologies inherently immune to electromagnetic interference.
- Potentiometric which use the motion of a wiper along a resistive mechanism to detect the strain caused by applied pressure.

For measuring the backpressure developed by the two particulate filters, four piezoresistive pressure transducers have been chosen. The need for measuring backpressure in terms of gauge pressure and not pressure drop has excluded the differential pressure sensors option. However, differential pressure measurements are considered necessary for estimating the filters soot loading. For this reason pressure sensors are to be installed before and after the filters[4] so that simultaneous readings of system backpressure and pressure drop across the filters can be achieved.

The four pressure sensors were acquired by the German company Wika and the selected model is the S-10 Pressure Transmitter (figure 40). This model offers continuous measuring ranges between 0…0.1 and 0…1,000 bar and is capable of operating with aggressive media such as exhaust gas (34). However, to ensure proper sensor operation the media temperature has to be maintained under $100^{o}C$, so special configurations must be realised in order to cool the exhaust gas to the desired temperature without affecting the sensor response. In order to achieve accurate and prompt backpressure readings a proper measuring range of 0 to 1 bar gauge pressure has been selected. The sensor provides two-wire current output of 4-20mA and its accuracy is defined as less than ±0.50% of the selected measuring span. Detailed sensor specifications are provided in appendix I pages 114 - 117.

Figure 40: S-10 pressure transmitter (34)

---

[4] See section 3.1 p.29

3.2.4 DPF Soot Load Estimation

The system backpressure is highly related to the DPF soot loading since the accumulated PM impedes the exhaust gas flow through the filters. As a consequence, pressure drop across the filters develops and the system backpressure increases. For this reason, a precise knowledge of the actual trapped soot mass inside the DPF is required. It is a state of the art to estimate indirectly the soot loading in a DPF via the measurement of the differential pressure developed across the filter combined with the use of specific on-line models. However, this method highly depends on soot characteristics and the exhaust flow rate through the filter. In addition, the estimation models need calibration in any new setup and to do this the soot load of the DPF must be known while tuning the parameters. Moreover, because it is difficult to know the soot distribution in the filter, the mass estimation based on the differential pressure sensor can be less accurate, especially for certain types of engine's operation cycles (35).

However, a new approach, based on a microwave measurement technique, that enables direct and contactless in-operation soot load detection, has been developed. Microwaves are impressed into the filter by a vector network housing via coaxial antennas and the scattering parameters (transmission-reflection), which are a function of frequency, are measured. The filter canning acts as cavity resonator, in which the electro-magnetic waves form resonant modes at characteristic frequencies. These are highly influenced by the permissibility and conductivity of the filter. As the DPF is being loaded, the accumulated soot alters the system's conductivity, due to the soot's different dielectric properties, hence its resonant frequencies (figure 41). As a result this shift of the resonant frequencies as well as the respective changes in the attenuation of the radio waves can be measured to determine the soot load inside the filter. This method has already been used to control the active regeneration of diesel particulate filters in city buses. Despite its merits, however, there is a major and obvious drawback concerning the method's sensitivity. The high exhaust gas temperatures alter the resonator geometry and the system's electrical conductivity, leading to a decreasing resonance frequency (36). As a result, the soot load measurements depend highly on the exhaust gas temperature so necessary compensation has to be considered.

In 2009 General Electric Sensing and Inspection Technologies announced the ACCUSOLVE Advanced Diesel Particulate Soot Sensor, also named the "soot sensor", which utilizes radio frequency technology to enable accurate measurement of accumulated soot in DPF, providing real-time soot loading data and real time closed loop control of the DPF regeneration process (37). The launch of the RF-sensor from GE demonstrated that the need for more precise

measurements of DPF soot load will lead to the gradual abandonment of the differential pressure measurement. Although the RF-sensor presents a clear temperature and soot distribution dependence, it doesn't depend on the exhaust gas flow and its response is prompt and more accurate.

For the time being, the lack of adequate experience, the high RF-sensor cost as well as the need for obtaining immediate reading of the system backpressure, led to the selection of the differential pressure measurement as the DPF soot load estimation method. For this reason except for the pressure sensors that are to be installed before the two filters, two additional similar pressure sensors are also to be installed after the filters[5], so by extracting the readings of the pressure sensors across each filter, the respective soot load estimation can be derived.
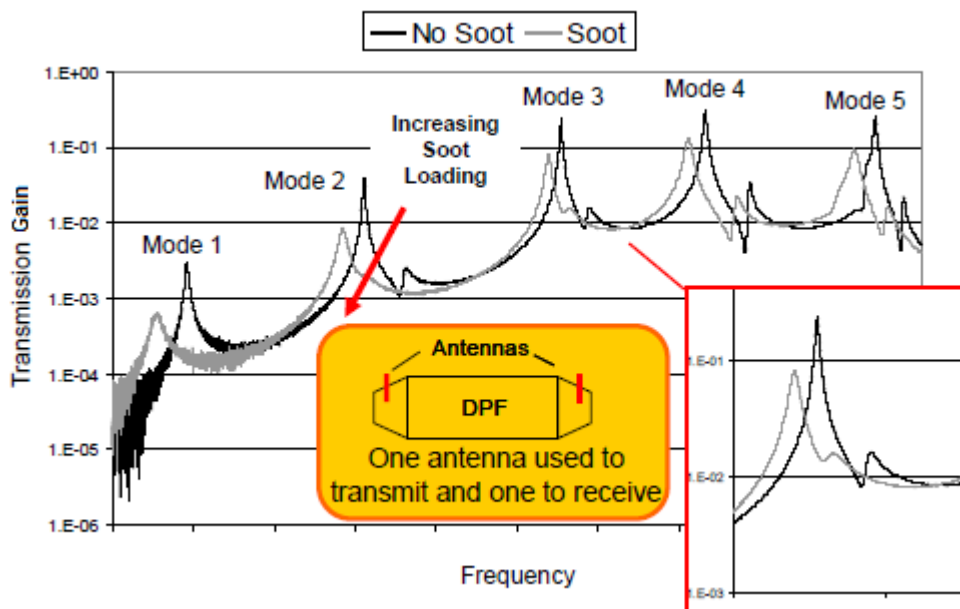
Figure 41: Resonant modes shift due to soot loading (36)

Figure 42: Accusolve advanced DPF soot sensor (37)

---

[5] See section 3.1 p.29

3.3 Exhaust Gas Flow Control

The only parameter that determines the overall system performance, hence its efficiency is the exhaust gas flow that is led through the particulate filters. Excessive exhaust gas flow through the filters will lead to a high increase of smoke emission reduction but also to an increase of system backpressure to undesirable levels as well as to early filter contamination. On the other hand, small exhaust gas filtration may lead to less engine backpressure and increased filter life span but the smoke reduction achieved may not be sufficient. As a consequence, the exhaust gas flow control, which is to be achieved via two butterfly valves[6], is crucial for the EBS operation and optimisation.

Initially, the exhaust gas will be totally bypassed until engine steady state operation is achieved. Therefore, the acknowledgement of the exhaust gas flow that is led to the particulate filters is easy since it can be derived from one single flow measurement across the main exhaust duct. However, system optimisation may impose partial bypassing of the exhaust gas. As a result in order to estimate the exhaust gas flow through the filters, one additional measurement across the bypass duct is necessary. For obtaining these measurements a flow measurement sensor has been considered in the EBS.

3.3.1 The SOMAS Butterfly Valves

The two special butterfly valves, manufactured from the Swedish company SOMAS, are wafer design so they are suitable to be mounted between flanges. They are made of stainless steel (special alloys may be used for applications with aggressive media) and their nominal size ranges from DN80 to DN1200 (for exhaust gas applications the maximum valve dimension is limited to DN800) in order to cover a vast range of pipe ducts. The main characteristic of these valves is their advanced triple eccentric design which includes a unique disc shape made of solid stainless steel (or other suitable materials) seat which remains unaffected by high flow velocities and temperatures and renders the valves capable of handling a wide range of liquids, gases and steam within a broad temperature range (up to 600°C). Furthermore, they can be used as control on/off and shut-off valves and their tightness class is in accordance with EN60534-4 Class V as standard (38). According to the characteristic curve of the flow as regards the valve opening angle (figure 43), high flow increase is observed after 50° while its maximum value

---

[6] See section 3.1 p.29

(100%) is achieved for 80° opening angle. For higher angle values the flow starts to decrease due to the increase of the pressure drop across the valve.
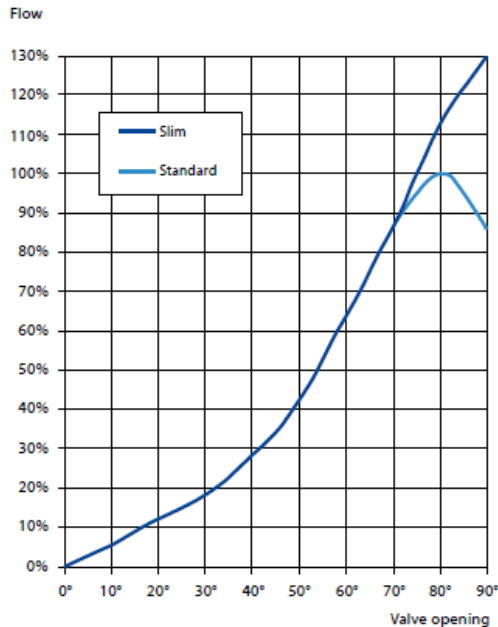
Figure 43: Characteristic curve of the flow as a function of the valve opening angle (38)

Figure 44: SOMAS butterfly valves for exhaust gas (38)

For the specific application (EBS) which features exhaust pipe duct of 323.8mm outer and 313.5 mm inner diameter, the SOMAS butterfly valve for exhaust gas (figure 44) DN 300 has been selected. Its overall specifications (e.g. pipe geometry factor, capacity factor, resistance factor, etc) and selection tables are presented in appendix I pages 118 - 121.

The SOMAS valves are delivered assembled with pneumatic actuators. The actuators are manufactured by SOMAS in a compact design and have a torque curve corresponding to the torque demand for ball segment, butterfly, and ball valves. Their main characteristic is the low-friction seals which allow for a low starting torque. Moreover, the springs of the actuators are supplied in a cartridge in order to reduce the risk of injury and to simplify maintenance.

The pneumatic actuators provided by SOMAS (figure 45) are divided into three categories:

- Double acting actuators
- Single acting actuators – spring to close
- Single acting actuators – spring to open

All three types consist of a piston which receives the force applied by the pressurised air (4 – 8 bar) supply and moves in a linear way. The linear motion from the piston is then converted into a rotary motion via a linkage mechanism. In figure 46 the curve that shows the output torque from the actuator as a function of the actuator shaft angle is provided. Maximum torque is achieved in the closed position which corresponds to the demand of ball segment valves, ball valves and metal seated butterfly valves. For the latter, the dynamic torque can be high in case of high differential pressure across the valve. This increased torque demand is normally covered by the actuator selection tables (39).

Figure 45: SOMAS pneumatic actuators (39)
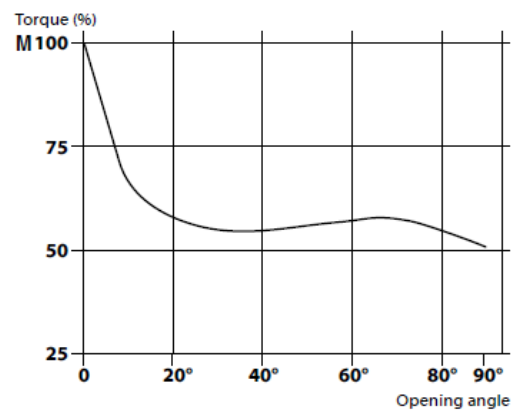
Figure 46: Characteristic curve of the actuator torque output as a function of the shaft angle (39)

The double acting actuators or DA don't have springs and the piston motion is reversed by pressurised air supply (figure 47). On the other hand, the single acting actuators have special springs for the reverse operation. In single acting actuators the springs either close (SC) or open (SO) the valves in case of failure while in DA actuators the fail safe operation is determined via selecting the desired depressurising strategy. The SOMAS pneumatic actuators overall specifications as well as the selection tables are provided in appendix I pages 122 - 124. The selected model of the pneumatic actuators of the EBS is the A31-DA-F14.

The SOMAS butterfly valves are delivered fully assembled and factory tested as complete units with the pneumatic actuators and the respective electro-pneumatic positioners. The positioners provide a vital interface for the valves operation since they allow remote electronic control of the butterfly valves. The selected model is the SIPART PS2 electro-pneumatic positioner of the Siemens Company.

The SIPART PS2 positioner offers many advantages, like simple installation and automatic commissioning (self-adjustment of zero and span), possible local and remote operation, very high-quality control thanks to an online adaptation procedure, negligible air consumption in stationary operation, ''tight shut-off'' function (ensures maximum positioning pressure on the valve seat) and few moving parts, hence insensitive to vibrations. It can also be used in various applications (from the food and pharmaceutical industry to the chemical/petrochemical one) and is suitable for single and double acting actuator. As far as the process communication is concerned, they are provided in versions of 0/4-20mA control communication without/with HART signal or with either PROFIBUS PA or FOUNDATION Fieldbus (FF) communication interface.

The SIPART PS2 electro-pneumatic positioner consists of a highly-integrated microcontroller and works in a complete different way to normal positioners. The positioner moves the actuator to a valve position corresponding to the selected setpoint. Additional function inputs can be used to block the valve or to set a safety position. A binary input is present as standard in the basic device for this purpose. Comparison of the setpoint and the actual value takes place electronically in the microcontroller. If the microcontroller detects a deviation, it uses a 5-way switch procedure to control piezoelectric valves, which regulates the flow of air into and from the chambers of the pneumatic actuator or it blows it in the opposite direction. The microcontroller then outputs an electric control command to the piezoelectric valve in accordance with the size and direction of the deviation (deviation between setpoint w and control output x). The piezoelectric valve converts the command into a pneumatic positional increment. The positioner outputs a continuous signal in the area where there is a large control deviation (high-speed zone); in areas of moderate control deviation (slow-speed zone) it outputs a sequence of pulses. No positioning signals are output in the case of a small control deviation (adaptive or variable dead zone). The linear or rotary motion of the actuator is detected by the mounting assembly and transferred to a high-quality potentiometer made of plastic conductive material over a shaft and a non-floating gear transmission (40).

The positioner also offers the option for installing a module which provides a two wire 4-20mA position feedback signal. This module, named I_Y, is indispensable for developing and optimising the EBS. Apart from the I_Y module, the positioner offers an alarm module which provides signalling of two limits of the travel or angle by binary signals. The two limits can be set independently as maximum or minimum values. The alarm module offers also a second binary input for alarm signals for triggering safety reactions (e.g. safety position) (41).

In figure 47 the SIPART PS2 electro-pneumatic positioner (detailed specifications provided in appendix I pages 125 - 131) is presented. The pneumatic connections of the positioner for the

inlet air and the positioning pressure are located on the right-hand side. The positioning pressure output ports Y1 and Y2 of the positioner are connected via two small tubes made of steel to the main chamber of the pneumatic actuator (figure 48). By alternating the pneumatic connections Y1 and Y2 a different valve safety position of in case of failure can be achieved.

Figure 47: SIPART PS2 electro-pneumatic positioner (40)
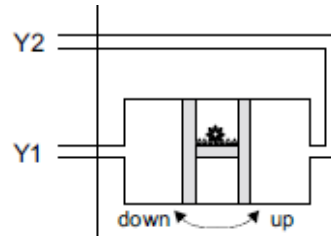
Figure 48: Pneumatic connection of positioner and actuator (41)

Due to the fact that the electro-pneumatic positioners were delivered mounted to the pneumatic actuators, the pneumatic connections of the positioners and the actuators were pre-determined. In case of failure (pneumatic or electrical) the valves are set to close as it is the mandatory safety position for valves that correspond to marine applications. The butterfly valves, the pneumatic actuators as well as the respective electro-pneumatic positioners were delivered in LME fully assembled as complete units ready for process installation (figure42).

Figure 49: SOMAS butterfly valve as delivered in LME

3.3.2   Exhaust Gas Flow Measurement

Except for optimised exhaust gas flow control, the EBS imposes the need for exhaust gas flow measurements. There is a variety of flow sensors now in the market, each of them depending on different operation principles. The most common flow sensors are the velocity flow meters which feature a special probe at the edge of which there is a vane wheel sensor. This kind of sensors measures directly the flow velocity inside a duct. The probe is inserted in the duct in a proper way so that the sensor is located right in the middle. The flow which passes through the duct excites the vane wheel which starts rotating according to the flow velocity. Then, the wheel rotation speed is measured and an estimation of the flow velocity can be derived. Although these sensors are simple, easy to operate and capable of measuring flow velocity of aggressive media, the need for steady velocity profile, as well as the fact that they interfere with the flow pose some limits to their operation. In order to overcome these limits additional flow sensors have been developed, like the differential pressure flow meters which calculate the flow by measuring the pressure drop over obstructions inserted in the flow, the positive displacement flow meters which measure process fluid flow by precision-fitted rotors as flow measuring elements and the open channel flow meters which estimates flow through an open channel by measuring the height of a liquid as it passes over an obstruction as a flume or weir in the channel. Finally, there are also the mass flow meters which measure mass flow rate directly and are divided in two categories. The thermal flow meters, which calculate flow by measuring the heat loss, conducted to the passing fluid and the Coriolis flow meters. The latter feature rotating U-shaped tubes which start to oscillate due to the applied Coriolis force by the passing fluid. The flow is calculated by measuring the inflicted oscillations.

For implementing exhaust gas measurements, LME disposes a velocity flow meter manufactured by the German company Hontzsch. The flow meter features the corrosion resistant vane wheel sensor ZS25 (figure 50) which is suitable for exhaust gas measurements (capable for operating up to 500°C) and yields a large measuring span of 1.4 to 120 m/s. The vane wheel rotation speed scanning is realised via a non-contact inductive proximity switch. Moreover, the sensor can operate to a large extent irrespective of the density and composition of the gas and keeps the pressure drop due to the sensor presence to a low level. Finally, the flow meter has an integrated transducer which produces output analogue signal of 4-20mA (42). Detailed sensor specifications are provided in appendix I pages 132 – 136.

Despite the sensor applicability to exhaust gas applications the need for long straight duct for implementing accurate measurements imposes a big challenge. In case of full exhaust

bypassing flow measurements can be limited to one and the procedure is simplified since a suitable spot on the exhaust duct far from elbows and duct reduction – enlargement can be found[7]. However, if additional measurements on the bypass duct are needed (in case of partial bypassing), the applicability of the sensor is highly limited considering the lack of sufficient straight duct length[8]. Therefore, the accurateness of the measurements is disputed. As a result obtaining a velocity profile in the selected measuring spot is necessary in order to determine the preciseness of the flow measurements. The velocity profile is derived by measuring the flow velocity in different sensor insertion lengths, on the same spot and for the same flow conditions (figure 51).

Figure 50: Hontzsch velocity flow sensor ZS25 (42)
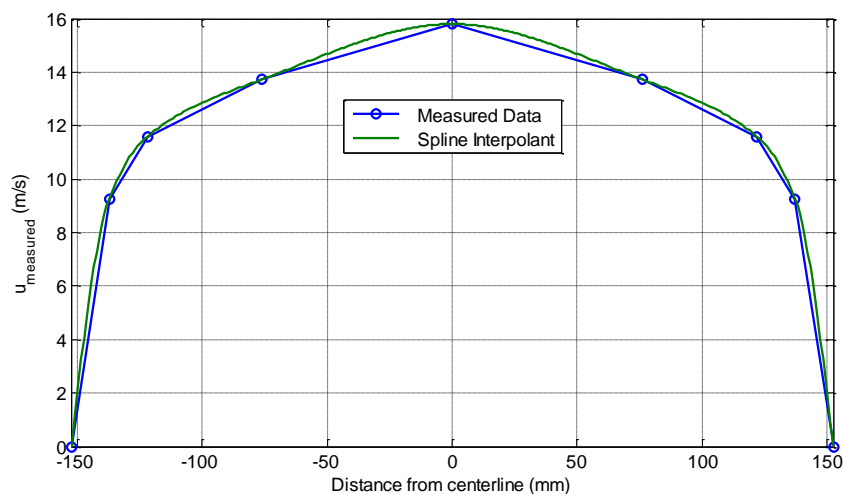
Figure 51: Measured flow velocity profile (43)

---

[7] See section 3.1 page 29 flow position 1
[8] See section 3.1 page 29 flow position 2

3.4 Additional Measurements and Devices

For achieving optimised EBS control several additional sensors and electronic devices are necessary. Due to the big dimensions of the exhaust duct, the EBS is characterised by high heat inertia. For this reason temperature readings are indispensable for identifying the exhaust gas properties as well as for controlling the exhaust flow through system. The necessary temperature measurements are to be obtained at three positions on the exhaust duct, two of them before the particulate filters and one before the bypass duct[9]. Early tests did prove a temperature difference between the two particulate filters which wasn't expected to be in such a degree from the computational simulations during the system design. This temperature difference may be an indication that the filters were not regenerated perfectly before their delivery at LME. Moreover, in order to ensure electrical isolation of the analogue signals, special isolating amplifiers are needed to support high-quality measurements. Finally, for the analogue signals reading a data acquisition unit, capable of providing numerous and simultaneous analogue inputs and outputs, is incorporated in the EBS.

3.4.1   Temperature Measurements

For temperature measurement many methods have been developed, most of them relying on measuring some physical property of a working material that varies with temperature. The most common temperature sensors that are used in industrial applications are (44):

- Thermistors
- Resistance Temperature Detectors (RTD)
- Thermocouples
- Pyrometer
- Infrared

A thermistor is a type of device whose resistance varies significantly with temperature, more so than in standard resistors. The resistance variation of the thermistors is considered as high and non-linear. As a result, they are useful as temperature detectors within a limited temperature range, typically $-90^{o}C$ to $130^{o}C$. Thermistors are mainly made of ceramic or polymer materials (32).

---

[9] See section 3.1 page 29

The RTDs share the same operation principle with the thermistors but due to the fact that they are made of pure metals, their response is more linear and are useful over larger temperature ranges. Most RTD elements consist of a length of fine coiled wire wrapped around a ceramic or glass core. The element is usually quite fragile, so it is often placed inside a sheathed probe to protect it. The RTD element is made from a pure material, typically platinum, nickel or copper (45). A resistance made of nickel is characterised by high temperature sensitivity leading to non-linearity, hence limited operation range. On the other hand, a resistance made of copper varies linearly with temperature but in such a way that leads to extensive sensor dilatation. Therefore, for large temperature ranges only platinum is considered appropriate as it presents linear behaviour even at very high temperatures (above 600°C). For this reason Pt100[10] has been developed as an industry standard of which the majority of RTDs are made (32).

A thermocouple is a temperature-measuring device consisting of two dissimilar conductors that contact each other at one or more spots. Any junction of dissimilar metals will produce an electric potential related to temperature. Thermocouples for practical measurement of temperature are junctions of specific alloys which have a predictable and repeatable relationship between temperature and voltage. Different alloys are used for different temperature ranges. Properties such as resistance to corrosion may also be important when choosing a type of thermocouple. Thermocouples are usually standardised against a reference temperature of 0 degrees Celsius (46). The most common are the types T (copper/constantan[11]), E (chromel[12]/constantan), J (iron/constantan), and K (chromel/alumel[13]) which can be used in a temperature span which ranges from -250°C to 1300°C (32).

As far as the pyrometer and the infrared temperature sensors are concerned, they are non-contacting devices which intercept and measure thermal radiation. While pyrometer operation is based on measuring the irradiance[14] of the target object (47), infrared temperature sensors measure only the infrared zone of the thermal radiation which is directly connected to the object temperature. These measuring devices are suited almost exclusively to the measurement of moving objects or any surfaces that cannot be reached or touched, but their accuracy is not as high.

---

[10] Pt100 is a RTD made of platinum that takes the value of 100 Ω at 0°C.
[11] 55% Cu + 45% Ni
[12] ~90% Ni + 10% Cr
[13] 95% Ni + 2% Al + 2% Mn + 1% Si
[14] Stefan-Boltzmann law defines irradiance as $j^{*}=\varepsilon\sigma T^{4}$, where ε is the emissivity of the object, σ the constant of proportionality and T the temperature (47).

For implementing the necessary temperature measurements on the EBS and considering maximum exhaust gas temperature of 300°C to 350°C, three RTDs made of Pt100 have been acquired. The sensors are manufactured by the German company Wika and the selected model is the TR10-C (figure 52). The sensor is connected via a three wire configuration (for eliminating deviations due to the lead resistance) to a T19 transmitter (figure 53) which is mounted within the cap of the connection head (48). The transmitter provides two-wire analogue signal of 4-20mA which corresponds to a measuring span of 0°C to 400°C. The sensor measurement deviation is defined according to DIN EN 60770 as ±0.50% of the selected measuring span (49). Detailed sensor and transmitter specifications are provided in appendix I pages 137 - 139 and 140 - 141.

Figure 52: TR10-C resistance temperature detector (48)

Figure 53: T19 transmitter (49)

3.4.2   Isolating Amplifiers and Data Acquisition System

For achieving high-quality signals, hence more accurate measurements, noise reduction of the sensors outputs has to be ensured. Moreover, electrical isolation of the analogue signals is essential for the safety of the system, since voltage variations could damage both the sensors and the data acquisition system (DAQ). Furthermore, the sensors output signals are in the form of analogue electrical current of 4-20mA. This signal form is suitable for long-travelling signals (high distance between sensors and DAQ system), since it ensures immune to voltage-noise signals. However, signal conversion from electrical current to voltage is necessary considering the DAQ system input is the form of voltage, 0-10 V. For these reasons, special isolating amplifiers, capable of satisfying these requirements, have been purchased. The selected isolating amplifiers (figure 54) are small compact devices, manufactured by the German company Phoenix Contact, which provide 3-way electrical isolation of the analogue signals, as well as signal conversion for connecting the installed sensors to the DAQ system. The selected models are the MINI MCR-SL-I-U-4 and MINI MCR-SL-UI-UI-NC. The first provides fixed signal

conversion and isolation of input electrical current 4-20mA to output voltage 0-10 V (50). As a consequence, it will be interposed for the electrical connection of the output signals of the sensors with the DAQ system. On the other hand, the second provides numerous possible combinations for signal conversions as the inputs and outputs can be configured via dual in-line package (DIP) switches (51). Therefore, it has been selected for the electrical connection of the output signals of the DAQ system with the electro-pneumatic positioners (U-I conversion) for the valves operation. Both of them feature prompt response (at approximately 3.5 ms), electrical isolation according to EN 61010 and limit frequency of 3 dB at approximately 100 Hz. The technical specifications are provided in appendix I pages 142 - 146.

Figure 54: Phoenix Contact MCR 3-way isolating amplifier (50)

As far as the DAQ system is concerned, LME disposes the DS1103 controller board (figure 55) of the dSPACE company which is a powerful controller board for rapid control prototyping. The board features accurate and high-speed 16-bit channels for 36 A/D (16 multiplexed channels equipped with 4 sample & hold A/D converters) and 8 D/A converters. Both input and output range of the converters is ±10 V. Furthermore, the board includes 32-bit parallel digital I/O channels organised in four 8-bit groups and a single CAN channel (52). The DS1103 controller board, whose technical specifications are presented in appendix I pages 147 - 148, is the main controller of the Caterpillar 3176B engine.
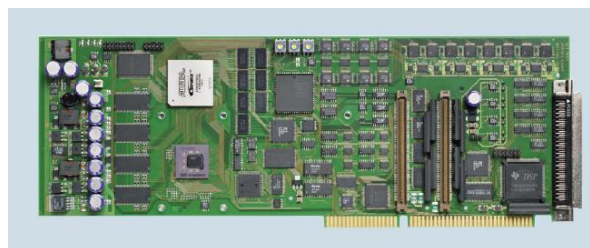
Figure 55: DS1103 controller board (52)

Chapter 4: Exhaust Bypass System Installation

4.1 Exhaust Bypass System Construction – Delivery - Assembly

The EBS is considered as part of the research project SEKTE (*Smoke Emission Abatement System for Fast Passenger Ships Manoeuvring in Island Harbours)* that is currently conducted in LME. In this context, the initial system design was conceived and created in the laboratory (figure 56) and then it was delivered to a piping constructions industry named Loukis which undertook the system construction due to its specialisation in marine exhaust systems. The EBS construction took place in the facilities of the Loukis industry in Piraeus (figure 57) and it was properly supervised in order to ensure compliance with all standards and to minimise possible deviations from the original design. The initial system design, which is presented in appendix II page 149, included five separate duct parts, connected to each other via bolts, two wafer design butterfly valves and two DPFs connected to the exhaust duct via clamps. For facilitating the manufacture process and eliminating possible mistakes, the two butterfly valves (complete units with actuators and positioners) as well as one DPF were delivered in the piping industry so that verification of the actual duct dimensions could be possible. Moreover, due to the fact that the initial design included clamp connection of the two DPFs with the exhaust duct, special caution was given for the manufacture of the connection surfaces. The EBS construction lasted almost ten days and it was followed by the system disassembly so that its transportation to the laboratory could be possible. The disassembled system was delivered and reassembled in the exhaust processing unit (room I.13) of LME/NTUA on Thursday, June 6, 2013.
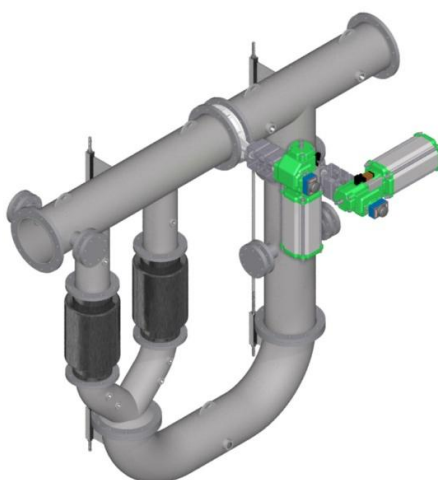
Figure 56: Exhaust bypass system initial design

Figure 57: EBS construction in Loukis industry

The reassembly and installation of the EBS in LME started early in the morning and lasted approximately 8 hours. Initially the whole system was delivered in separate parts (figure 58) and it was transferred to the installation point (room I.13) by an overhead crane and a couple of manual pallet jacks (figures 59, 60 and 61). The butterfly valves were delivered separately (figure 62) as complete units with the actuators and the positioners in their special boxes provided by the manufacturer (figure 63). Finally, the two DPFs of the EBS were collected (figures 64 and 65); the first one delivered by Loukis industry, where it was given in order to ease the piping construction, while the second was kept in the laboratory's storage room.

Figure 58: System delivery in separate parts

Figure 59: Parts transfer with the overhead crane

Figure 60: Parts transfer to room I.13

Figure 61: Parts deployment at room I.13

Figure 62: Butterfly valves transfer in their special boxes

Figure 63: Butterfly valves as delivered in LME

Figure 64: The first DPF as delivered by Loukis industry

Figure 65: The two DPFs collected before their installation

With the completion of the system transfer to the deployment point, the necessary preparation for its installation initiated. This included the uninstalling of the previous exhaust duct which was to be replaced by the exhaust bypass duct. Initially, the installed insulation was removed (figure 66) and a chain system, which worked like a manual lift, was installed in order to hold and uninstall the previous exhaust duct (figure 67). After all previous gaskets were removed, the assembly of the straight upper part of the EBS started. This consisted of two straight exhaust duct parts which were connected to each other via the first butterfly valve (figure 68). Since the valve is wafer design, the connections at every point was realised via bolts. The assembled upper straight part was then lifted by chains to the installation point (figure 69) and it was incorporated via bolt connections to the existing exhaust duct (figure 70). For achieving sealed connections between the flanges of the separate parts of the system, new gaskets were installed to avoid exhaust gas leakage. Then, the second butterfly valve and the vertical part of the exhaust duct (figure 71) were installed. Due to the increased dimensions of the butterfly valves, they were positioned properly in order to overcome encountered space limits. The next task included the assembly of the two DPFs with the respective two-channel exhaust duct. The connections between the particulate traps and the exhaust duct were realised via clamps (figure 72) which imposed the need for special connection surfaces at the ends of the particulate traps and the exhaust duct. In order to enable the installation of the lower straight part of the EBS, the assembled part of the DPFs had to be lifted by chains (figure 73). Then, the lower straight part was installed and connected via bolts and gaskets to the system (figure 74). Finally, the upper edges of the lifted DPFs had to be connected via clamps to the upper straight exhaust duct at the respective receptors (figure 75). Although this connection method (clamps) offered some serious advantages (low-cost, reduced weight and flexibility considering the easy installation-removal in case of filters replacement), it proved time-consuming as well as inefficient in terms of exhaust duct sealing. Indeed, due to the fact that the filters were used before their installation to the EBS, they presented small differences at their edges. The exhaust duct connection surfaces which would be the receptors of the particulate traps were constructed based on the DPF which was delivered to Loukis industry. Therefore, the assembly of the particulate traps to the exhaust duct proved very difficult and rose questioning regarding the process sealing.

The EBS installation was completed at the end of the day (figure 76) and a quick inspection of all the existing connections (welds, flanges, clamps) was carried out. The overall installation was considered successful, although questioning regarding the DPFs connection remained.

Figure 66: Removal of the insulation

Figure 67: Removal of the previous exhaust duct

Figure 68: Assembly of the upper straight part

Figure 69: Lifting the assembled upper straight part

Figure 70: Installation of the straight upper part

Figure 71: Installation of second butterfly valve and vertical part

Figure 72: DPFs connection with the two-channel duct

Figure 74: Installation of the lower straight part

Figure 73: Lifting the DPFs part

Figure 75: Final installation of the DPFs

Figure 76: The initially installed exhaust bypass system

4.2 Exhaust Bypass System Modifications

After the full installation of the system in LME, some early tests were carried out in order to examine the system performance and check the duct sealing, especially at the clamp connections of the DPFs. The first tests were conducted while operating the Caterpillar 3176b engine at about 40% load and only for the upper straight part of the EBS (valve 1 open) due to a technical problem encountered in valve 2, which remained closed. While the upper straight part of the EBS demonstrated the high-quality of the manufacture process of Loukis industry (the welds were almost perfect), the complete tests which entailed tests carried out by the bigger and older (hence smoky) MAN B&W Holeby L16/24 engine at 90% load confirmed the existing questioning regarding the clamp connections sealing (figure 77). These proved almost completely inefficient since except for the chocking smell emanated by the leaky exhaust duct, smoke deriving from the DPFs connections could be visually observed. Therefore, modifications concerning the DPFs part, especially the four connections of the particulate traps with the exhaust duct were necessary. Loukis industry undertook the project and suggested that the only way to achieve high-sealing and simultaneously non-permanent connections was via flanges. However, this connection method would increase the total system weight and the process for welding the flanges at the ends of the filters was somewhat sophisticated considering the small and rough edges of the filters. Finally, this connection method imposed the need for installing additional compensators in order to receive vibrations and vertical dilatations. The tasks lasted a few days and included the removal of the DPFs, the flanges welding at the connection points and the compensators installation before the filters (figure78). Then, the extracted part was re-installed on the EBS (figure 79) and the tests demonstrated sufficient process sealing at all points (both upper straight and bypass part).

Figure 77: Initial clamp connections

Figure 78: Flange connections and compensator

Figure 79: Modified exhaust bypass system

4.3 Sensors Process Connection

The sensors mounting included the installation of all temperature and pressure sensors, the opacity meter and the flow meter. The latter was not to be installed permanently on the system since corrosion from the exhaust gas had to be avoided. The sensors mounting started with the installation of the G1000 SDM. The smoke sensor consists of two optic heads which feature a G 1'' female thread for process connection. Despite the fact that Green Instruments provided a couple of 200 mm long 1'' welding sockets for connecting the optic heads with the smoke channel, two special socket pipes were produced in the laboratory (figure 80). These featured smaller overall length but also increased thread length for process connection (design provided in appendix II page 150). For the smoke monitor installation special configurations (figure 81) were initially predicted during EBS design, which also included a couple of sealing flanges (figure 82). The two sealing flanges had 1'' female thread in the middle and 8 G ½'' female threads in circular pattern for bolt connection. The socket pipes were inserted into the sealing flanges which were respectively connected to the exhaust duct via bolts. Special attention had to be given to the alignment of the sockets, so that they were centred right opposite each other. In order to verify proper alignment, a pipe longer than the funnel diameter was inserted into the socket holes (figure 83). After the socket pipes installation, the optic heads of the sensor were installed and the brass nuts were tightened to secure the optic cables. Finally, the monitoring unit was mounted on the plasterboard close to the sensor installation point (figure 84).

Figure 80: Socket pipes produced in the laboratory
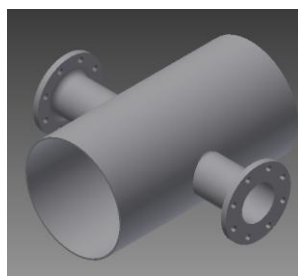
Figure 81: Configurations on the exhaust duct for SDM installation
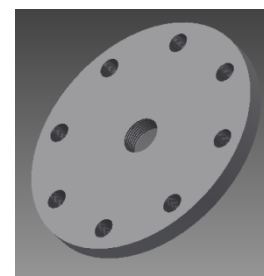
Figure 82: Sealing flanges

Figure 83: Inserting the pipe during alignment check

Figure 84: G1000 SDM installed on the system

The pressure sensors were provided with G ½'' B thread for process connection while the exhaust duct was equipped with G ½'' fittings. Although the pressure sensors could be directly connected to the duct fittings, the need for exhaust gas cooling due to the limited permissible temperature of the measuring media (100°C) dictated the use of fine (1/8'' diameter) inox tubes. Therefore, special adaptors for the connection of the inox tubes to the sensors and the exhaust duct had to be purchased. These adaptors, manufactured by the Parker Company, featured a 1/8'' special conical reception for the inox tubes and a ¼'' BSPP thread. For the connection of the 1/4'' BSPP thread to the G ½'' male thread of the sensors, special unions were produced in the laboratory with G 1/4'' female thread for connection with the Parker adaptors and G ½'' female thread for connection with the sensors (figure 85). In addition, in order to connect the Parker adaptors to the duct fittings, unions featuring a G ¼'' female thread and a G ½'' male thread were purchased. All the adaptors, unions and tubes of the sensors process connection are presented in table 4. The pressure sensors were mounted on a metal plate which was tied with special clamps on a rod positioned behind the filters (figure 86). According to the initial EBS design the rod was installed to enhance the mechanical strength of the system as well as to receive vertical dilatations. Finally, the inox tubes were cut at the desired length to connect each pair of Parker adaptors (sensor – fitting) after a sufficient number of spirals was considered to achieve exhaust gas cooling below the maximum permitted temperature.

Part No	Name	Description	#
1	Union	Union G 1/2'' F -/- G 1/4'' F	4
2	Parker Fitting	Parker adaptor G 1/4'' M -/- Conical 1/8'' M	8
3	Inox Tube	Inox tube 1/8''	4
4	Hexagonal Union	Union Hexagonal G 1/4'' F -/- G 1/2'' M	4

Table 4: Accessories list for pressure sensors process connection

Figure 85: Pressure sensor - union - Parker adaptor

Figure 86: Pressure sensors mounted on the plate

Figure 87: Pressure sensors process connection

The three new temperature sensors (RTDs) had 250 mm insertion length and G ½'' male thread for process connection. According to the EBS design, the pipe duct at the temperature sensors installation point had an external diameter of 219 mm (inner 200 mm) and G ½'' fittings 100 mm long. Therefore, the two temperature sensors, installed before the filters, (figure 88) were inserted almost in the middle of the pipe duct for ensuring more accurate measurements. The third temperature sensor was mounted on a central position of the exhaust duct before the EBS for measuring exhaust temperature, comparing it with the other temperature measurements (before the filters) and estimating the EBS heat inertia. For connecting the third RTD on the exhaust duct, an old G ½'' adaptor of the pipe duct was used.

Finally, near the third temperature sensor, another pressure sensor was installed, which would act as an alarm unit in case of overall system backpressure increase. This sensor (PTX 1400), made from Druck Company, was similar to the newly acquired pressure sensors (S-10), but it differed in the measuring range (0 – 6 bar absolute). It featured current output of 4-20mA and G ¼'' female thread for process connection. The sensor was installed in a similar way as the other pressure sensors (Parker adaptors – inox tubes) with the only difference that the sensor

could be directly connected to the Parker adaptor. The accessories for the PTX 1400 process connection were: 2 Parker adaptors (G ¼'' male thread to conical 1/8'' connection for tube), inox tube with a sufficient spirals number and 1 hexagonal union featuring G ¼'' female to G ½'' male thread. The third temperature sensor and the PTX 1400 pressure sensor, all mounted on the exhaust duct before the EBS, are presented in figure 89.
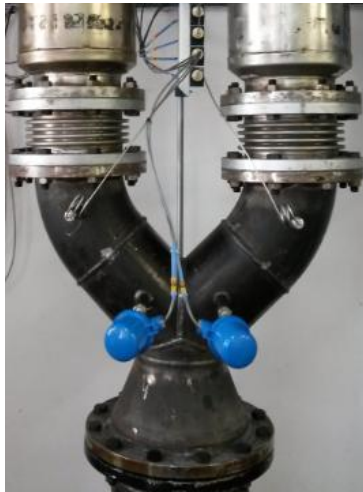
Figure 88: Temperature sensors installed before the filters

Figure 89: Temperature and pressure sensor mounted on exhaust duct before EBS

Finally, as far as the flow meter installation is concerned, no permanent instrument connection was considered. The flow measuring positions were two and the sensor would be alternately installed according to the desired measurement. The first position was on the old exhaust duct before the EBS, near the temperature and pressure sensor measuring positions. The flow meter would be installed via a G 1 ½'' fitting (as shown in figure 89) which imposed the need for a suitable adaptor since the sensor diameter was 1''. The laboratory, disposed such an adaptor as previous exhaust gas flow measurements had been obtained in this position. On the other hand, the second position was on the bypass duct of the EBS. The provided fitting was G 1 ¼'' and the adaptor, which the laboratory disposed, didn't fit. As a result, a new adaptor for connecting the flow meter to the pipe duct was produced. The adaptor featured a G 1/14'' hexagonal nipple (figure 90) in which a metallic barrel (figure 91) was inserted to provide 1'' fitting for the sensor. In case of sensor removal, a 1'' taper (figure 92) was made for process sealing. The barrel was constrained via a M5 blind screw, while the sensor – taper by a smaller M4 one. The adaptor with the taper mounted is presented in figure 93 while its design is

provided in appendix II page 151. For ensuring sufficient process sealing at all measuring positions on the exhaust duct, different copper washers were used according to the required size.
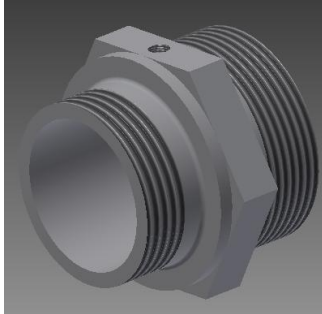
Figure 90: Hexagonal Nipple
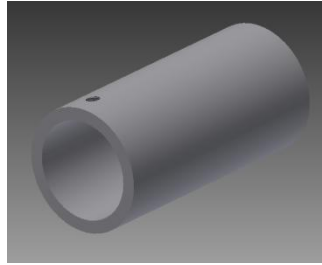
Figure 91: Barrel for providing 1'' fitting
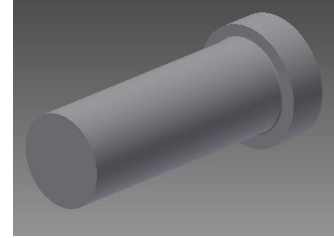
Figure 92: 1'' taper for process sealing

Figure 93: Flow meter adaptor for the second measuring position

4.4 Electrical Connections

For facilitating the instruments electrical connections, a metallic rail was mounted along the plasterboard behind the EBS (figure 94) in order to support the cables of the signals and the power supply. Then, two multi-channel (12 pairs each) Li YCY cables were installed (figure 95) in order to transfer the signals (room I.13) to the DAQ system which is placed in the engine room. Total system signals are presented in table 5.

Sensors							
Item	Instrument Tag	Signal Description	Signal Range	Sensor Type	Manufacturer	Physical range	Physical value unit
1	PT132	Exhaust Pressure, filter 1, outlet	4-20mA	Pressure Transmitter	WIKA	0 - 1	bar [g]
2	PT133	Exhaust Pressure, filter 2, outlet	4-20mA	Pressure Transmitter	WIKA	0 - 1	bar [g]
3	PT134	Exhaust Pressure, filter 1, inlet	4-20mA	Pressure Transmitter	WIKA	0 - 1	bar [g]
4	PT135	Exhaust Pressure, filter 2, inlet	4-20mA	Pressure Transmitter	WIKA	0 - 1	bar [g]
5	PT131	Exhaust Pressure, main	4-20mA	Pressure Transmitter	Druck	0 - 6	bar [a]
6	TT131	Exhaust Temperature, main	4-20mA	Pt100	WIKA	0 - 400	deg ^{o}C
7	TT134	Exhaust Temperature, filter 1, inlet	4-20mA	Pt100	WIKA	0 - 400	deg ^{o}C
8	TT135	Exhaust Temperature, filter 2, inlet	4-20mA	Pt100	WIKA	0 - 400	deg ^{o}C
9	FT131	Flow meter	4-20mA	Vane Wheel	Hontzsch	0.4-120	m/s
10	OPA131	Opacimeter	4-20mA	Opacity	Green Instruments	0-100%	N/A
11	ZT131	Valve 1 Position Feedback	4-20mA	Iy Module - Positioner	Siemens	0-100%	N/A
12	ZT132	Valve 2 Position Feedback	4-20mA	Iy Module - Positioner	Siemens	0-100%	N/A
Actuators							
Item	Instrument Tag	Signal Description	Signal Range	Actuator Type	Manufacturer	Physical range	Physical value unit
1	ZY131	Valve 1 Actuator	4-20mA	Electro-pneumatic	Siemens	0-100%	N/A
2	ZY132	Valve 2 Actuator	4-20mA	Electro-pneumatic	Siemens	0-100%	N/A

Table 5: List of sensors - actuators

For the sensors wiring Li YCY cables were used which consist of copper conductors insulated by PVC and twisted in pairs. These are separated by plastic from the tinned copper braid which is covered by PVC jacket. These cables are suitable for eliminating noise impact as long as the tinned copper braid is grounded.

65

All pressure and temperature sensors need 24 VDC power supply in order to be activated and provide 4 – 20mA output signal (passive signals). The flow meter also needs 24 VDC power supply but it provides an active 4-20mA signal. The opacity meter is powered by 220 VAC, providing 4-20mA active signal while the electro-pneumatic positioners need 4 -20mA input current of voltage less than 10 VDC for their operation. Finally, the positioners dispose the I_y module which needs 24 VDC power supply to provide the output signal (valve position feedback).

The signal cables were connected to terminals according to the signal type (active/passive) and the respective power supply. Then, the signals were led to the multi-channel cables (figure 96), also connected to terminals, in order to be transferred to the engine room. All terminal stations as well as the power supplies were mounted in an electrical panel (A1) which was installed in room I.13. The panel was based on two vertical beams (figure 97) since it couldn't be installed on the plasterboard because of its high weight. Its initial design is presented in appendix II page 152.

Figure 94: Metallic rail for wiring support
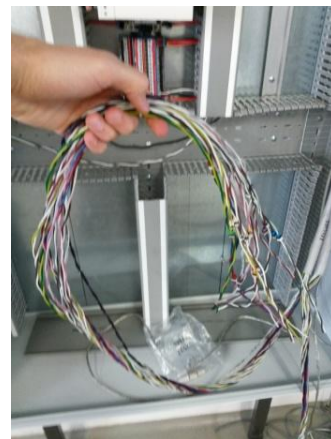
Figure 96: Multi-channel cables ready to be connected to terminals in panel A1

Figure 95: Multi-channel Li YCY cables

Figure 97: The panel as installed in room.13

After the panel installation (figure 98) and its full assembly (terminal stations, power supplies and internal cable connections) the multi channel cables were connected to the respective isolating amplifiers which were located in panel Y12-H14 in the engine room. This panel includes the Caterpillar 3176b engine controller since it contains all the necessary electrical connections and the DAQ system (DS1103). Then, the isolating amplifiers (signal converters), which were installed below the DAQ module in the panel, were connected to the DAQ system (figure 99) via Li YCY cables which featured BNC connectors at their ends. In table 6 the list of the installed isolating amplifiers is presented. For the opacity and the flow velocity signals Mini MCR-SL-I-U-4 isolator type could be used, but due to low-availability, the supplier provided only 10 isolators of this type. Therefore, for these signals the Mini MCR-SL-UI-UI-NC model was used. The isolating amplifiers were mounted on a vertical rail, which was installed in the panel, and they were bridged together for their power supply. Then, one of them was connected to a 24 VDC power supply located in the panel. Finally, all signals were given suitable tags in order to be easily distinguished from one another and all cables were marked for ensuring correct re-corrections in case of a sensor removal.

Isolating Amplifiers						
Item	Instrument Tag	Signal Description	Output Signal	Input Signal	Isolator Type	Manufacturer
1	OPA131	Opacity	0-10 VDC	4-20mA	Mini MCR-SL-UI-UI-NC	Phoenix Contact
2	FT131	Flow Velocity	0-10 VDC	4-20mA	Mini MCR-SL-UI-UI-NC	Phoenix Contact
3	PT131	Exhaust Pressure, main	0-10 VDC	4-20mA	Mini MCR-SL-I-U-4	Phoenix Contact
4	PT132	Exhaust Pressure, filter 1, outlet	0-10 VDC	4-20mA	Mini MCR-SL-I-U-4	Phoenix Contact
5	PT133	Exhaust Pressure, filter 2, outlet	0-10 VDC	4-20mA	Mini MCR-SL-I-U-4	Phoenix Contact
6	PT134	Exhaust Pressure, filter 1, inlet	0-10 VDC	4-20mA	Mini MCR-SL-I-U-4	Phoenix Contact
7	PT135	Exhaust Pressure, filter 2, inlet	0-10 VDC	4-20mA	Mini MCR-SL-I-U-4	Phoenix Contact
8	TT131	Exhaust temperature, main	0-10 VDC	4-20mA	Mini MCR-SL-I-U-4	Phoenix Contact
9	TT134	Exhaust temperature, filter 1, inlet	0-10 VDC	4-20mA	Mini MCR-SL-I-U-4	Phoenix Contact
10	TT135	Exhaust temperature, filter 2, inlet	0-10 VDC	4-20mA	Mini MCR-SL-I-U-4	Phoenix Contact
11	ZY131	Valve 1 Pneumatic Actuator	4-20mA	0-10 VDC	Mini MCR-SL-UI-UI-NC	Phoenix Contact
12	ZY132	Valve 2 Pneumatic Actuator	4-20mA	0-10 VDC	Mini MCR-SL-UI-UI-NC	Phoenix Contact
13	ZT131	Valve 1 Position Feedback	0-10 VDC	4-20mA	Mini MCR-SL-I-U-4	Phoenix Contact
14	ZT132	Valve 2 Position Feedback	0-10 VDC	4-20mA	Mini MCR-SL-I-U-4	Phoenix Contact

Table 6: List of installed isolating amplifiers in panel Y12-H14
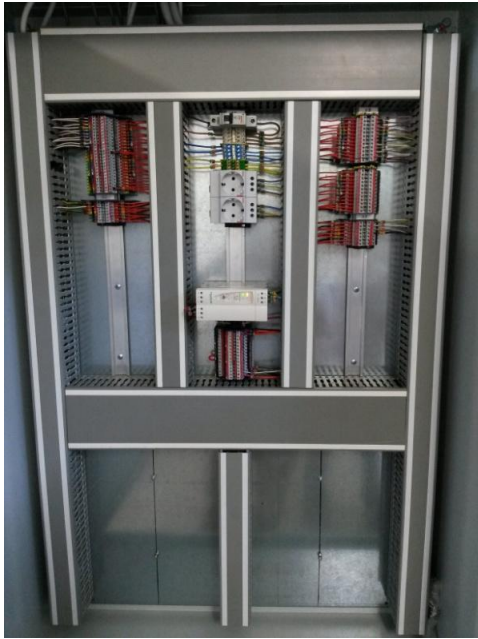
Figure 98: Electrical panel A1 installed in room I.13
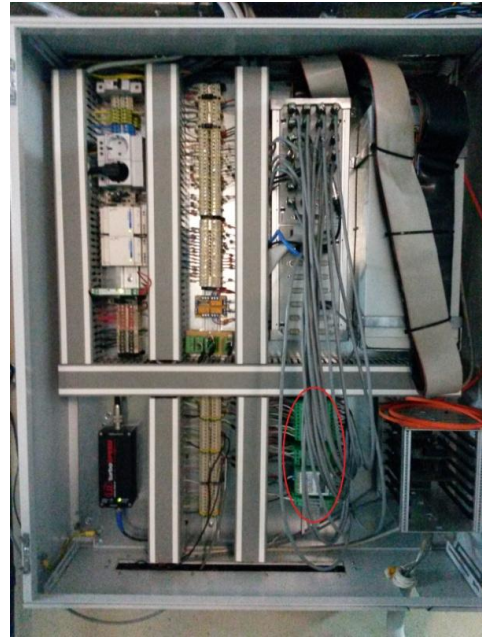
Figure 99: Electrical panel Y12-H14 with DAQ module and isolating amplifiers (red demarcation)

Before all electrical connections were installed, the necessary drawings were created to facilitate the tasks and ensure that possible mistakes that could lead to serious problems (short-circuits) would be avoided. In figure 100 the electrical connections of the electro-pneumatic positioner of the butterfly valve 1 is presented. The ZY-131 is an actuator signal for the valve operation. An opening – closing command is given by the controller which corresponds to an output voltage signal (0-10 V), that is transmitted to the respective isolating amplifier for conversion to electrical current of 4-20mA. The electrical current is transferred to terminal station –X9 of the panel A1 and then via internal connections to terminal station –X2 from which it is transmitted to the channels 6, 7 of the positioner and activates the valve operation. On the other hand, the ZT-131 is a sensor signal for providing valve position feedback. The 4-20mA signal is powered by 24 V supply and it is transferred from the positioner channels 61, 62 to terminal station –X1 (passive signals) of the panel A1. Then, it is transmitted from terminal station –X8 via the multi-channel cables to the respective isolating amplifier for conversion to 0 - 10 V. Finally, the voltage signal is sampled by the DAQ system via an analogue input port. In figure 101 the wiring design of the EBS for the Caterpillar 3176b engine is presented. NY and PY are the engine rpm and brake actuator signals, respectively, and FE is a sensor signal for the achieved brake torque. The electrical drawings for the connections of every sensor and device of the EBS, as well as the overall wiring design of the system signals (sensors – actuators) for both engines are provided in appendix II pages 153 - 166.
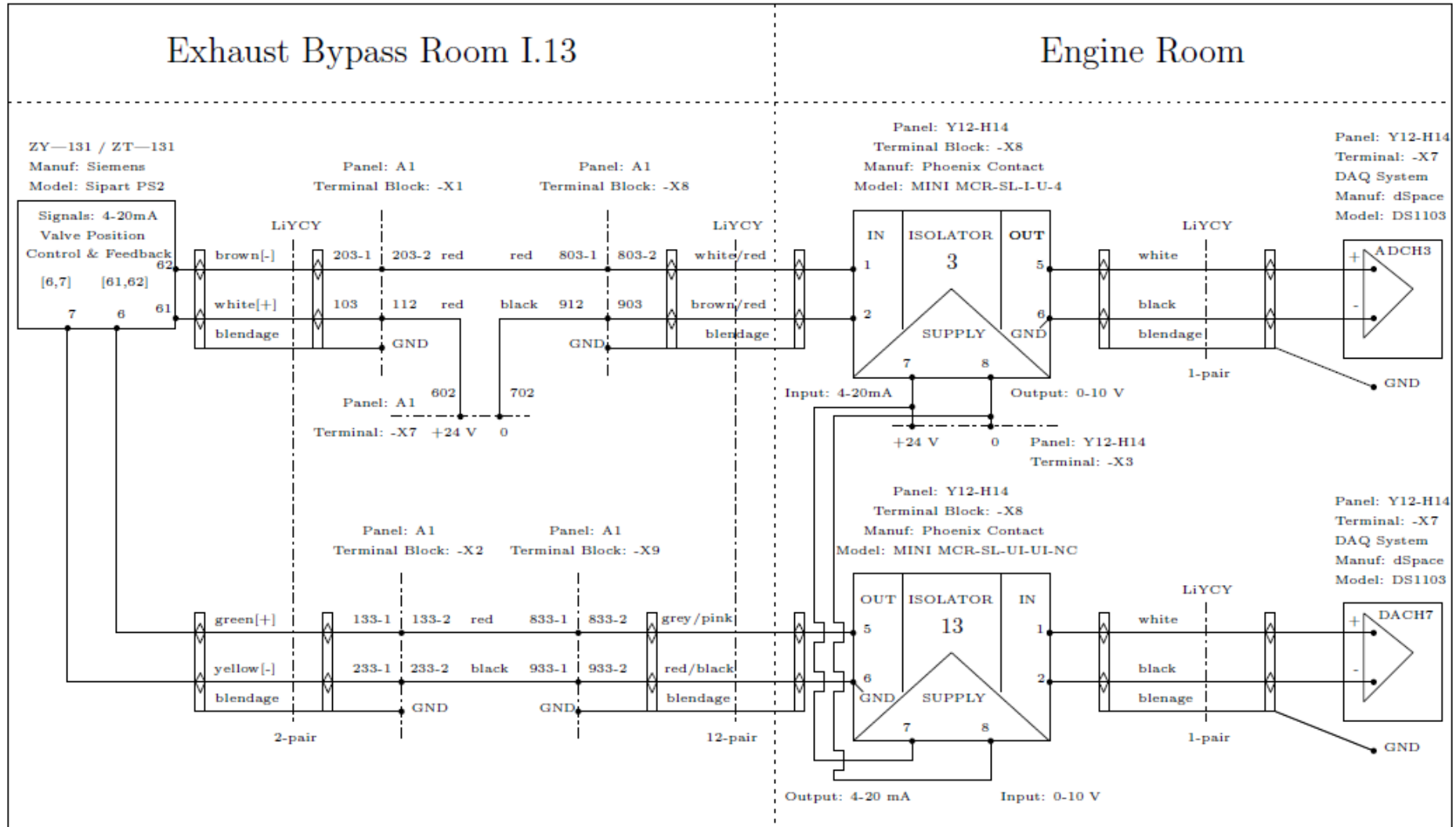
Figure 100: Electrical connection of butterfly valve positioner 1
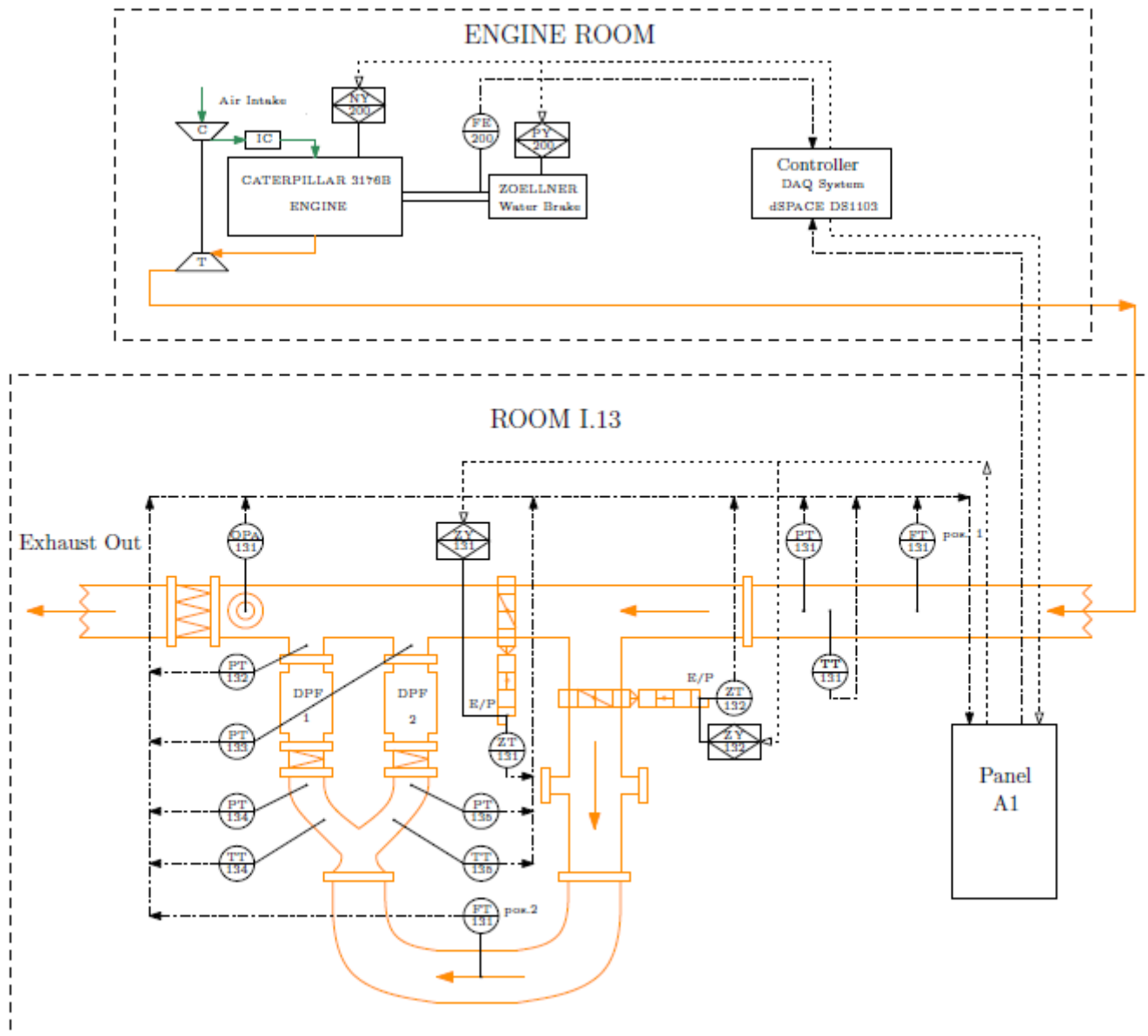
Figure 101: Wiring Design of the EBS for the Caterpillar 3176b engine

4.5 Additional Tasks

The full assembly of the EBS also included the installation of an air supply subsystem and the pipe duct insulation. The first task was carried out before the sensors mounting as it was necessary for the pneumatic actuators operation (need of at least 5.5 bar air supply). Moreover, the purge air system of the G1000 SDM needed air supply of 1 -2 bar for securing the lenses from fouling. The second task comprised the pipe duct insulation which was installed for avoiding increased heat radiation.

4.5.1   Air Supply Subsystem Installation

The installed low-pressure air supply subsystem included an air supply source, copper tubes, a station for air distribution (pneumatic actuators – SDM) and elastic air hoses. For the SDM purge air supply, an air supply filter regulator was indispensable for ensuring sufficient pressure drop, evening out pressure variations as well as withholding impurities. The air supply source already existed in room I.13 and it provided air of 7 bar from an receiver of the laboratory. The air supply source was connected to copper tubes (figure 102) which led to an air distributor located on a station (small, non-metallic, rectangular plate) which was mounted on the plasterboard close to both butterfly valves and SDM measuring position 1. Apart from the air distributor, the station also featured an air supply filter regulator, a flow meter and a second air distributor for securing sufficient air supply to both lenses of the opacity sensor (figure 103). All the necessary connections after the first air distributor was realised via elastic air hoses. The station was designed in such a way that it could be easily removed and re-installed in case of SDM removal.

Figure 102: Air supply subsystem (air supply source in the left)

Figure 103: Station featuring air distributors, air supply filter regulator, flow meter and elastic air hoses

4.5.2 Pipe Duct Insulation Installation

After the sensors mounting had been completed, some preliminary tests were conducted in order to verify the entire system functionality. Next and last step was the placement of insulation on the exhaust bypass duct. The work was carried out in three days by Loukis industry (the same industry that constructed the bypass pipeline) and included placement of the main insulation – stone wool and the protective outer aluminium sheet (figures 104 and 105). The stone wool is a fibrous insulating material used in technical applications and consists of silica – aluminium fibres. It has excellent thermal and sound insulation properties and can withstand temperatures of 700 – 850 $^{\circ}$C. However, particular attention should be paid when handling this material because it may cause irritation to the skin, the eyes and the respiratory system (53). For the outer sheath of the insulation, aluminium foil was used because of its ability to retain gloss for a long time period after its placement. During the installation of insulation, all sensors were removed in order to be protected and were re-installed in their positions after the completion of the work. However, due to the increased thickness of the insulation (approximately 6 -7 cm), the pressure fittings had to be lengthened so that they could remain accessible. The final form of the exhaust bypass system is demonstrated in figure 106. In addition, a draft of the room I.13 front view is provided in appendix II page 167.

Figure 104: Installation of the exhaust pipeline insulation

Figure 105: Placement of the insulation outer sheath (aluminium foil)

Figure 106: Final form of exhaust bypass system

Chapter 5: Opacity Measurements Onboard

5.1 Introduction

As part of the research project SEKTE which also included the EBS installation and experimentation, measurements, regarding engine emissions and operating parameters, were obtained onboard a high speed vessel. These measurements were realised to serve as a reference for the subsequent project. Moreover, in combination with corresponding measurements in the experimental engine test-bed, they could contribute to estimating the effectiveness of the smoke reduction system as well as the possibilities of such a system being permanently installed on a ship. The onboard measurements were conducted during a typical route of the ship in Greek islands and comprised readings of several major parameters of the engine operation (impeller torque – speed, fuel consumption, in-cylinder pressure, emissions and opacity). However, in the context of this thesis only the opacity and engine power (for explaining the opacity behaviour) measurements are presented.

5.2 Ship Specifications

The onboard measurements were realised on the Speedrunner 3 high speed vessel (figure 107) owned by Aegean Speed Lines (ASL). The ship disposes 4 Ruston 20RK 270MK II medium speed engines (figure 108) coupled to 4 KaMeWa 112F11 water jets for its propulsion. The ship and engine technical specifications are provided in table 7 and 8 respectively.

Figure 107: ASL Speedrunner 3

Ship Type	High Speed Vessel
Deadweight	340 [t]
Speed	34 [knots]
Length	100.4 [m]
Breadth	17.00 [m]
Depth	10.70 [m]
Drought	4.60 [m]
Pax Capacity	800
Garage Capacity	170 cars or 145 cars plus 6 buses

Table 7: Speedrunner 3 specifications

Engine Type	Turbocharged Diesel Engine
Operation Cycle	4-X
Cylinders Number	20
Engine Configuration	V
Volume	20 x 17.5 [lt]
Diameter	270 [mm]
Stroke	305 [mm]
Compression ratio	12.3 : 1
Turbocharger pressure	3.5 [bar]
Maximum Power	6875 [kW] at 1000 [rpm]

Table 8: Ruston 20RK 270MK II
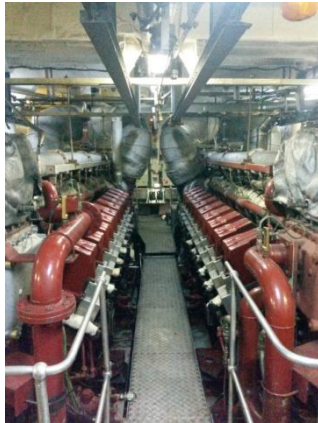
(a)

(b)

Figure 108: Ruston 20RK 270MK II

The equipment was deployed in the fore engine room and the measurements were collected on one of the four identical engines of the ship (specifically from the second main propulsion engine). For the opacity readings, the G1000 SDM was mounted on the exhaust duct of the engine after it had been removed from the EBS. Moreover, strain gauges and an inductive proximity sensor were placed on the impeller, for obtaining torque and speed measurements. By multiplying the measured torque and speed values, the impeller power is calculated. The impeller is the shaft that is located after the clutch and drives the coupled water jet. In figure 109 the top view of the ship engine room is provided.
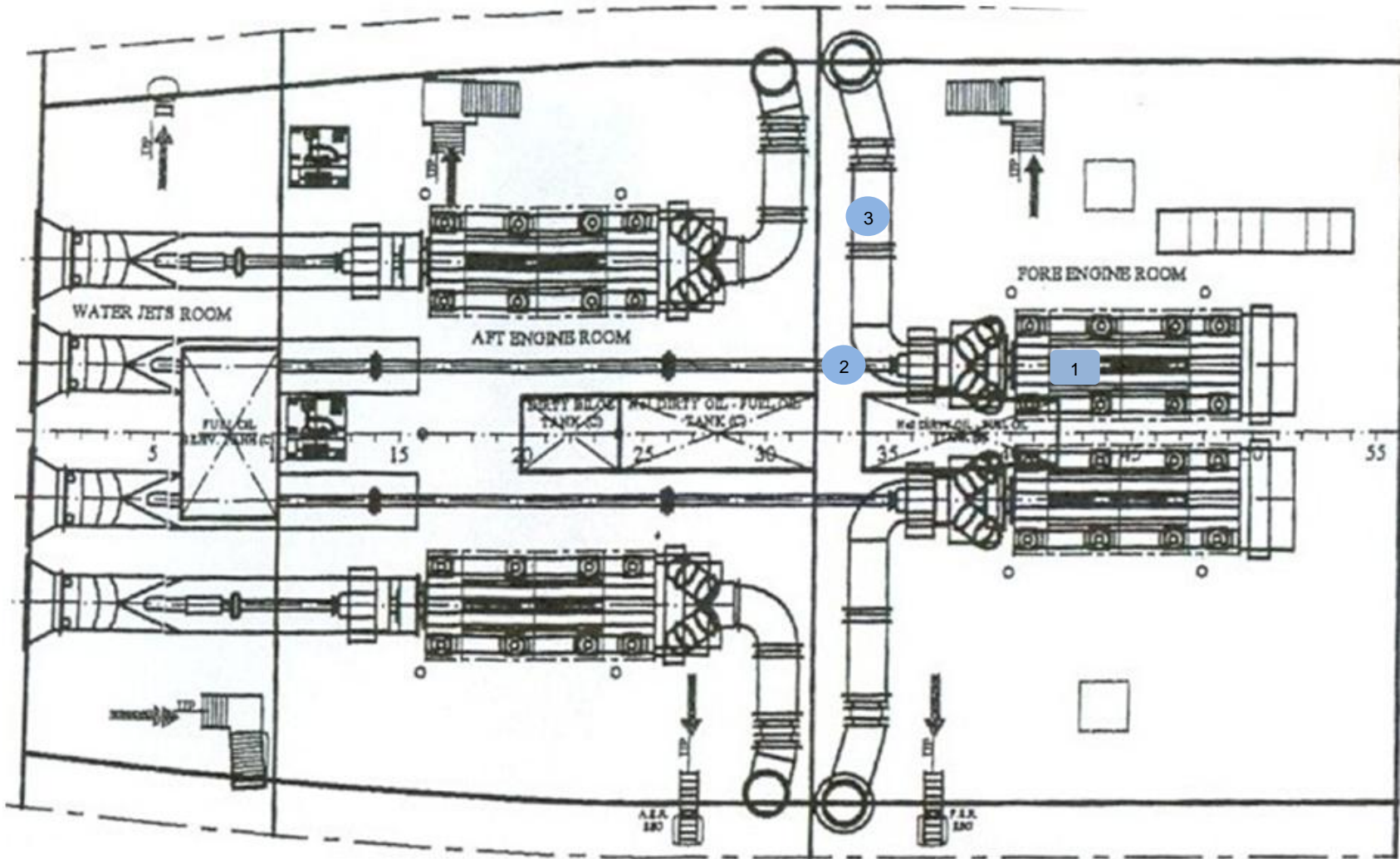
Figure 109: Top view of the ship engine room where the second main engine [1], the impeller [2] and the exhaust duct [3] are presented

5.3 Equipment Installation

The G1000 SDM was installed on the exhaust duct of the second main propulsion engine of the ship. During the last ship dry-docking (March 2014), ASL made some modifications for enabling the onboard measurements. As far as the opacimeter is concerned, two holes were opened on the exhaust duct in order to receive the sensor. The two welding sockets provided by Green Instruments were delivered to ASL and were installed on the pipe duct. In order to ensure perfect alignment, a guiding pipe (figure 110) was used during sockets welding.

The sensors installation was scheduled two days before the ship trip and lasted a few hours. The opacity sensor was mounted on the pre-installed welding sockets on the exhaust duct. Then, the monitoring unit was tied with ropes close to the optic heads in order to secure the optic cables. In addition, the purge air supply station was removed from room I.13 and placed in the ship close to the optic heads of the opacity sensor (figure 111). The station was connected via air hoses to the low-pressure air supply system of the ship. Finally, all the necessary electrical connections were made which included the sensor power supply (220 VAC) and output signal (4-20mA). In figure 112 the G1000 SDM as installed on the ship pipe duct is presented.

For measuring the impeller torque, a strain gauge was installed on the shaft after the clutch. The strain gauge was connected to a signal transmitter which transfers the signal via wireless connection to a receiver. Then, the receiver converts and transmits the analogue signal (4-20mA) to the portable DAQ system of the laboratory. Moreover, an inductive proximity sensor was installed in order to measure the impeller speed. The sensor was connected to a signal converter responsible for transforming the measured pulses to analogue signal (4-20mA) and transmitting it to the portable DAQ system. Both torque and speed sensors, as installed on the impeller, are presented in figure 113.

The portable DAQ system of LME (figure 114) disposes signal conversion modules (made by National Instruments) which receive and record data in the form of 4-20mA analogue signals. For the signals recording - presentation a software was developed on the NI LabView platform. The DAQ system was placed close to the sensors in order to avoid high cable lengths in the engine room.

Figure 110: Guiding pipe for ensuring welding sockets alignment

Figure 112: G1000 SDM installed on exhaust pipe duct

Figure 111: Purge air supply station placed in the ship

Figure 113: Torque and speed sensors installed on impeller

Figure 114: Portable DAQ system

5.4 Measurements Analysis

The measurements were performed during a typical ship route scheduled on 06/06/2014. The ship itinerary (figure 115) included departure from the port of Piraeus at 16:30 pm, arrival at the port of Serifos at 19:00 pm, departure at 19:10 pm for the port of Sifnos (arrival at 19:35) and then departure at 19:45 pm for the port of Milos (arrival 20:45 pm). Finally, the ship departed from the port of Milos at 21:00 pm and arrived at Piraeus in midnight.
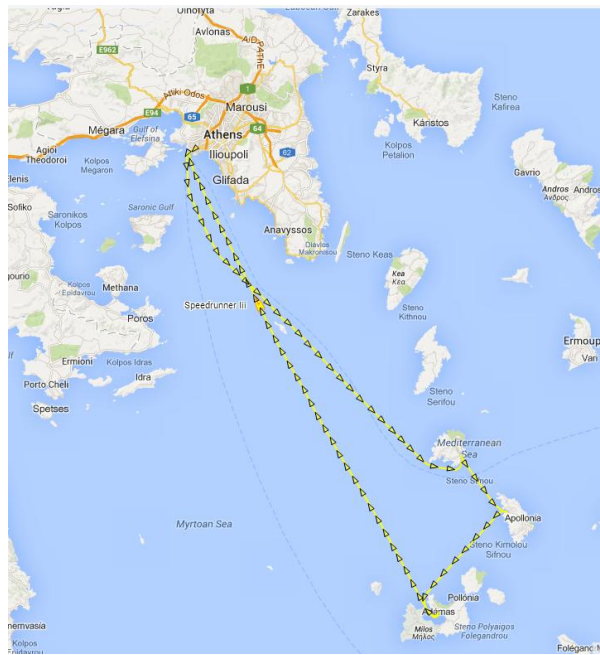
Figure 115: Speedrunner 3 scheduled route (Piraeus -> Serifos -> Sifnos -> Milos -> Piraeus)

The data acquisition started at 16:30 pm and lasted throughout the whole trip including time periods of ship manoeuvring in island ports. In addition, data recording continued even during engine clutch off at the port of Milos. So the acquired measurements provided an overall profile of the engine performance throughout the whole ship itinerary. In figure 117 the opacity measurements are presented which correspond to the impeller power measurements[15] provided in figure 118. The opacity percentage corresponds to the measuring range of the G1000 SDM.

The general trend is that opacity is kept at relatively low levels especially during engine operation at steady state conditions. However, three major overshoots (80 − 100%) are observed which correspond to extreme engine load increase such as engine start-up and clutch

---

[15] Power was calculated as a product of the measured impeller torque and speed ($P = T \times \omega$).

on at the port of Piraeus and the second clutch on at the port of Milos. Moreover, overshoots of 40 – 50% can also be observed which are directly correlated to the engine's load increase after the ship departure from the islands ports. Furthermore, some smaller overshoots (30 - 40%) can be distinguished which are related to engine transient loadings during ship manoeuvring in the islands ports. The opacity overshoots last only a couple of minutes but they are prominent due to the bright background and the sensitive environment of the island ports.

In general, it is easily inferred that least opacity can be achieved when diesel engine operates at MCR (Maximum Continuous Rating). In this steady state condition, the combustion is almost perfect and the emissions are reduced to the lowest level. During full load departure of Speedrunner 3 (engine operating at 96% of MCR) opacity is kept at very low levels (below 5%). Moreover, when the engine operates in steady state conditions at reduced loads (80% of MCR) during the return trip[16], the opacity is increased but it is still kept at reasonable levels (about 15%). However, when the engine operates in transient loadings during ship manoeuvrings, opacity increases further which is a direct result of low-quality (incomplete) combustion.

The exhaust bypass system targets almost exclusively the opacity overshoots met during steep increases of the engine's load. These represent a very small profile in the overall opacity measurements but their intensity and duration (approximately a couple of minutes), pose serious challenges. In figures 116 and 119, photos of the Speedrunner 3 funnel during ship departure from the ports of Piraeus and Sifnos are provided, which demonstrate the increased smoke emission during the engine load increase.

Figure 116: Photos of the Speedrunner 3 funnel during ship departure from Piraeus port

---

[16] During the return trip, the ship is almost empty, so the resistance is less; hence the impeller power requirement is reduced.
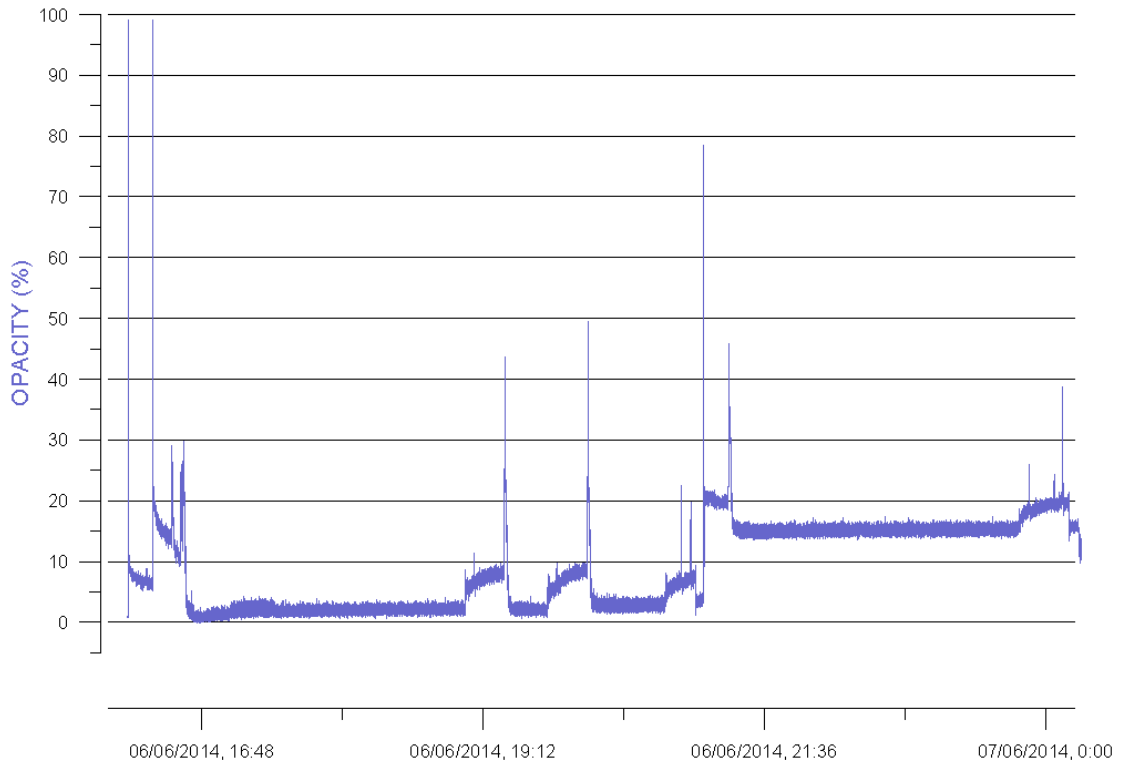
Figure 117: Opacity measurements onboard
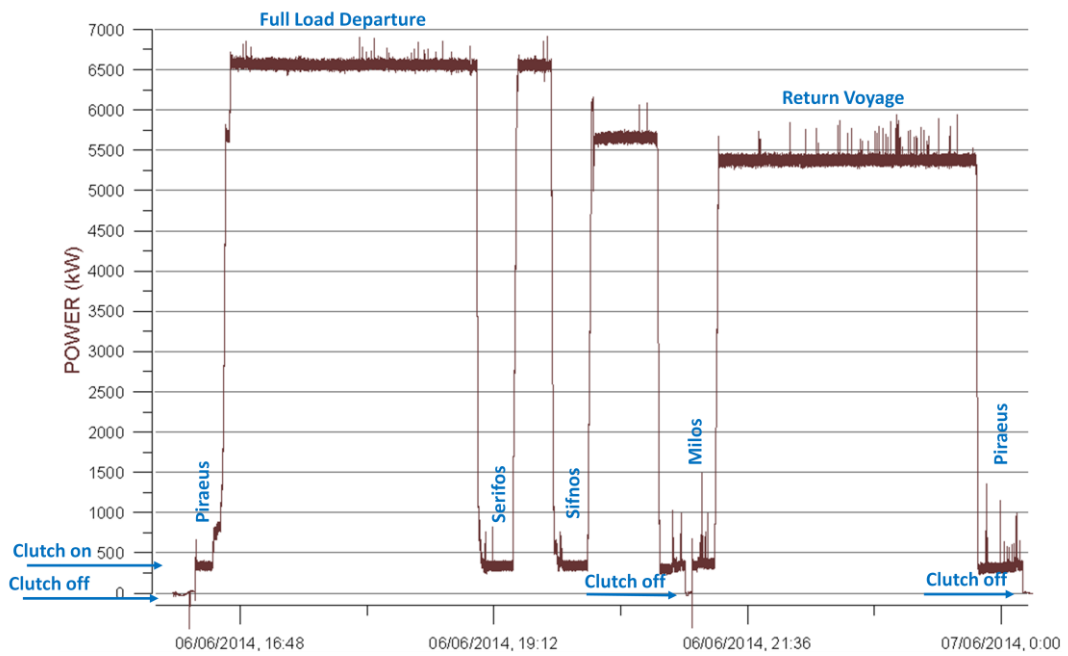
Figure 118: Impeller power measurements

(a) 0-20s

(d) 40 - 50s

(g) 85 – 95s

(b) 20 – 30s

(e) 50 – 60s

(h) 95 – 105s
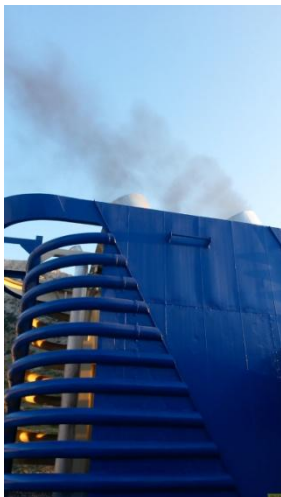
(c) 30 – 40s

(f) 60 – 85s

Figure 119: Photos of the Speedrunner 3 funnel during ship departure from the port of Sifnos (0s)

5.5 Conclusion

The opacity measurements onboard didn't' provide any unexpected result. Smoke emission is negligible (even 0% opacity) when the engine operates close to MCR since combustion is almost perfect. At lower engine loads, the quality of the combustion stars to deteriorate and the result is increased smoke emission which, however, is still considered low (opacity below 15%). The biggest challenge is during rapid - steep increase of the engine load which ''shocks'' the engine operation and as result adversely affects the combustion in the cylinders. Despite the small duration of this phase (a couple of minutes at most) smoke emission is prominent due to its high intensity. In this case, opacity reaches higher values (above 40%) and the smoke is visible even at a long distance from the ship funnel. Therefore, a smoke emission reduction method should be considered for ensuring low opacity levels. Finally, the opacity measurements demonstrated increased opacity values (close to 25%) during ship manoeuvring in the islands, which does not pose great challenges, at least as long as it remains at these reasonable levels.

The exhaust bypass system could provide solution in case of high smoke emission, since it could enable the PM collection during the periods of steep engine loading. In addition, during engine steady state operation, the system could be deactivated for avoiding early filter clogging. Moreover, the short period of the PM collection could lead to smaller DPFs, which is vital due to the limited space found on this type of ships.

The onboard opacity measurements could prove very valuable also for determining the EBS input activation signal. For instance, measuring exhaust gas opacity for activating the EBS could lead to increased signal delay, hence increased smoke emission before the EBS activation. Considering the high correlation between engine loading profile and smoke emission, increased slope of the engine loading profile could be used as activation signal for the EBS. Steep increase of the engine load would be recognised and the EBS would be activated for capturing the produced PM before its emission to the atmosphere. This method would decrease EBS activation delay and could lead to system efficiency increase.

Finally, the measurements performed onboard could serve as reference for the opacity measurements conducted in the laboratory and could provide real-time numerical indication of the exhaust gas opacity met in marine applications.

Chapter 6: Experiments with Exhaust Bypass System

6.1 Preparation for the Experiments

After the EBS full installation and the conduction of the onboard opacity measurements, the preparation for the experiments with the new system was initiated. At first, the newly installed signals and commands were incorporated in the Caterpillar 3176b control panel. Except for the standard signals of the EBS, which were described in section 3, three new signals had to be considered in order to facilitate the assessment of the system operation. The first one was the engine speed, as measured on the engine crankshaft, the second was the achieved torque load as measured on the shaft of the hydraulic break and, finally, the third was a temperature signal close to the engine exhaust. Both engine speed and break load signals, which had already been integrated in the engine control panel (DS1103), were processed by special low-band filters for eliminating high-frequency noise. Moreover, the engine control panel featured the necessary command signals for determining the engine-break operation. These were the engine speed and the torque load command signals (figure 120). All sensor and command signals of the caterpillar 3176b engine control panel (DS1103) are presented in figure 121.
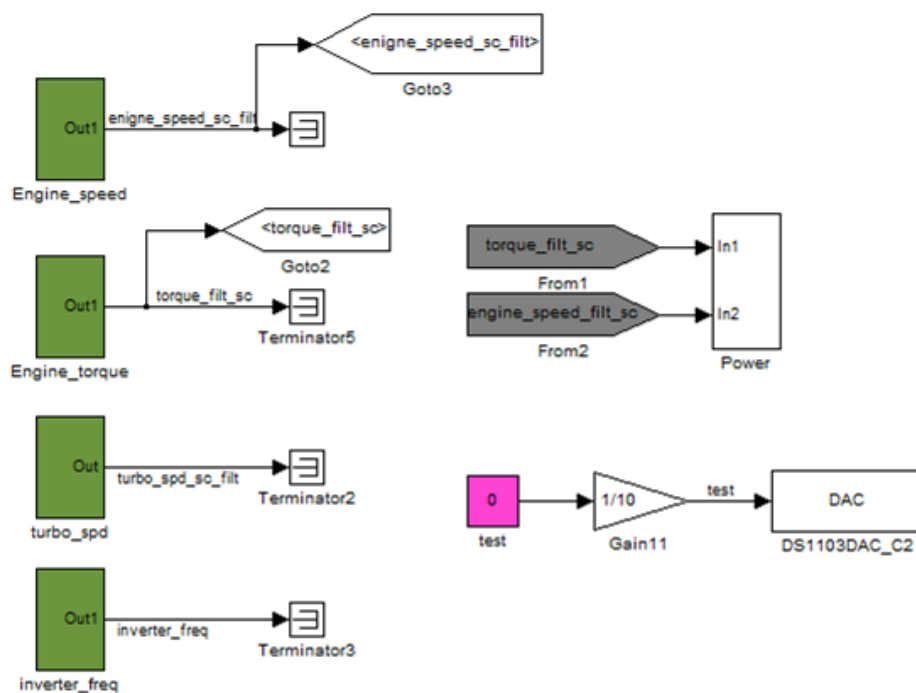
Figure 120: Command and sensor signals for the engine-break operation
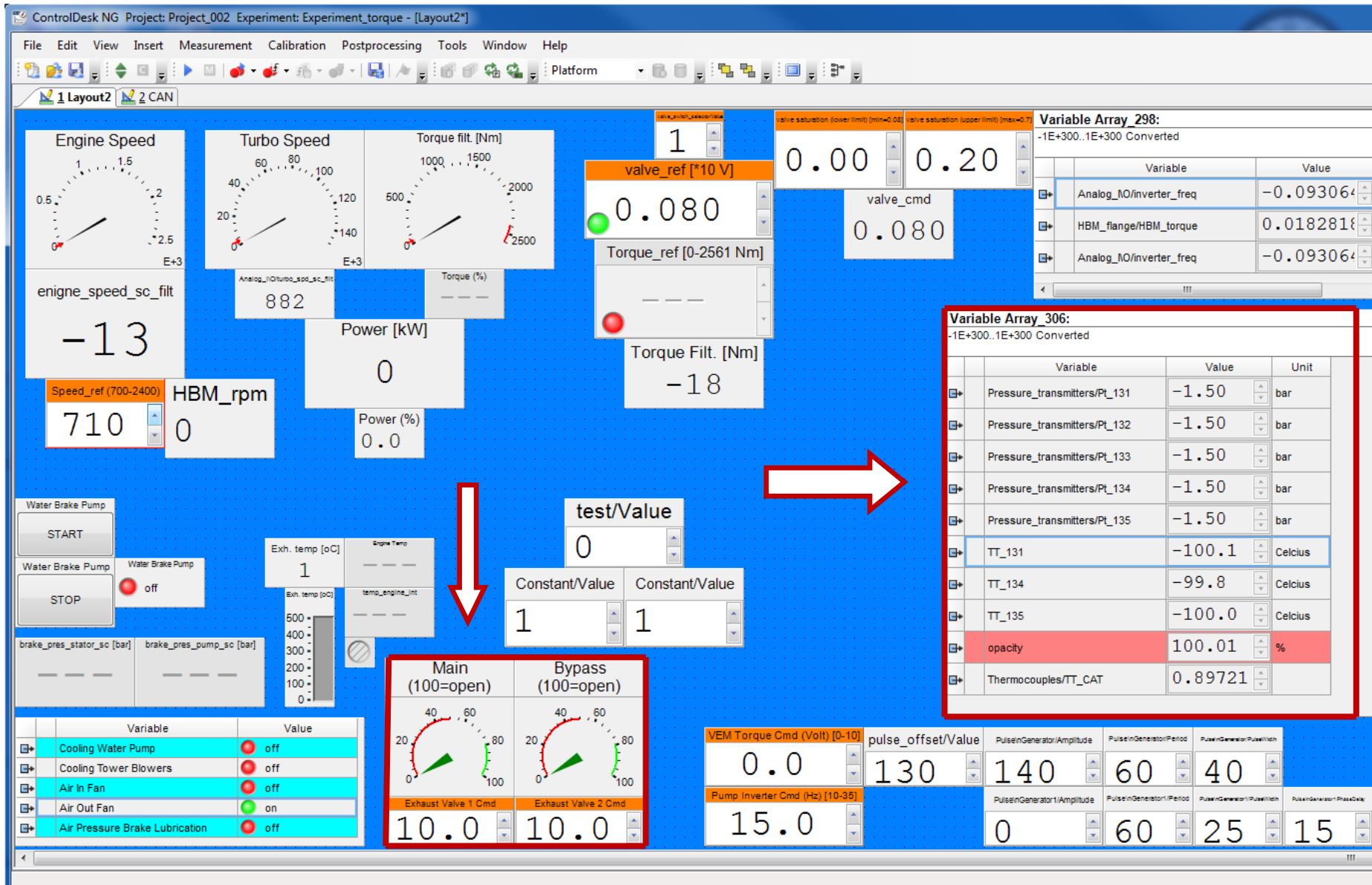
Figure 121: Caterpillar 3176b control panel with newly installed signals and commands (shown by the arrows)

For the data acquisition, a suitable program was developed on the Matlab/Simulink platform for enabling the analogue input signals recording and for providing the necessary interface between computer and DAQ hardware. The DS1103 analogue input and output channels were modelled as data acquisition blocks in Simulink. Each analogue input channel (sensor signal) was connected to the respective data recording – ''sink'' block while the analogue output signals were connected to suitable ''source'' block according to the output signal form. Finally, the transfer functions were also modelled in Simulink as ''Gain'' blocks, which were interposed between the DAQ and ''source'' – ''sink'' blocks. The latter were represented by the ''To File'' block which recorded the collected data in the form of .mat files for enabling their processing in Matlab. All EBS sensor and command signals as modelled in Simulink are provided in figure 122.

The transfer function of each signal, which was calculated based on the measuring span of the sensor and the respective signal range, is presented in table 9. FT131, which is the signal of the flow velocity, is not included in the table since it was not installed for the experiments.

Signal	Measuring range	Signal	Transfer Function
PT131	0 - 6 [bara]	$0 - 10$ [V]	$[bar] = 0.6 \cdot [V]$
PT132	$0 - 1$ [barg]	$0 - 10$ [V]	$[bar] = 1.012 + 0.1 \cdot [V]$
PT133	$0 - 1$ [barg]	$0 - 10$ [V]	$[bar] = 1.012 + 0.1 \cdot [V]$
PT134	$0 - 1$ [barg]	$0 - 10$ [V]	$[bar] = 1.012 + 0.1 \cdot [V]$
PT135	$0 - 1$ [barg]	$0 - 10$ [V]	$[bar] = 1.012 + 0.1 \cdot [V]$
TT131	$0 - 400$ [^{o}C]	$0 - 10$ [V]	$[C] = 40 \cdot [V]$
TT134	$0 - 400$ [^{o}C]	$0 - 10$ [V]	$[C] = 40 \cdot [V]$
TT135	$0 - 400$ [^{o}C]	$0 - 10$ [V]	$[C] = 40 \cdot [V]$
OPA131	$0 - 100$ [%]	10 - 0 [V]	$[\%] = 100 - 10 \cdot [V]$
ZY131	$0 - 100$ [%]	$0 - 10$ [V]	$[V] = 0.1 \cdot [\%]$
ZT131	$0 - 100$ [%]	$0 - 10$ [V]	$[V] = 0.1 \cdot [\%]$
ZY132	$0 - 100$ [%]	$0 - 10$ [V]	$[\%] = 10 \cdot [V]$
ZT132	$0 - 100$ [%]	$0 - 10$ [V]	$[\%] = 10 \cdot [V]$

Table 9: Transfer functions of EBS signals
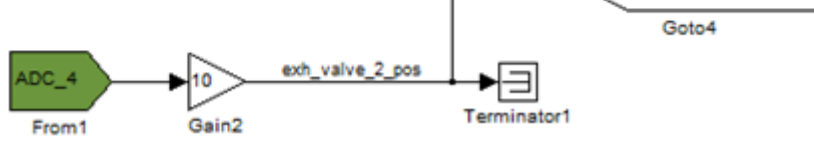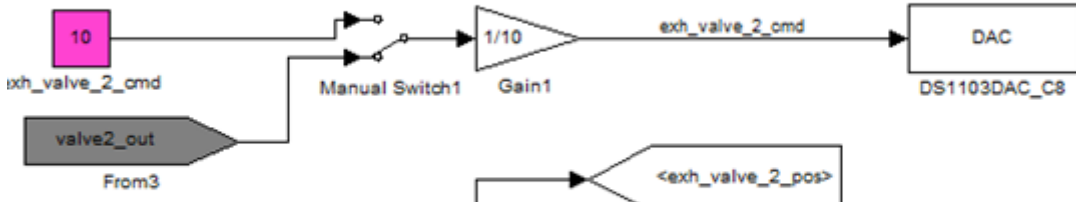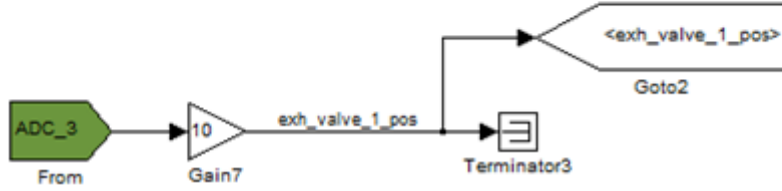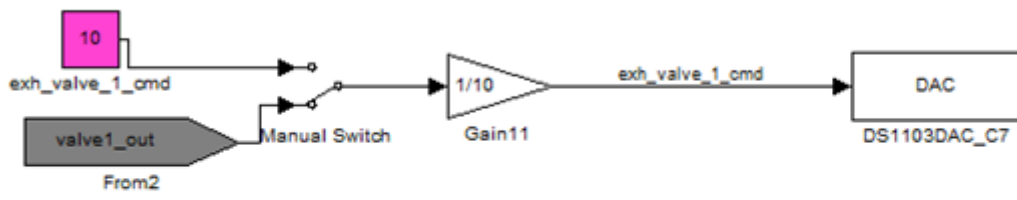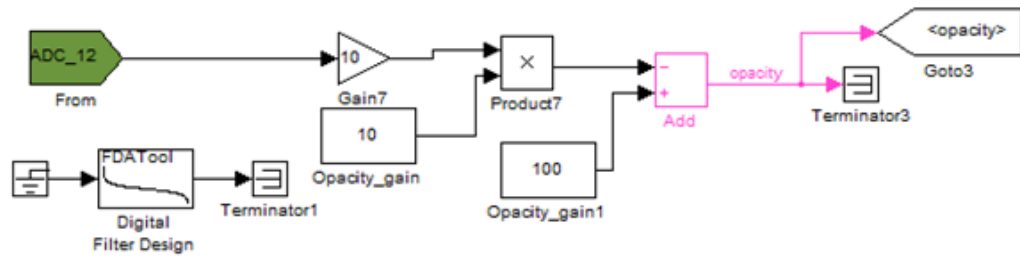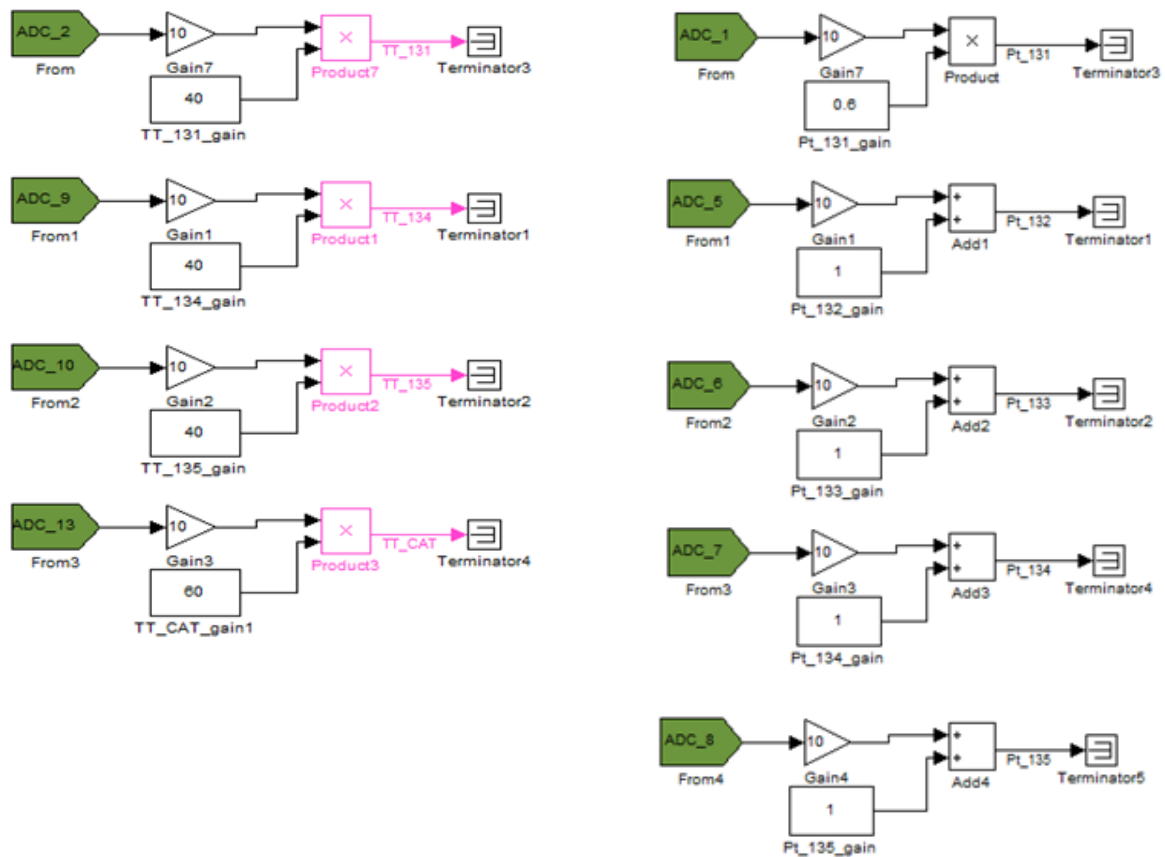
Figure 122: EBS sensor and command signals as modelled in Simulink

The first experiments of the EBS were performed with the Caterpillar 3176b engine and included engine loading at constant speed and manual handling of the valves according to the opacity values. As a result a first estimation concerning the EBS operation could be derived. Moreover, proper operation of all sensors and actuators could be verified before developing more complex EBS control systems. The sample time was defined as 1000 samples per second and it was maintained throughout all experiments.

After the first experiments, a first approach of closed-loop control of EBS was developed on the Stateflow environment of Matlab. This platform enables modelling and simulating combinatorial and sequential decision logic based on state machines and flow charts (54). The flow chart, which was developed for the EBS control, is presented in figure 123.
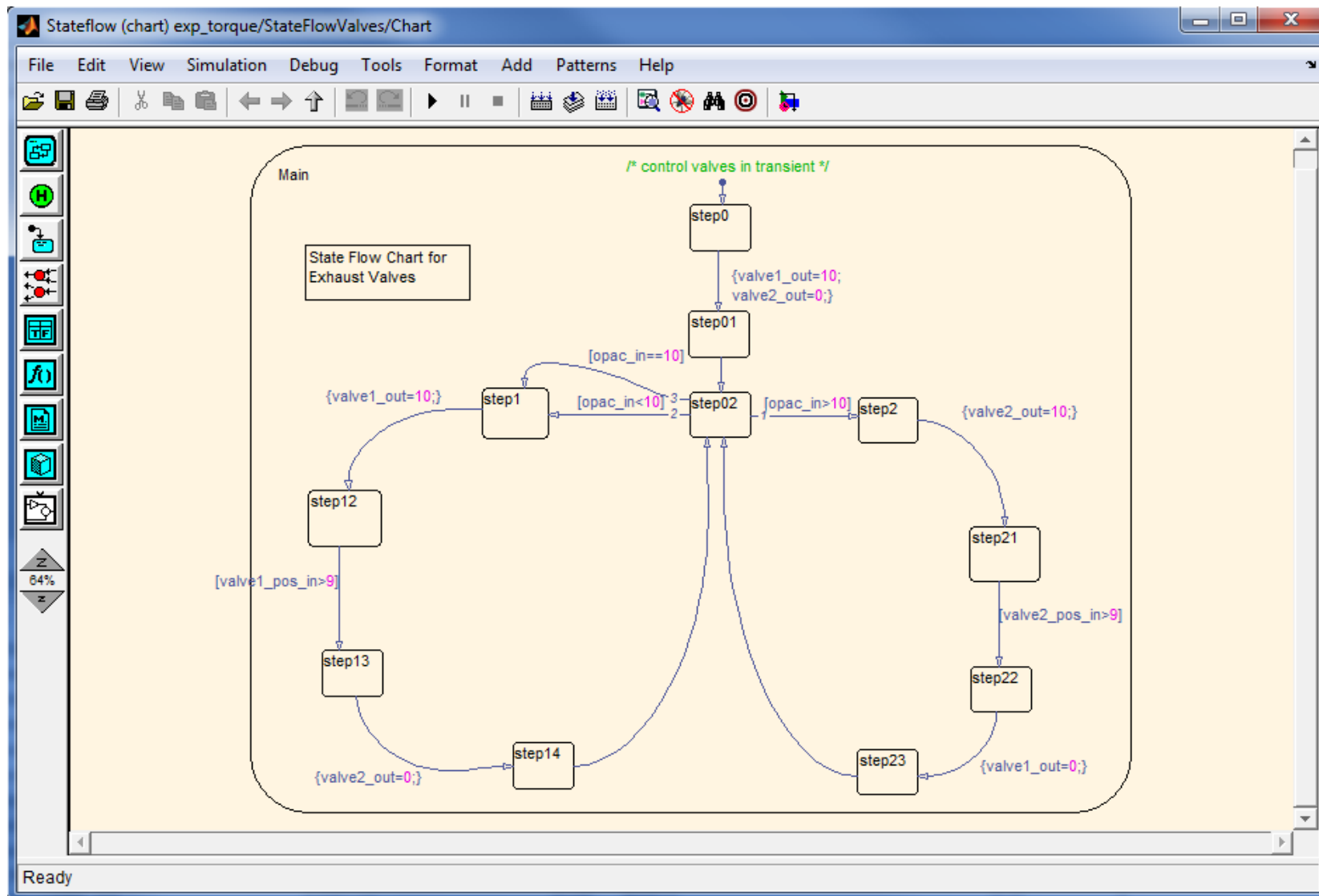
Figure 123: Stateflow chart as developed for EBS control

At first the system confirms proper initial positioning of the exhaust valves[17]. Then, the opacity signal is controlled and according to its value the EBS activation is decided. If opacity exceeds 10% valve 2 (bypass) is opened. After a 90% (at least) opening of valve 2 is verified, valve 1 is fully closed and exhaust gas is being filtered. This loop is continuous as long as opacity is kept above 10%. If the opacity signal is below or equal to 10%, valve 1 is opened (or remains open) and valve 2 is closed (or is kept closed). The loop is, finally, completed by controlling the opacity signal again.

The Stateflow chart was modelled in Simulink and connected to the necessary I/O signals of the DAQ blocks (figure 124). Then, the experiments were conducted with sample time defined as 1000 samples per second.
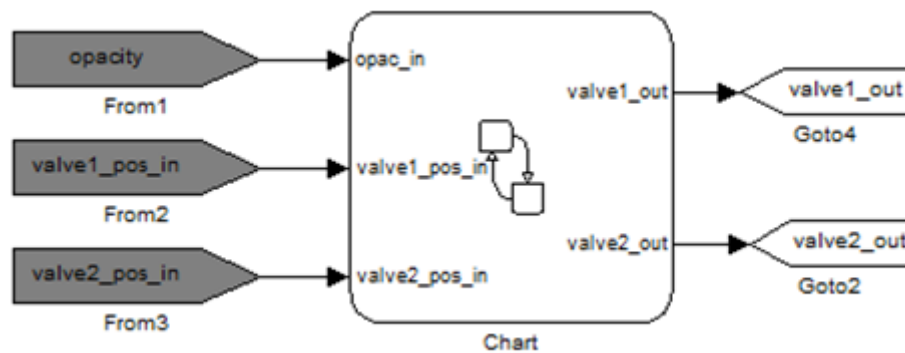
Figure 124: Stateflow block connected to the respective signal blocks in Simulink

Finally, due to the need for testing the EBS with higher engine loading, experiments with the MAN B&W Holeby L16/24 engine were performed. The EBS was activated before the engine loading in order to investigate the DPFs performance with high opacity exhaust gas. Moreover, the overall backpressure developed due to the EBS, as well as the pressure drop across the filters could be measured and assessed. Unfortunately, the engine-break operation was determined by a separate controller (Woodward Atlas) and because of the fact that junction box was not installed simultaneous torque and engine speed measurements were not available. However, the engine operated at nominal speed (1200 rpm) and the engine was loaded at 30% (1194 Nm) of MCR (500 kW). The sample time was maintained at 1000 samples per second.

---

[17] Valve 1 is the exhaust valve located on the main exhaust duct, while valve 2 is the exhaust valve located on the bypass part of the exhaust duct. With the first valve open and the second closed, all exhaust gas is emitted unfiltered.

6.2 Results Analysis

6.2.1 Caterpillar 3176B, Valves: Manual Handling
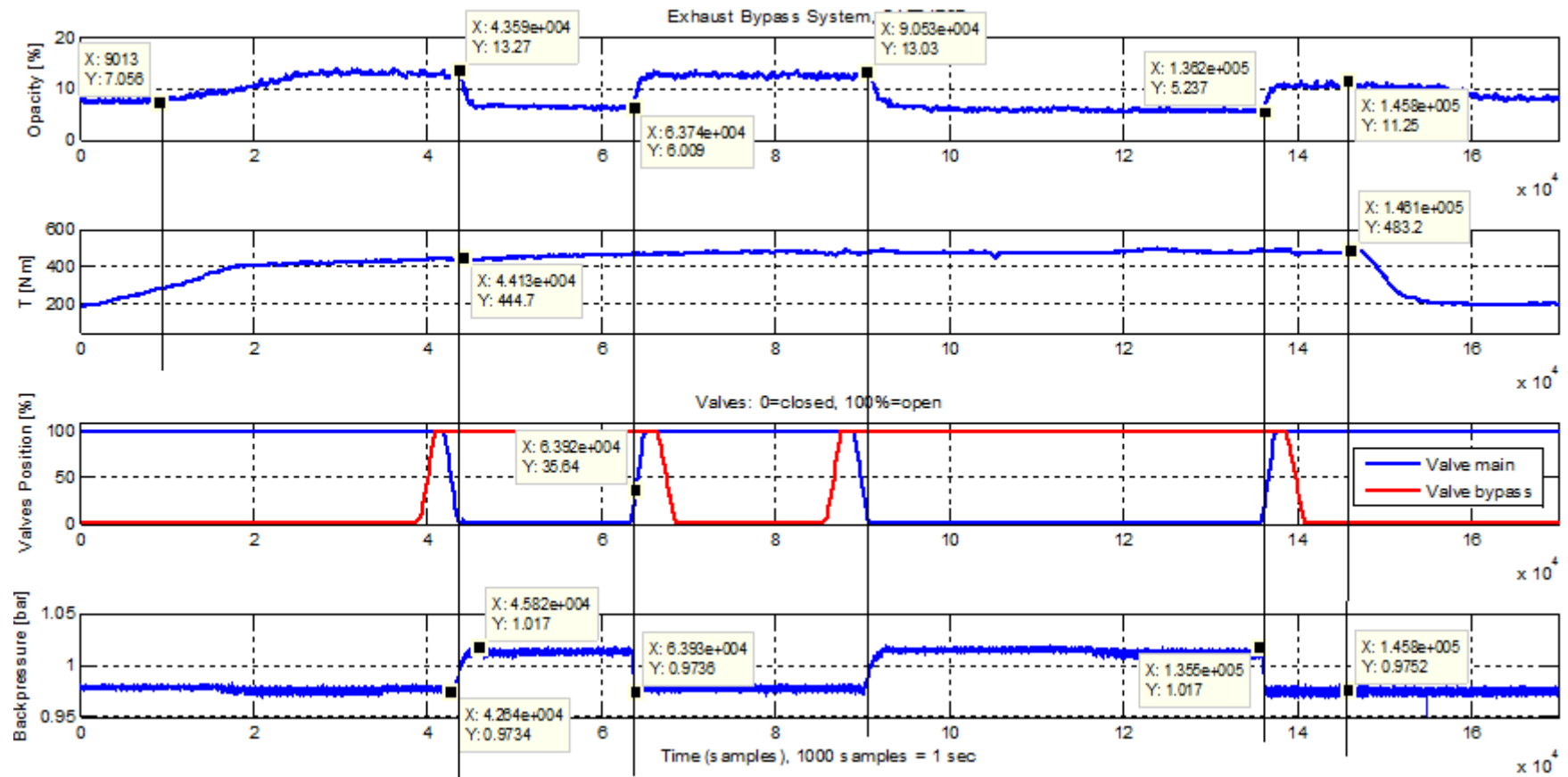
Figure 125: Opacity, torque, valves position and backpressure measurements with CAT3176B, valves: manual handling
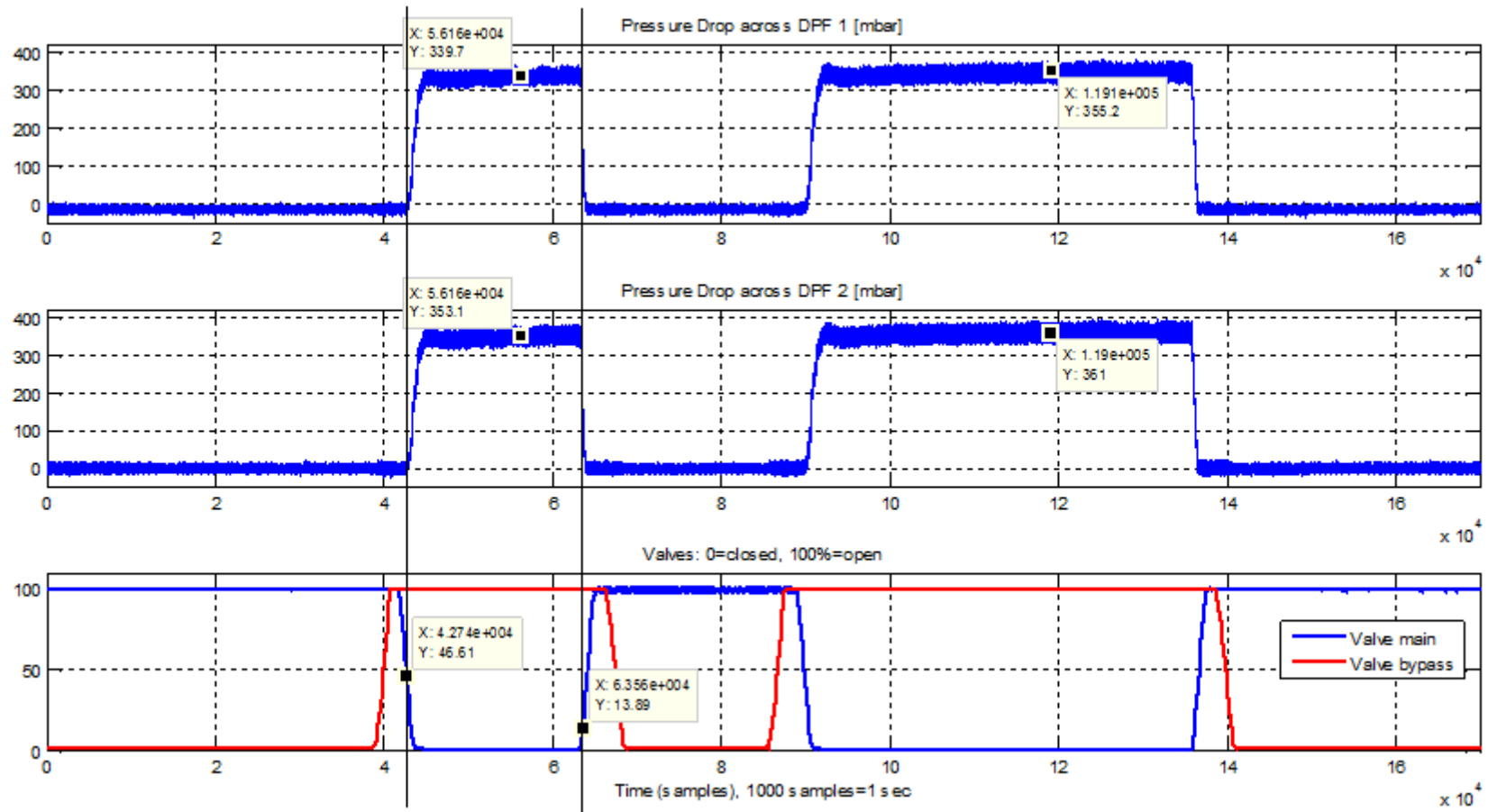
Figure 126: Pressure drop across DPF 1, DPF 2, and valves position measurements with CAT3176B, valves: manual handling
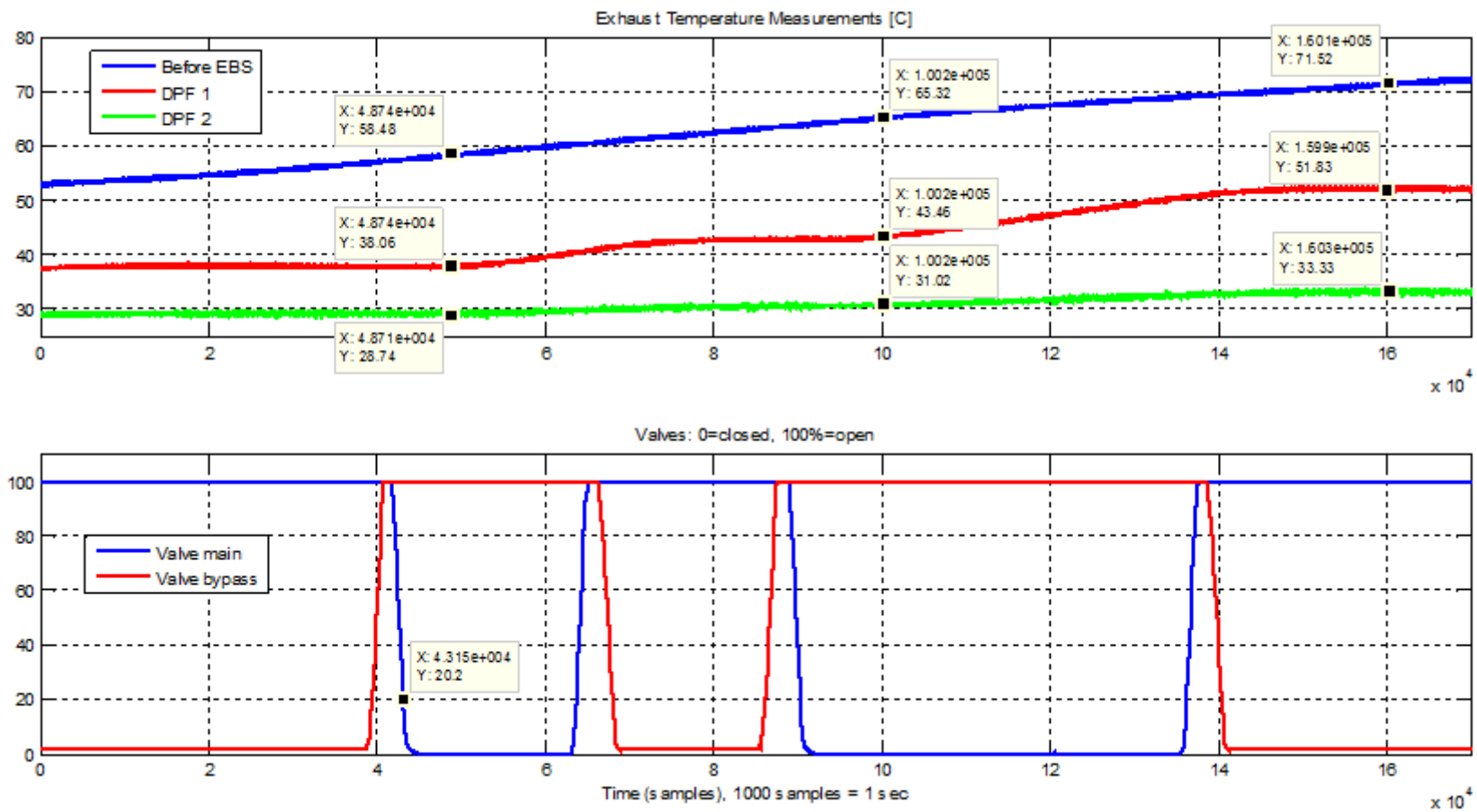
Figure 127: Temperature before EBS, DPF 1, DPF 2 and valves position measurements with CAT3176B, valves: manual handling

In figure 125 the opacity, torque, valves position and system backpressure measurements are presented. The engine loading includes engine load increase from 200 Nm to 500 Nm at constant engine speed 1600 rpm. In terms of power the engine is loaded from 7.5% of MCR (449.6 kW) to 18.6% (83.7 kW). Initially, opacity signal delay of about 9000 samples (9s) is observed which is expected due to the fact that the sensor is located at the end of the EBS in room I.13 and at low loads the exhaust gas velocity is small. However, at higher loads the signal delay tends to decrease because of the higher exhaust gas velocity. At 200 Nm, opacity is approximately 7% while at 500 Nm it is increased to 13% showing an increase of 6%, which is related to worse combustion conditions in the cylinders due to higher but still very low engine load. Then, EBS is activated by opening valve 2 (bypass) and closing valve 1 (main). By the time valve 1 is closed, opacity starts to decrease demonstrating the exhaust gas filtering. In reality, opacity starts to decrease simultaneously with the valve 1 closing since exhaust gas is forced to pass through the bypass duct. The DPFs cause an opacity reduction of 7% which means that opacity doesn't ''follow'' the engine load increase as it is below 7% which was its value at 200 Nm engine load. After a while, EBS is deactivated by repositioning the exhaust valves and opacity is increased at 13% which is its previous value before EBS activation. Then, EBS is reactivated and opacity is again reduced to 6%. However, the opacity values tend to decrease to 5% which is a result of better combustion due to the stabilization of the engine load. The opacity reduction due to improvement of combustion starts roughly 100s after the load increase. Finally, EBS is deactivated and opacity is increased to 11% proving the fact that the engine starts to operate in steady-state conditions. The engine load is then reduced to 200 Nm and opacity respectively decreases to 7.5% with tendency for further decrease to its initial value of 7%.

As far as the system backpressure is concerned, pressure increases of 43.6 mbar (first EBS activation) and 43.4 mbar (second EBS activation) are observed. The sensor readings are not considered accurate, at least in absolute values, because the sensor indicates initial exhaust gas pressure of 0.97 bar (it should be above 1.012 bar). However, this constant error can be eliminated by measuring the pressure drop caused by the EBS.

In figure 126 the pressure drop measurements across the two filters are presented. The pressure drops across DPF 1 are 340 mbar (EBS first activation) and 350 mbar (EBS second activation) while the respective ones across DPF 2 are a little higher 350 mbar (first activation) and 360 mbar (second activation). This slight difference (10 mbar) between the pressure drops across the two filters is a clear indication of different initial soot load. Moreover, the differential pressure developed across the filters is considered high but fortunately the overall system backpressure is kept at reasonable levels.

Finally, in figure 127 the temperature measurements are provided which demonstrate the different heating and exhaust gas filtering of the two DPFs as well as the high system heat inertia. At first the exhaust temperature before the EBS shows linear increase of small gradient (7°C per 50s) due to the low engine load. The exhaust temperatures before the two filters are kept constant when EBS is deactivated since no exhaust gas passes through the filters. However, during EBS activation both DPF temperatures show a non-linear increase which lasts as long as exhaust gas passes through the filters. In addition, the exhaust temperature before the DPF 2 is continuously lower than the respective one before the DPF 2, which is a clear proof that less exhaust gas passes through the second filter. The temperature difference between the two DPFs continuously increases (10°C, 12°C, 18°C) and considering the increased pressure drop measured across DPF 2, higher soot loading of the second filter can be inferred. Furthermore, the exhaust gas tends to flow through DPF 1 at increased amounts due to lower pipeline length.

6.2.2   Caterpillar 3176B, Valves: Stateflow Control
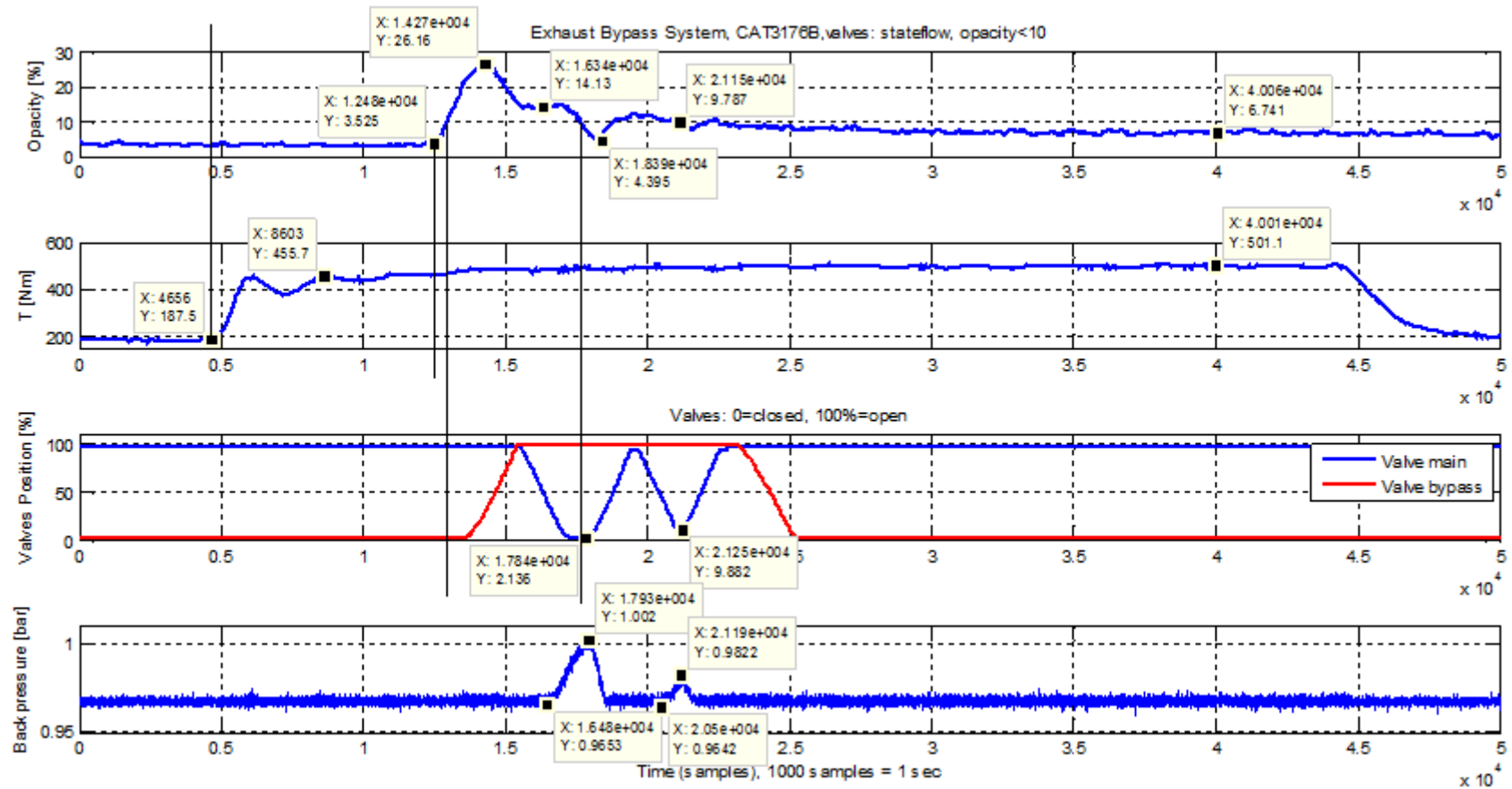
Figure 128: Opacity, torque, valves position and backpressure measurements with CAT3176B, valves: stateflow control
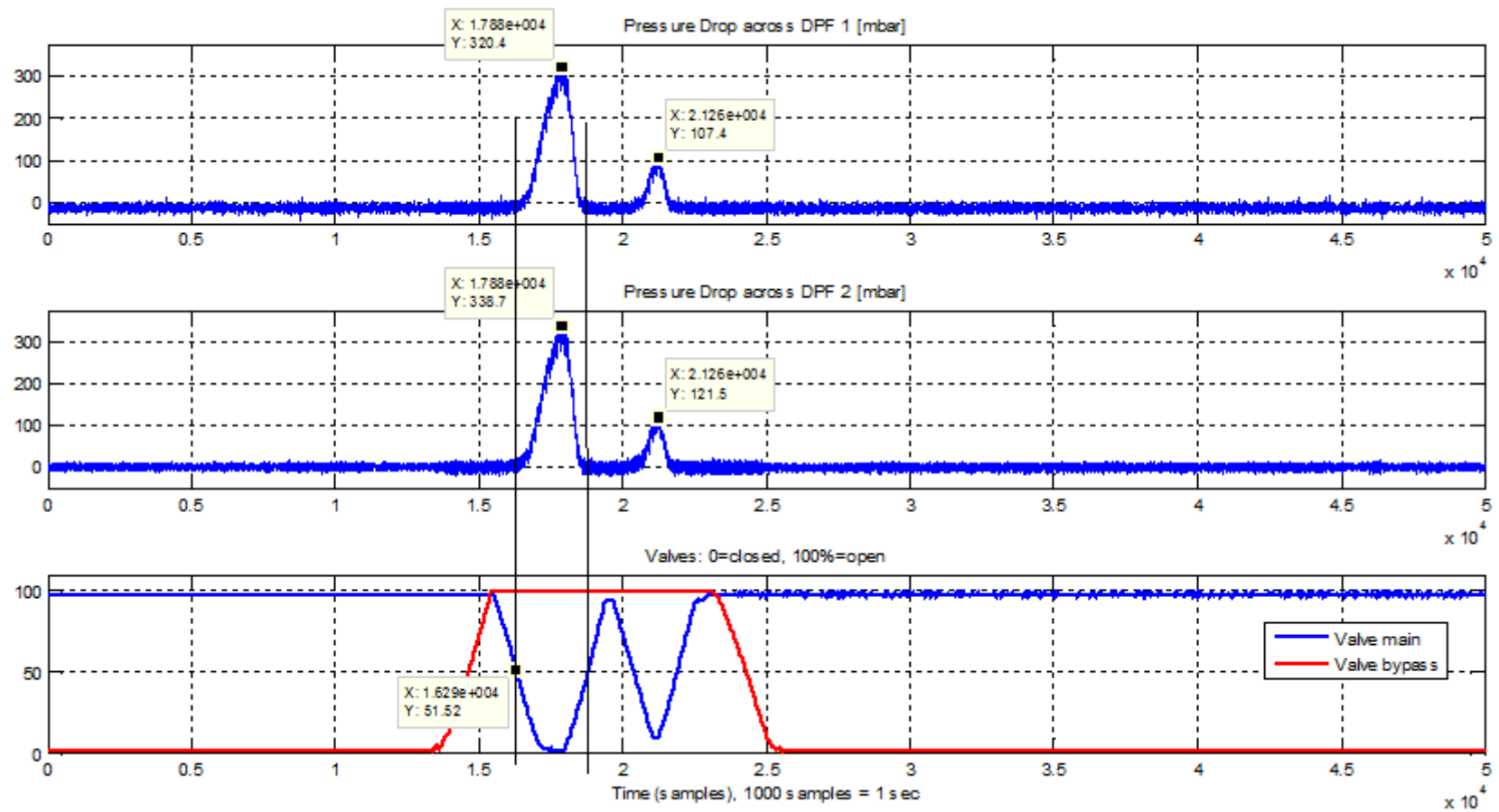
Figure 129: Pressure drop across DPF 1, DPF 2, and valves position measurements with CAT3176B, valves: stateflow control
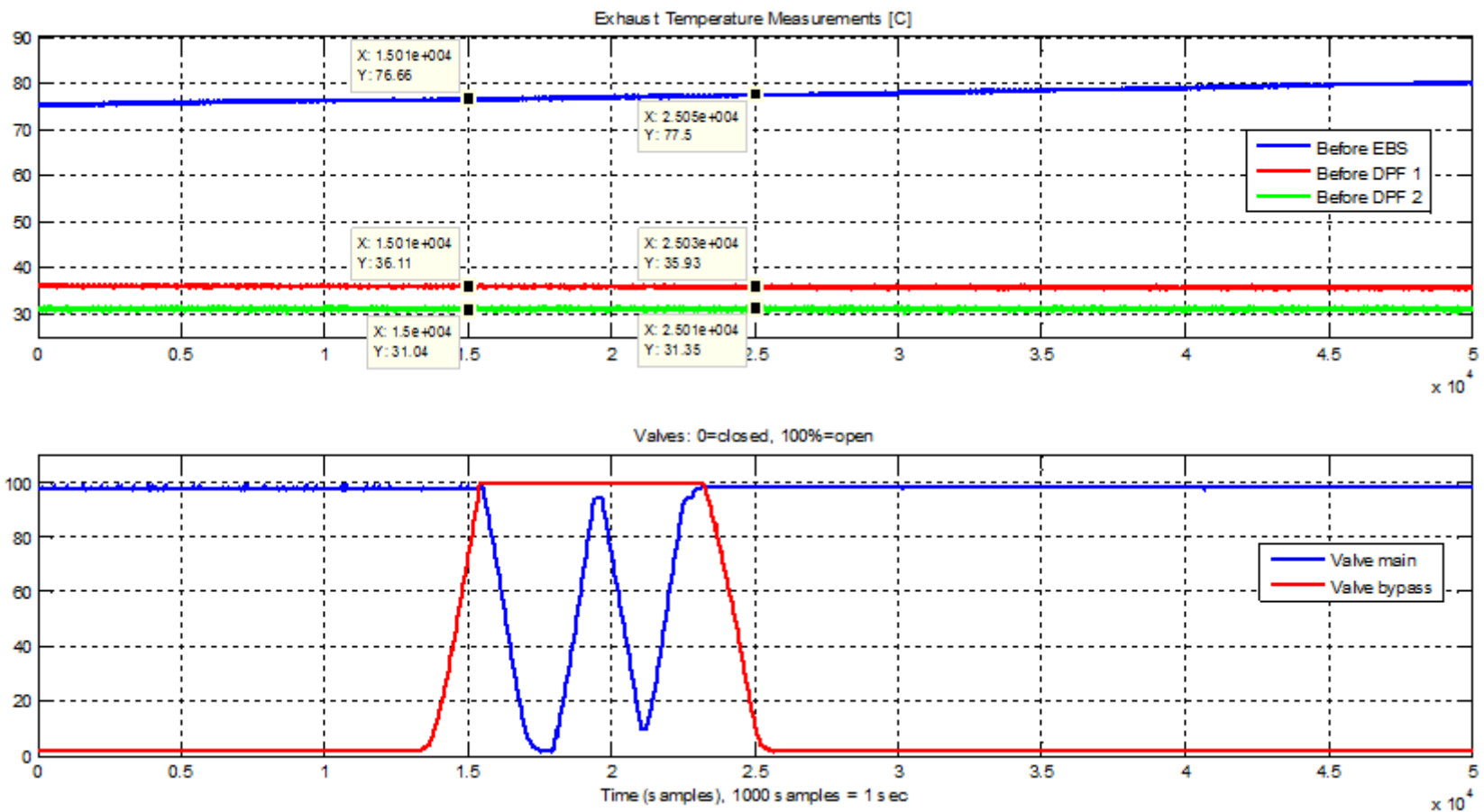
Figure 130: Temperature before EBS, DPF 1, DPF 2 and valves position measurements with CAT3176B, valves: stateflow control

In figure 128 the opacity, torque, valves position and system backpressure measurements with Caterpillar 3176B engine and stateflow valves control are presented. The engine loading includes engine load increase from 200 Nm to 500 Nm at constant engine speed 1600 rpm. In terms of power the engine is loaded from 7.5% of MCR (449.6 kW) to 18.6% (83.7 kW). Initially, the opacity signal delay is approximately 8000 samples (8s) but tends to decrease (due to the increased exhaust gas velocity. At 200 Nm, opacity is approximately 4% while at 500 Nm it is increased to 26% showing a sharp increase of 22%. Stateflow control dictates EBS activation if opacity exceeds 10%. Therefore, valve 2 (bypass) opens which is followed by the closing of valve 1. Due to the fact that initially the engine load profile is unstable, the imposed load deviates as it instantaneously decreases below 400 Nm. As a result, opacity is rapidly reduced to 14% where it is stabilized according to the stabilization of the engine load at 500 Nm. It's worth mentioning that the opacity value during this transient loading is in complete accordance with the opacity measured in the previous experiment for the same transient loading. Then, opacity is further reduced due to the EBS activation and quickly decreases to 4%, showing a 10% reduction. By the time opacity is less than 10% stateflow control dictates the EBS deactivation which initiates by opening valve 1. As a consequence exhaust gas starts to flow through the main duct[18] and opacity is increased again to 12%, which triggers the EBS re-activation. Because of the fact that valve 2 remains open, valve 1 re-closes immediately, forcing the exhaust gas to flow through the DPFs and opacity decreases to 9%. Then, EBS deactivates completely (both valves are moved to the initial positions) while opacity is kept low (7%) as the engine starts to operate in steady-state conditions and the combustion is improved.

As far as the system backpressure is concerned, it is considered low since the overall pressure increase caused by the EBS is small during both EBS activations. At first the maximum pressure drop is 36.7 mbar (10% opacity reduction) while during the second EBS activation, it is 18 mbar (3% opacity reduction).

In figure 129 the pressure drop measurements across the two filters are presented. The pressure drops across DPF 1 are 320 mbar (EBS first activation) and 107 mbar (EBS second activation) while the respective ones across DPF 2 are a little higher 339 mbar (first activation) and 122 mbar (second activation). The increased values of the pressure drop developed across the filters indicate possible clogging of the filters due to mal-regeneration before their installation on the system. Furthermore, the difference between the pressure drops across the two filters (15 – 20 mbar) is higher than this measured in the previous experiment (10 mbar).

---

[18] Exhaust gas tends to flow through the shortest pipeline length or/and through regions of less pressure

This strongly suggests that the two DPFs were not regenerated equally before their installation on the EBS, as DPF 2 is clearly more loaded with soot. Nevertheless, despite the increased differential pressure across the two filters, the overall system backpressure is still low.

In figure 130 the temperature measurements are provided which demonstrate the increased system heat inertia. The exhaust temperature in the duct before EBS shows a slight increase (1°C per 10s), but remains low (about 77°C), while the exhaust temperatures before the filters are lower (36°C for DPF 1 and 31°C for DPF 2) and don't present any gradient even during EBS activation. Finally, the temperature difference (5°C) between the two DPFs is noteworthy as it proves the exhaust gas maldistribution between the two filters during EBS activations. Except for the suspected increased soot load of DPF 2, there is also the suggestion that the system design is not optimal. Considering that more exhaust gas tends to flow through DPF 1[19] the exhaust velocity met before DPF 2 is lower and as a consequence static pressure before the filter is higher. This may lead to increased pressure drop across the filter.

---

[19] Shorter pipeline length

6.2.3 MAN B&W Holeby L16/24, Valves: Manual Handling
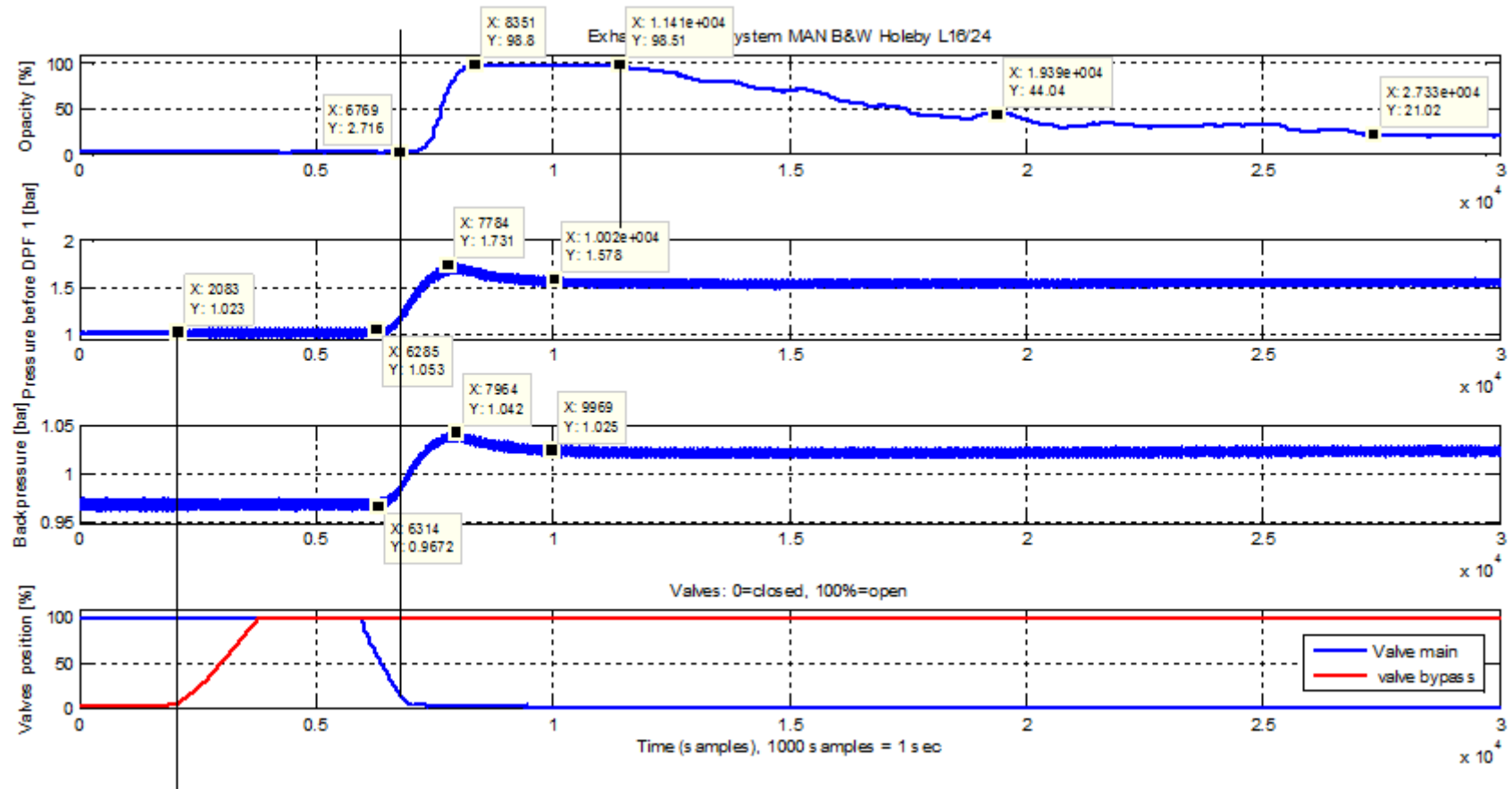
Figure 131: Opacity, backpressure and valves position measurements with MAN B&W Holeby L16/24, valves: manual handling
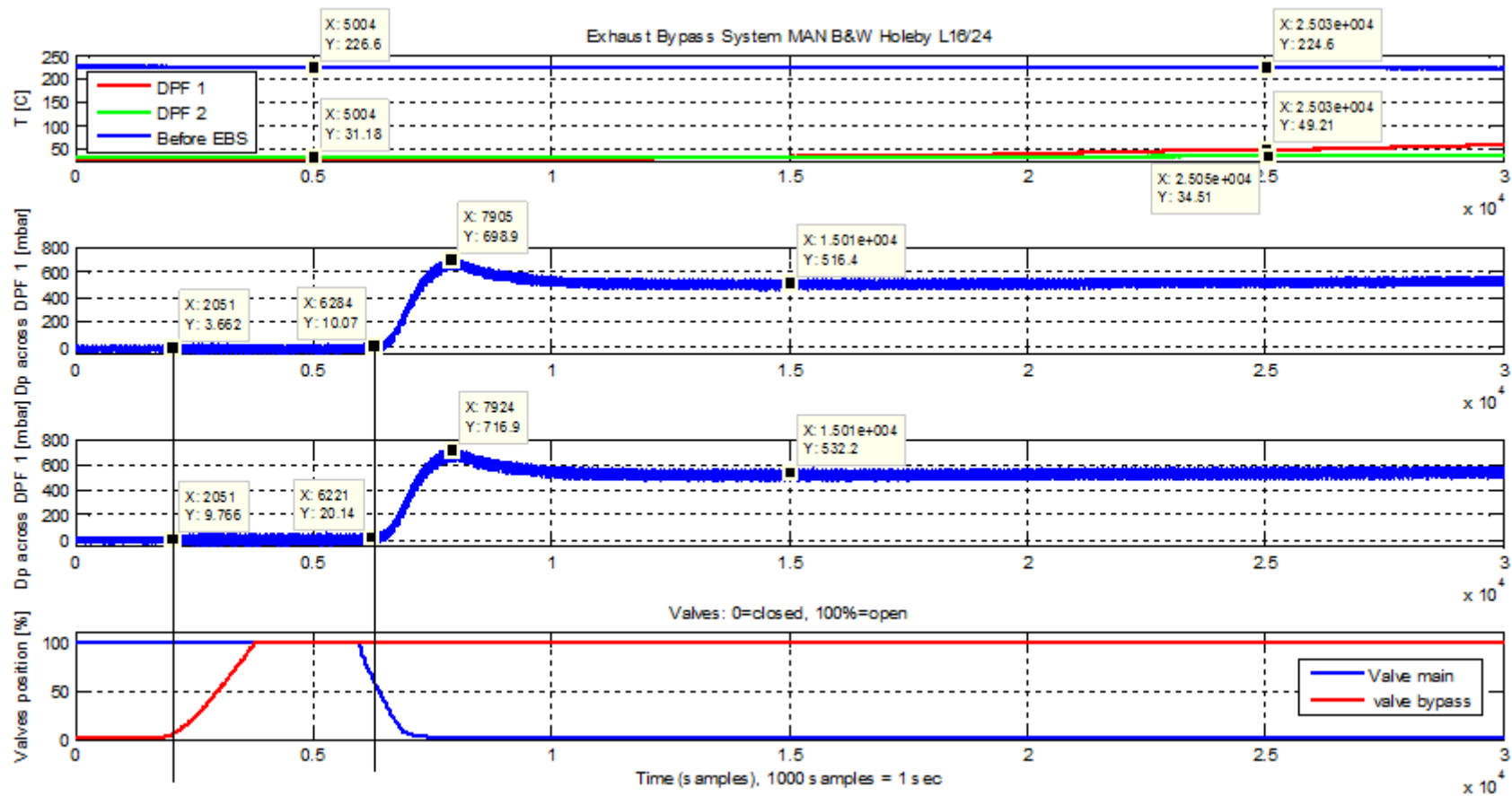
Figure 132: Temperature, pressure drop across DPF 1, DPF 2 and valves position measurements with MAN B&W Holeby, valves: manual handling

In figure 131 the opacity, backpressure before DPF 1 and EBS as well as the valves position measurements with the MAN B&W Holeby L16/24 engine are presented. Unfortunately, torque measurements are not available because the engine controller wasn't connected to the DS1103, so only measurements directly related to the EBS were collected. The engine initially is idle (10% of MCR) and it operates at nominal revolutions 1200 rpm. The imposed engine loading includes load increase from 398 Nm to 1194 Nm at constant engine speed which in terms of power corresponds to power increase from 50 kW (10%) to 150 kW (30% of MCR). At first opacity is 3% which corresponds to idle engine operation but due to the imposed sharp load increase it is increased to 99%. Opacity remains at 99% for approximately 3s (3000 samples) and then decreases to lower values. The opacity reduction is gradual but continuous (54% reduction after 8s and 77% after 16s). The EBS activation starts at 2000 samples (2s) and is completely finished (valve 2 opened and valve 1 closed) after 5s. Despite the fact that EBS is activated at 7s (7000 samples) opacity starts to decrease at 11s (1141 samples). Obviously this is attributed to the opacity signal delay which can be roughly estimated at 4s. Finally, opacity is reduced to 20% showing a total reduction of 79% due to the exhaust gas filtering as well as the engine loading stabilisation.

As far as the system backpressure is concerned, two measurements are presented, the first one corresponding to the exhaust pressure measured just before DPF 1, whilst the other to the exhaust pressure measured before the EBS by the defective sensor. Both of them present similar behaviour but they differ in absolute values. The exhaust pressure before DPF 1 increases 30 mbar simultaneously with valve 2 opening. The highest increase (680 mbar) is presented when valve 1 fully closes which forces all exhaust gas to flow through the filters. Then, the pressure is decreased and stabilised at 1.5 bar. The exhaust pressure measured before EBS behaves the same showing maximum increase of 75 mbar (valve 1 opening) and pressure reduction of 20 mbar before its stabilisation. The absolute values of the pressure before EBS are not presented because they are considered inaccurate.

In figure 132 the temperature and the valves position measurements are provided. Moreover, the pressure drop measurements across the two filters are presented. The temperature measured before EBS is 225°C and it remains constant while the temperature measured before each filter is much lower (31°C for both DPFs) and tends to increase unevenly due to the prolonged EBS operation. Specifically, after 20s the temperature before DPF 1 is increased 18°C to 49°C, while the temperature before DPF 2 is increased only 3°C to 34°C. This strengthens the suggestion that the exhaust flow is mal-distributed through the two filters which is a result of either different DPFs soot load or defective system design.

Finally, the differential pressure measured across the two filters shows similar behaviour with the exhaust pressure measurements provided in figure 131. Specifically, the pressure drop across DPF 1 instantly increases to 10 mbar after the opening of valve 2. Then, after the full EBS activation which forces the exhaust gas to flow entirely through the filters, the pressure drop increases to approximately 700 mbar before its reduction and stabilisation at 516 mbar. The pressure drop across DPF 2 behaves exactly the same though its absolute values are continuously 10 – 18 mbar higher according to the previous experiments. Therefore, it can be derived that DPF 2 is more clogged than DPF 1 due to increased initial soot or ash load in the filter.

6.3 Conclusion

The experiments with the exhaust bypass system provided fruitful results concerning the achieved opacity reduction and the consequent backpressure developed. The first experiment included 300 Nm engine loading at constant speed and manual handling of the exhaust valves. At first the initial concern of high opacity signal delay was confirmed as it lagged 9s after the engine load increase. This is considered an unfavourable factor for the system efficiency as long as opacity signal serves as the trigger signal for the EBS activation. Moreover, when activated the EBS inflicted a rapid 54% opacity reduction (from 13% to 6%) while overall backpressure was kept low since it was increased only 43 mbar. The pressure drop developed across the filters was approximately 340 - 350 mbar with the latter representing the pressure drop across DPF 2. Although this pressure drop was quite high, the overall system backpressure was kept at reasonable levels. Furthermore, the temperature measurements demonstrated high system heat inertia and indicated mal-distribution of the exhaust flow through the filters as DPF 1 was heated more quickly.

The second experiment comprised a first effort for closed loop system control by using the stateflow environment for the valves operation. Opacity of 10% was defined as the trigger signal for the EBS activation and the engine was loaded the same way as in the first experiment. The opacity signal delay was measured 8s and the EBS reduced exhaust opacity approximately 70% from 14% to 4%. The overall backpressure was still kept at low levels as it was increased 36.7 mbar. Despite the small system backpressure the pressure drop across DPF 1 was 320 mbar while across the second filter was 19 mbar higher (339 mbar). The increased pressure drop across DPF 2 suggested higher filter soot loading which could be explained by insufficient regeneration of the filters before their installation on the EBS. In addition, the temperature measurements demonstrated again the high system heat inertia as no temperature gradient was presented on the DPFs during the EBS activation. Moreover, the difference between the temperatures of the two filters was a second clear indication of exhaust flow mal-distribution, as DPF 1 was heated again more quickly. Finally, the stateflow control of the valves provided promising results. However, the system control was not optimal due to the fact that opacity signal was not suitable for this type of control as every time that opacity was reduced below 10%, valve 1 was opened which led to opacity increase because of the EBS deactivation. As a consequence the system efficiency was reduced as the opacity abatement was diminished.

The third and final experiment included 796 Nm engine loading of MAN B&W Holeby L16/24 engine at constant engine speed. The EBS was activated and the opacity started to decrease after 4s. The reduction was gradual and continuous (55% after 8s, 79% after 16s) till the opacity stabilisation at 20%. The opacity signal delay can be roughly estimated at 4s by measuring the time period between the EBS full activation and the initiation of the opacity reduction. It is worth mentioning that opacity is initially increased to 98% and it remains there for approximately 3s. The overall system backpressure was increased 75 mbar after the EBS activation. In addition, exhaust pressure measurements before DPF 1 were collected which presented a pressure increase of 680 mbar before the filter. Then, the exhaust pressure before DPF 1 was stabilised at 1.5 bar. Furthermore, the pressure drop across the two filters was 700 mbar for DPF 1 and 717 mbar for DPF 2. The high pressure drop measured across the filters indicated increased soot/ash load in the filters. Finally, the temperature measurements confirmed the system high heat inertia as the temperature gradients were very small. Moreover, the different exhaust temperatures before the two filters strongly suggested that the EBS design was not optimal as DPF 1 presented higher temperature gradient (hence increased exhaust gas flow).

As far as the system backpressure measurement (PT131) is concerned, the absolute values were considered inaccurate due to probable defective sensor. However, by measuring the pressure increase (differential pressure) caused by the EBS activation, the constant error was eliminated and a rough estimation of the imposed system backpressure could be derived.

Chapter 7: Conclusions - Recommendations

In the context of this thesis a smoke emission abatement system was developed and installed in the exhaust processing room I.13 of LME. The system consisted of a bypass duct connected to the exhaust system, two DPFs for PM collection and two butterfly valves for exhaust gas flow control. The DPF selection was based on achieving minimum pressure drop, as well as minimum filter dimensions. The exhaust bypass system would be activated by repositioning the two exhaust valves only during engine transient loading. This was a basic prerequisite for the system design in order to avoid early clogging of the filters due to increased soot deposition. It is worth mentioning that the initial DPFs connection via clamps proved ineffective as it led to high exhaust gas leakage. The consequent flange connections offered high process sealing but also less flexibility in case of filter replacement and increased system weight.

For estimating the system efficiency, a suitable sensor, capable of measuring the exhaust opacity, was installed on the exhaust duct after the filters. Moreover, two pressure sensors were mounted across each filter for measuring the developed pressure drop, while the overall system backpressure was measured by a fifth pressure sensor mounted just before the EBS. Finally, three RTDs were also incorporated in the system for providing useful temperature readings before the filters and the EBS. All sensors were mounted and connected based on drawings which were produced in order to provide full system documentation. The sensors output signals were electrically isolated and converted by newly installed isolating amplifiers before their collection by the DAQ system. The complete installation of the system included the placement of an electrical panel, an air supply subsystem as well as the exhaust duct insulation.

Before conducting experiments with the exhaust bypass system, opacity measurements on the ASL Speedrunner 3 high speed vessel, were performed. The opacity readings were possible after the installation of the opacimeter on the exhaust duct of one of the four ship engines. The measurements demonstrated very low exhaust opacity (below 5%) when the engine operated close to MCR, while at lower engine loads opacity was increased to 15%. The biggest challenge, in terms of smoke emission, was presented during engine load increase, which inflicted consequent opacity increase to 40%. Furthermore, the opacity measurements onboard indicated the strong correlation between the engine loading profile and the exhaust opacity which could prove very useful for optimising the smoke abatement system by decoupling its activation from the opacity signal which is characterised by high delay.

The experiments with the exhaust bypass system included engine loading at constant speed, EBS activation according to the measured exhaust opacity and full exhaust gas filtering. All experiments demonstrated high opacity signal delay (8 – 9s) which led to system efficiency reduction. The opacity abatement was relatively high (54% – 70%) while the system overall backpressure presented only a small increase of 37 – 75 mbar. However, the pressure drop developed across the filters was quite high (340 – 700 mbar). This was a clear indication of high initial filters soot load due to possible mal-regeneration before their installation on the EBS. Finally, the temperature measurements pointed out high system heat inertia as the temperature gradients were kept low. Moreover, the increased heating of DPF 1 compared to DPF 2 suggested that more exhaust gas passed through the first filter. This was a clear indication of increased clogging of DPF 2 as well as not optimal system design considering the fact that the exhaust gas preferred to follow the shortest pipeline path, through the less loaded filter.

As far as future work is concerned, the EBS installation offers a variety of possible system operations for achieving less smoke emission. At first the defective pressure sensor, installed before the EBS, should be replaced for ensuring accurate backpressure measurements. Furthermore, the system activation should be decoupled from the opacity signal as the latter is characterised by high delay. Possible solution is correlating the EBS activation to the engine loading profile which may lead to an increase of the system efficiency due to higher opacity reduction. Moreover, tests with partial exhaust gas filtering can be performed in order to extend the life span of the filters without significantly diminishing the total opacity abatement. In the end, an optimised closed loop system control should be implemented in order to achieve higher smoke emission reduction, less backpressure and low contamination of the DPFs.

Figure 133: ASL Speedrunner 3 leaving the port of Serifos

108

Bibliography

1. **Doug Woodyard.** *Pounder's Marine Diesel Engines and Gas Turbines.* Oxford : Elsevier, 2009.

2. **N.P. Kyrtatos.** *Marine Diesel Engines, Design and Operation.* Athens : Symmetria, 1993.

3. **D.A. Cooper.** *Exhaust emissions from high speed passenger ferries.* Goteborg : Atmospheric Environment, 2001.

4. **Kazuyuki Maeda, Yutaro Wakuri, Koji Takasaki, Shin-ichi Morishita.** *Exhaust Emissions from Marine Diesel Engines Using Residual Fuel.* s.l. : M.E.S.J., 1998.

5. **DieselNet.** *DieselNet.* [Online] [Cited: 9 July 2014.] https://www.dieselnet.com/standards/.

6. **Timothy V. Johnson.** *Diesel Emission Control in Review.* Detroit : SAE International, 2007.

7. **Irvin Glassman, Richard A. Yetter.** *Combustion.* Fourth. London : Elsevier, 2008.

8. **Tatsuro Tsukamoto, Tomohiro Miyoshi, Kenji Ohe, Hiroshi Okada.** *Characteristics of Particulate Emission from Marine Diesel Engines - Comparison between High Speed Four Stroke Engine and Low Speed Two Stroke Engine.* s.l. : M.E.S.J., 1999.

9. **Laurie Goldsworthy.** *Exhaust Emissions from Ship Engines - Significance, Regulations, Control Technologies.* s.l. : A&NZ Mar LJ, 2010.

10. **Malin Alriksson, Ingemar Denbratt.** *Low Temperature Combustion in a Heavy Duty Diesel Engine Using High Levels of EGR.* Warrendale : SAE International, 2006.

11. **K.D. Rakopoulos, D. Th. Xountalas.** *Combustion - Pollution of Reciprocating Internal Combustion Engines.* Athens : Fountas, 1998.

12. **CIMAC.** *Background information on black carbon emissions from large marine and stationary Diesel engines – Definition measurement methods, emission factors and abatement technologies.* Frankfurt : CIMAC, 2012.

13. **G. Livanos, E. Kanellopoulou, N. Kyrtatos.** *Marine Diesel Engine Transient Operation with Reduced Smoke Emissions.* s.l. : JIME, 2006.

14. **G. Papalambrou, N. Alexandrakis ,N. Kyrtatos, E. Codan, I. Vlaskos, V. Pawlis, R. Boom.** *Smokeless Transient Loading of Medium/High Speed Engines Using a Controlled Turbocharging System.* Vienna : CIMAC Congress, 2007.

15. **Neundorfer.** *Neundorfer Particulate Knowledge.* [Online] [Cited: 14 July 2014.] http://neundorfer.com/knowledge_base/baghouse_fabric_filters.aspx.

16. **—.** *Neundorfer Particulate Knowledge.* [Online] [Cited: 14 July 2014.] http://www.neundorfer.com/knowledge_base/electrostatic_precipitators.aspx#itp.

17. **Wikipedia.** *Wikimedia Foundation.* [Online] [Cited: 14 July 2014.] http://en.wikipedia.org/wiki/Electrostatic_precipitator.

18. —. *Wikimedia Foundation.* [Online] [Cited: 14 July 2014.] http://en.wikipedia.org/wiki/Scrubber.

19. **G. Koltsakis, A. Stamatelos.** *Catalytic Automotive Exhaust Aftertreatment.* Thessaloniki : Elsevier Science, 1997.

20. **A.M. Stamatelos.** *On-line Regeneration Control for a Diesel Particulate Trap System.* Thessaloniki : Elsevier Science, 1993.

21. **Georgios Stratakis.** *Experimental Investigation of Catalytic Soot Oxidation and Pressure Drop Characteristics in Wall-Flow Diesel Particulate Filters.* Volos : University of Thessaly, 2004.

22. **Th. Zaxmanoglou, G. Kapetanakis, P. Karampilas, G. Patsiavos.** *Automotive Technology - Beyond 2000.* Athens : IDDEA, 2013.

23. **DieselNet.** *DieselNet.* [Online] [Cited: 28 July 2014.] https://www.dieselnet.com/tech/cat_substrate.php.

24. **Yiannis A. Levendis, Iraklis Pavlatos, Richard F. Abrams.** *Control of Diesel Soot, Hydrocarbon and NOx Emissions with a Particulate Trap and EGR.* s.l. : SAE International, 1994.

25. **P. Lauer.** *On the experience of first DPF operation at a medium speed 4-stroke Disel engine on board a commercial ocean going vessel.* Zurich : 16th ETH Conference on Combustion Generated Particles, 2012.

26. **A. Stamatelos, O. Zwgou.** *Calculations of DPF and bypass piping exhaust routing for the engines MAN B&W 5L16/24 and CAT 3176B.* Athens : Laboratory of Thermodynamics and Thermal Engines - University of Thessaly, 2014.

27. **DURAG.** *Filter Monitor Brochure.* Mendota Heights : DURAG, 2014.

28. **Delphi.** *Delphi Particulate Matter Sensor Brochure.* Michigan : Delphi, 2014.

29. **Green Instruments A/S.** *G1000 Smoke Density Monitor Manual.* Bronderslev : Green Instruments A/S, 2012.

30. **Wikipedia.** *Wikimedia Foundation.* [Online] [Cited: 6 August 2014.] http://en.wikipedia.org/wiki/Ringelmann_scale.

31. **Green Instruments A/S.** *G1000 Smoke Density Monitor Brochure.* Bronderslev : Green Instruments A/S, 2014.

32. **Kostas Kalaitzakis, Eutuxis Koutroulis.** *Electrical Measurements and Sensors.* Athens : Kleidarithmos, 2010.

33. **Wikipedia.** *Wikimedia Foundation.* [Online] [Cited: 7 August 2014.] http://en.wikipedia.org/wiki/Pressure_sensor.

34. **Wika.** *High-quality pressure transmitter for general industrial applications: Model S-10.* Klingenberg : Wika, 2012.

35. **John Hansson, Victor Ingestrom.** *A Method for Estimating Soot Load in a DPF Using an RF-based Sensor.* Linkopings : Linkopings Univeristy, 2012.

36. **M. Feulner, A. Muller, G. Hagen, D. Bruggemann, R. Moos.** *Microwave-based DPF Monitoring-Soot Load Determination and Influencing Parameters.* Bayreuth : Bayreuth Engine Research Center, 2013.

37. **General Electric.** *Accusolve Diesel Particulate Filter Soot Sensor.* Billerica : General Electric Sensing and Inspection Technologies, 2011.

38. **SOMAS.** *Datasheet Butterfly valve for exhaust gas applications Si-207 EN.* Saffle : SOMAS, 2014.

39. —. *Datasheet Pneumatic actuators Si-503 EN.* Saffle : SOMAS, 2012.

40. **Siemens AG.** *Electropneumatic positioners SIPART PS2 - US Edition.* Nurnberg : Siemens AG, 2009.

41. —. *Electropneumatic positioners SIPART PS2 with and without HART communications.* Nurnberg : Siemens AG, 2008.

42. **Honztsch.** *Flow measurement with sensors ZS25 at working temperatures up to +500 °C optional with integrated and configurable transducer UFA.* Hegnach : Honztsch, 2014.

43. **N. Vrettakos.** *Analysis of Cylinders Pressure Measurements of Maine Engines.* Athens : Laboratory of Marine Engineering NTUA, 2011.

44. **Wikipedia.** *Wikimedia Foundation.* [Online] [Cited: 20 August 2014.] http://en.wikipedia.org/wiki/Temperature_measurement.

45. —. *Wikimedia Foundation.* [Online] [Cited: 20 August 2014.] http://en.wikipedia.org/wiki/Resistance_temperature_detector.

46. —. *Wikimedia Foundation.* [Online] [Cited: 20 August 2014.] http://en.wikipedia.org/wiki/Thermocouple.

47. —. *Wkimedia Foundation.* [Online] [Cited: 20 August 2014.] http://en.wikipedia.org/wiki/Pyrometer.

48. **Wika.** *Threaded resistance thermometer Model TR10-C, with fabricated thermowell model TW35.* Klingenberg : Wika, 2013.

49. —. *Analogue temperature transmitters Model T19.10, configurable ranges, head mounting version.* Klingenberg : Wika, 2010.

50. **Phoenix Contact.** *MINI MCR-SL-I-U-4 Extract from the online catalog.* Blomberg : Phoenix Contact, 2014.

51. —. *MINI MCR-SL-UI-UI-NC Extract from the online catalog.* Blomberg : Phoenix Contact, 2014.

52. **dSPACE.** *DS1103 PPC Controller Board.* Paderborn : dSPACE, 2008.

53. **Wikipedia.** *Wikimedia Foundation.* [Online] [Cited: 1 September 2014.] http://en.wikipedia.org/wiki/Mineral_wool.

54. **MathWorks.** MathWorks. [Online] [Cited: 9 September 2014.] http://www.mathworks.com/products/stateflow/.

Appendix I: Instruments Technical Specifications

I.1 G1000 Smoke Density Monitor Specifications

Specifications - G1000 SDM

Lloyd's Register TYPE APPROVAL

Monitoring Unit incl. Digital Display

Power supply	Standard 210–250V AC – 50/60 Hz – 12 VA max. — optional 105–130 V AC or 20–30V DC
Ambient temperature	0°C – 55°C
Dimensions/weight	H×W×D: 300 × 200 × 150 mm / 5.5 kg (monitoring unit alone)
Enclosure	IP 65 Steel box
Display	0...100% opacity level (programmable)
Accuracy	Better than 2% of full scale
Output signal (linearized)	4...20 mA (4 mA ≈ 100% – 20 mA ≈ 0% Opacity) max. 800 Ω or 0...10V DC (0V ≈ 100% – 10V ≈ 0% Opacity) max. 10 mA
Alarm delay	Default 5 s (programmable 0–99 s)
Relay function	2 relays, volt free, freely configurable — default NC — max. 250V AC, max. 2A
Default alarm levels	Relay 1 at 20% opacity (= Ringelman 1) and Relay 2 at 30% opacity

Fiber Optic Cables

Optic fibers	Glass-fiber core in stainless steel sheathings with brass end tip
Operating temperature	Max. 240°C at the glass fiber tip behind the lenses – up to 500°C in the stack
Length of cables	Standard 4.5 m – optional 6.0 m, 7.5 m, or others
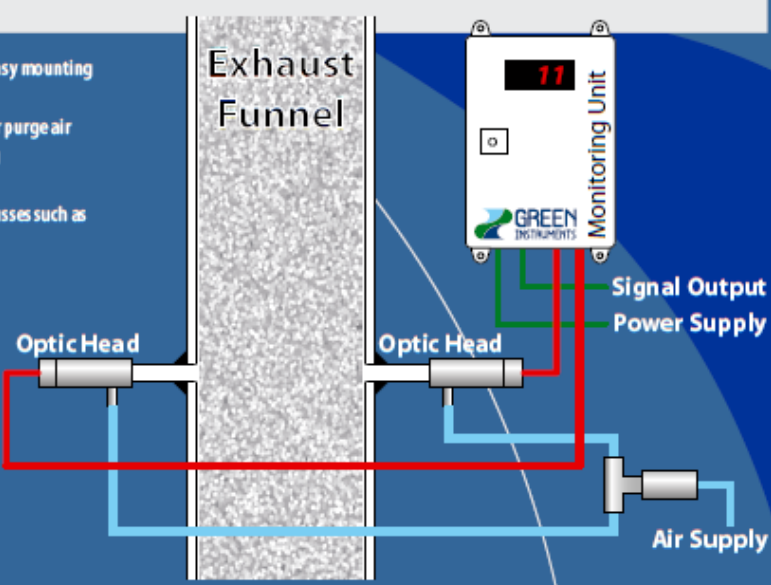
Optic Heads with Purge Air System

Welding sockets	34×200 mm (Ø×L) – sockets aligned opposite of each other
Scanning distance	1 m to 3 m – for shorter ranges one lens need to be removed or replaced
Head housing	H×W×D: < 120 × 100 × 60 mm – stainless steel – with purge-air connector
Purge air supply	10 NLPM – i.e. 5 NLPM for each head

Optional Equipment

- Welding and adjustment bracket for easy mounting
- Audit filter pens
- Purge air blower — filter-regulator for purge air
- Alarm annunciator for panel mounting
- Visualization and data logging
- Data-system integration via various busses such as as RS485 and CAN

I.2 S-10 Pressure Transmitter Specifications

Output signals

Signal type	Signal
Current (2-wire)	4 ...20 mA
	20 ...4 mA
Current (3-wire)	0 ...20 mA
Voltage (3-wire)	DC 0 ... 10 V
	DC 0 ... 5 V
	DC 1 ... 5 V
	DC 0.5 ... 4.5 V ratiometric

Other output signals on request.

Load in Ω

- Current output (2-wire):
  ≤ (power supply - 10 V) / 0.02 A

- Current output (3-wire):
  ≤ (power supply - 3 V) / 0.02 A

- Voltage output (3-wire):
  > maximum output signal / 1 mA

Voltage supply

Power supply
The power supply depends on the selected output signal
- 4 ... 20 mA: DC 10 ...30 V
- 20 ... 4 mA: DC 10 ...30 V
- 0 ... 20 mA: DC 10 ...30 V
- DC 0 ...5 V: DC 10 ...30 V
- DC 1 ...5 V: DC 10 ...30 V
- DC 0 ...10 V: DC 14 ... 30 V
- DC 0.5 ... 4.5 V ratiometric: DC 4.5 ...5.5 V

Reference conditions (per IEC 61298-1)

Temperature
15 ... 25 °C

Atmospheric pressure
860 ... 1,060 mbar

Humidity
45 ... 75 % relative

Power supply
DC 24 V

Mounting position
Calibrated in vertical mounting position with pressure connection facing downwards.

Accuracy specifications

Non-linearity (per IEC 61298-2)
≤ ± 0.2 % of span BFSL

Non-repeatability
≤ ±0.1 % of span

Accuracy at reference conditions
Including non-linearity, hysteresis, zero offset and end value deviation (corresponds to measured error per IEC 61298-2).

Accuracy	
Standard	≤ ±0.50 % of span
Option	≤ ±0.25 % of span [1]

[1] Only for measuring ranges ≥ 0.25 bar

Adjustability of zero point and span
Adjustment is made using potentiometers inside the instrument.
- Zero point: ± 5 %
- Span: ± 5 %

Temperature error at 0 ... 80 °C
- Mean temperature coefficient of zero point:
  - Measuring ranges ≤ 0.25 bar: ≤ 0.4 % of span/10 K
  - Measuring ranges > 0.25 bar: ≤ 0.2 % of span/10 K

- Mean temperature coefficient of span:
  ≤ 0.2 % of span/10 K

Long-term stability at reference conditions
≤ ±0.2 % of span/year

Time response

Settling time
- ≤ 1 ms
- ≤ 2 ms for output signal DC 0.5...4.5 V ratiometric and measuring ranges < 400 mbar, 10 psi

Operating conditions

Ingress protection (per IEC 60529)
For ingress protections see "Electrical connections"
The stated ingress protection only applies when plugged in using mating connectors that have the appropriate ingress protection

Vibration resistance (per IEC 60068-2-6)
20 g

Shock resistance (per IEC 60068-2-27)
1,000 g (mechanical)

Temperatures

Permissible temperature ranges		
	Standard	**Option**
Medium	-30 ... +100 °C	-40 ... +125 °C
Ambient	-20 ... +80 °C	-20 ... +80 °C
Storage	-40 ... +100 °C	-40 ... +100 °C

Materials

Wetted parts
Stainless steel

Non-wetted parts
- Case: Stainless steel
- Internal pressure transmission medium: Synthetic oil
- Clamping nut: PA
- Angular connector: PA
- O-rings at the clamping nut: NBR
- Flat gasket: VMQ

Instruments with a measuring range of > 25 bar relative do not contain any pressure transmission medium (dry measuring cell).

Process connections

Standard	Thread size
EN 837	G ¼ B
	G ½ B
DIN 3852-E	G ¼ A [1]
-	G ¼ female
ANSI/ASME B1.20.1	¼ NPT
	½ NPT
SAE J514 E	7/16-20 UNF with 74° taper
-	M20 x 1.5
-	G ½ male / G ¼ female
ISO 7	R ¼

1) Maximum overpressure limit 600 bar

Other process connections on request

Approvals, directives and certificates

Approvals
- CSA
- GOST

For further approvals see www.wika.com

CE conformity
- EMC directive 2004/108/EC, EN 61326 emission (group 1, class B) and interference immunity (industrial application)
- Pressure equipment directive 97/23/EC

Electrical connections

Available connections

Electrical connection	Ingress protection	Wire cross-section	Cable diameter	Cable lengths
Angular connector DIN 175301-803 A	IP 65	max. 1.5 mm²	6 ... 8 mm	-
Angular connector DIN 175301-803 with ½ NPT	IP 65	max. 1.5 mm²	-	-
Circular connector M12 x 1 (4-pin)	IP 67	-	-	-
Bayonet connector (6-pin)	IP 67	-	-	-
½ NPT conduit male, with cable outlet	IP 67	3 x 0.5 mm²	6.8 mm	1.5 m, 3 m, 5 m, 10 m, 5 ft, 10 ft, 20 ft, 30 ft, others on request
Cable outlet				
▪ Standard	IP 67	3 x 0.5 mm²	6.8 mm	1.5 m, 3 m, 5 m, 10 m, 5 ft, 10 ft, 20 ft, 30 ft, others on request
▪ not adjustable	IP 68	3 x 0.5 mm²	6.8 mm	1.5 m, 3 m, 5 m, 10 m, 5 ft, 10 ft, 20 ft, 30 ft, others on request
▪ adjustable	IP 68	3 x 0.5 mm²	6.8 mm	1.5 m, 3 m, 5 m, 10 m, 5 ft, 10 ft, 20 ft, 30 ft, others on request

Short-circuit resistance
S_+ vs. U_-

Reverse polarity protection
U_+ vs. U_-

Overvoltage protection
DC 36 V

Insulation voltage
DC 500 V

Connection diagrams

Angular connector DIN 175301-803 A

	2-wire	3-wire
U_+	1	1
U_-	2	2
S_+	-	3

Bayonet connector (6-pin)

	2-wire	3-wire
U_+	A	A
U_-	B	B
S_+	-	C

Angular connector DIN 175301-803 with ½ NPT

	2-wire	3-wire
U_+	1	1
U_-	2	2
S_+	-	3

½ NPT conduit male, with cable outlet

	2-wire	3-wire
U_+	red	red
U_-	black	black
S_+	-	brown

Circular connector M12 x 1 (4-pin)

	2-wire	3-wire
U_+	1	1
U_-	3	3
S_+	-	4

Cable outlets

	2-wire	3-wire
U_+	brown	brown
U_-	green	green
S_+	-	white
Shield	grey	grey

Dimensions in mm

Pressure transmitter model S-10

with angular connector DIN 175301-803 A

ø27
27
≈48
≈82
≈54
20
G1/2B
EN837
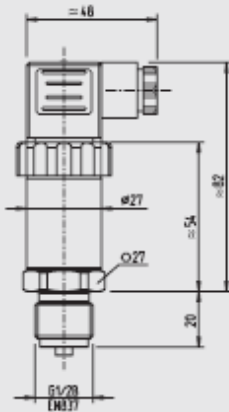
Weight: approx. 0.2 kg

with angular connector DIN 175301-803 with ½ NPT

ø27
27
≈44
≈82
≈54
20
G1/2B
EN837
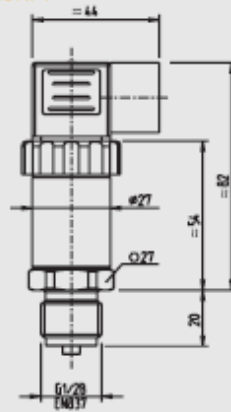
Weight: approx. 0.2 kg

with circular connector M12 x 1 (4-pin)

M12x1
ø27
27
≈67
≈54
20
G1/2B
EN837
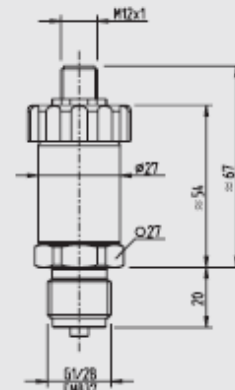
Weight: approx. 0.2 kg

with bayonet connector (6-pin)
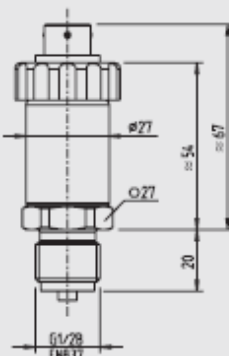
ø27
27
≈67
≈54
20
G1/2B
EN837

Weight: approx. 0.2 kg

with ½ NPT conduit male, with cable outlet

1/2NPT
ø27
27
≈73
20
G1/2B
EN837
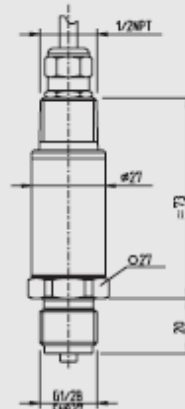
Weight: approx. 0.2 kg

with cable outlet, standard

ø27
27
≈54
20
G1/2B
EN837
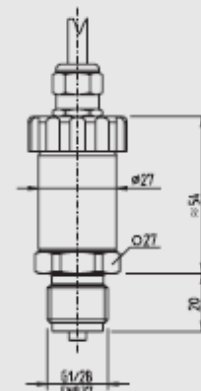
Weight: approx. 0.2 kg

with cable outlet, not adjustable

ø27
27
≈50
20
G1/2B
EN837

Weight: approx. 0.2 kg

with cable outlet, adjustable

ø27
27
≈57
20
G1/2B
EN837
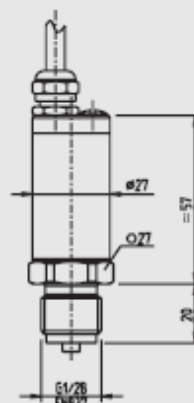
Weight: approx. 0.2 kg

I.3 SOMAS Butterfly Valve Specifications

Temperature performance

The VSS is designed to operate at very high temperature and still maintain tight shutoff over a long period of time. The standard material combination for VSS exhaust gas valve is based on 1.4408 material for applications up to 550°C.

	Temp	0°C	100°C	150°C	200°C	250°C	300°C	350°C	400°C	450°C	500°C	550°C	600°C	650-700°C
1.4408	PN 25	25	25	22.7	21	19.8	18.5	17.8	17.1	16.8	16.5	16.3	N/A	N/A
1.4552	PN 25	25	25	23.3	22.1	21	19.8	19.1	18.5	18.1	17.7	16.9	10.2	Contact SOMAS

Tightness class

The tightness class dependent on application to the chosen material in the seat ring.

Metal seat Code D EN 60534-4 V (ASME B16-104 Class V)

Flow characteristics
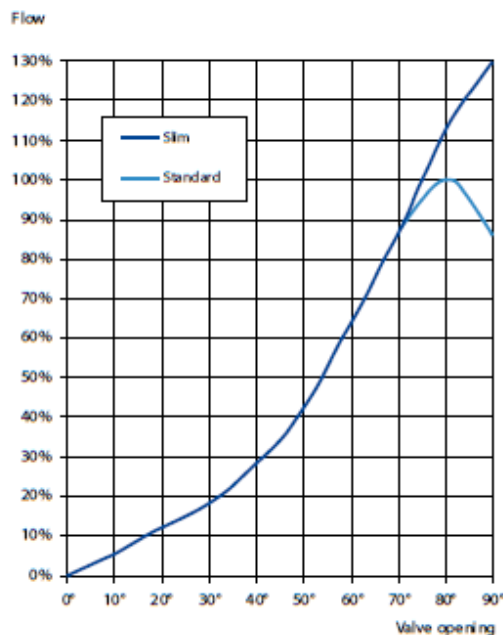
Liquid pressure recovery factor F_L

Factor	Opening angle								
F_L	0.88	0.86	0.82	0.80	0.74	0.68	0.61	0.60	0.59

Factor F_L is valid for all sizes

Factor F_{LP}

Factor	Opening angle								
F_{LP}	0.88	0.86	0.82	0.80	0.74	0.68	0.61	0.60	0.59

Factor F_{LP} is valid for all sizes

Pipe geometry factor F_P

Valve DN	Pipe DN	10°	20°	30°	40°	50°	60°	70°	80°	90°
80	100				0.99	0.99	0.96	0.93	0.91	0.93
	150	1.0	1.0	0.99	0.98	0.97	0.92	0.86	0.83	0.86
	200				0.97	0.94	0.88	0.81	0.77	0.81
100	150				0.98	0.97	0.93	0.88	0.84	0.88
	200	1.0	1.0	0.99	0.97	0.94	0.87	0.80	0.76	0.80
	250				0.96	0.93	0.85	0.77	0.72	0.77
125	150				0.98	0.95	0.91	0.91	0.88	0.91
	200	1.0	1.0	0.99	0.95	0.89	0.83	0.83	0.79	0.83
	250				0.93	0.86	0.78	0.78	0.74	0.78
150	200				0.98	0.95	0.91	0.91	0.88	0.91
	250	1.0	1.0	0.99	0.95	0.89	0.83	0.83	0.79	0.83
	300				0.93	0.86	0.78	0.78	0.74	0.78
200	250				0.99	0.98	0.96	0.93	0.91	0.93
	300	1.0	1.0	0.99	0.98	0.96	0.92	0.86	0.83	0.86
	350				0.97	0.94	0.88	0.81	0.77	0.81
250	300	1,00	1,00	1,00	0,99	0,99	0,97	0,95	0,93	0,95
	350	1,00	1,00	0,99	0,99	0,97	0,93	0,88	0,85	0,88
	400	1,00	1,00	0,99	0,98	0,95	0,90	0,83	0,80	0,83
300	350	1,00	1,00	1,00	1,00	0,99	0,98	0,96	0,95	0,96
	400	1,00	1,00	0,99	0,99	0,97	0,94	0,90	0,87	0,90
	500	1,00	1,00	0,99	0,97	0,95	0,89	0,82	0,78	0,82
350	400	1,00	1,00	1,00	1,00	0,99	0,98	0,97	0,96	0,97
	450	1,00	1,00	1,00	0,99	0,98	0,95	0,92	0,90	0,92
	500	1,00	1,00	0,99	0,98	0,97	0,92	0,87	0,84	0,87
400	450	1,00	1,00	1,00	1,00	0,99	0,99	0,97	0,97	0,97
	500	1,00	1,00	1,00	0,99	0,98	0,96	0,93	0,91	0,93
	600	1,00	1,00	0,99	0,98	0,96	0,91	0,85	0,82	0,85
450	500	1,00	1,00	0,91	1,00	0,99	0,99	0,98	0,97	0,98
	600	1,00	1,00	0,68	0,99	0,97	0,94	0,89	0,87	0,89
	650	1,00	1,00	0,62	0,98	0,96	0,91	0,86	0,82	0,86
500	600	1,00	1,00	1,00	0,99	0,99	0,97	0,95	0,93	0,95
	650	1,00	1,00	1,00	0,99	0,98	0,95	0,91	0,89	0,91
	700	1,00	1,00	0,99	0,98	0,97	0,93	0,88	0,85	0,88
600	650	1,00	1,00	1,00	1,00	1,00	0,99	0,99	0,98	0,97
	700	1,00	1,00	1,00	1,00	0,99	0,98	0,96	0,93	0,91
	800	1,00	1,00	0,99	0,99	0,97	0,94	0,90	0,84	0,80
650	700	1,00	1,00	1,00	1,00	1,00	0,99	0,99	0,98	0,97
	800	1,00	1,00	1,00	0,99	0,98	0,96	0,93	0,89	0,87
	900	1,00	1,00	0,99	0,98	0,97	0,93	0,88	0,82	0,78
700	800	1,00	1,00	1,00	1,00	0,99	0,98	0,97	0,96	0,97
	900	1,00	1,00	1,00	0,99	0,98	0,95	0,91	0,89	0,91
	1000	1,00	1,00	0,99	0,98	0,96	0,92	0,87	0,83	0,87
800	900	1,00	1,00	1,00	1,00	0,99	0,98	0,97	0,96	0,97
	1000	1,00	1,00	1,00	0,99	0,98	0,96	0,93	0,90	0,93
	1200	1,00	1,00	0,99	0,98	0,96	0,91	0,85	0,81	0,84

Standard disc - Capacity factor Kv and Resistance factor ξ

DN	Disc	0°	10°	20°	30°	40°	50°	60°	70°	80°	90°	ξ 80°
80	Std	0	14	31	48	73	108	165	203	235	205	1.17
100	Std	0	21	45	70	107	158	240	324	375	326	1.13
125	Std	0	35	75	116	177	262	400	520	605	523	1.06
150	Std	0	50	108	168	256	379	580	780	905	784	0.98
200	Std	0	89	193	299	457	675	1030	1390	1610	1397	0.98
250	Std	0	142	307	476	727	1076	1650	2211	2555	2222	0.95
300	Std	0	207	446	692	1058	1566	2400	3219	3720	3235	0.93
350	Std	0	279	602	934	1427	2111	3230	4341	5020	4362	0.94
400	Std	0	371	800	1242	1898	2809	4300	5775	6675	5805	0.91
450	Std	0	482	1039	1618	2472	3661	5630	7555	8732	7594	0.85
500	Std	0	584	1258	1951	2981	4413	6760	9071	10485	9117	0.90
600	Std	0	853	1839	2851	4375	6448	9880	13256	15325	13223	0.87
700	Std	0	1157	2494	3867	5909	8746	13400	17981	20780	18071	0.88
800	Std	0	1525	3289	5100	7793	11534	17670	23711	27405	23830	0.86

Relation between Kv and Cv: Kv = 0.86 x Cv

Slim disc - Capacity factor Kv and Resistance factor ξ

DN	Disc	0°	10°	20°	30°	40°	50°	60°	70°	80°	90°	ξ90°
600	Slim	0	853	1839	2851	4357	6448	9880	13256	17324	19923	0.52
650	Slim	0	1002	2160	3349	5117	7573	11604	15569	20347	23400	0.52
700	Slim	0	1157	2494	3867	5909	8746	13400	17981	23491	27015	0.52
800	Slim	0	1525	3289	5100	7793	11534	17670	23711	30980	35627	0.51

Max. allowable pressure drops/torque figures

Maximum allowable pressure drops are valid at 20° C (see below).

Valve DN	PN	Max. pressure drop. bar at opening angle			Torque min. at ΔP		Torque min. at ΔP		Torque max. shaft
		0°	60°	80°	bar	Nm	bar	Nm	Nm
80	25	25	15	6	≤ 10	100	> 10	120	150
100	25	25	15	6	≤ 10	120	> 10	165	220
125	25	25	14	6	≤ 10	180	> 10	220	260
150	25	25	12	2.7	≤ 10	200	> 10	250	300
200	25	25	9	1.8	≤ 10	250	> 10	290	350
250	25	25	7.5	1.7	≤ 10	400	> 10	500	600
300	25	24	6.5	1.6	≤ 10	500	> 10	620	750
350	25	22	5.5	1.5	≤ 8	800	> 8	1000	1200
400	25	20	5	1.43	≤ 8	1000	> 8	1350	1600
450	25	18	4.7	1.25	≤ 7	1350	> 7	1900	2250
500	25	15	4.4	1.19	≤ 6	1900	> 6	2700	3250
600	25	12	4	1.13	≤ 5	2400	> 5	2900	3500
650	25	10	3.9	1.1	≤ 5	2800	> 5	3250	3750
700	25	8	2.7	0.75	≤ 4	3200	> 4	4200	5000
800	25	8	2.6	0.75	≤ 4	4000	> 4	5000	6000

DN 450 - 1200
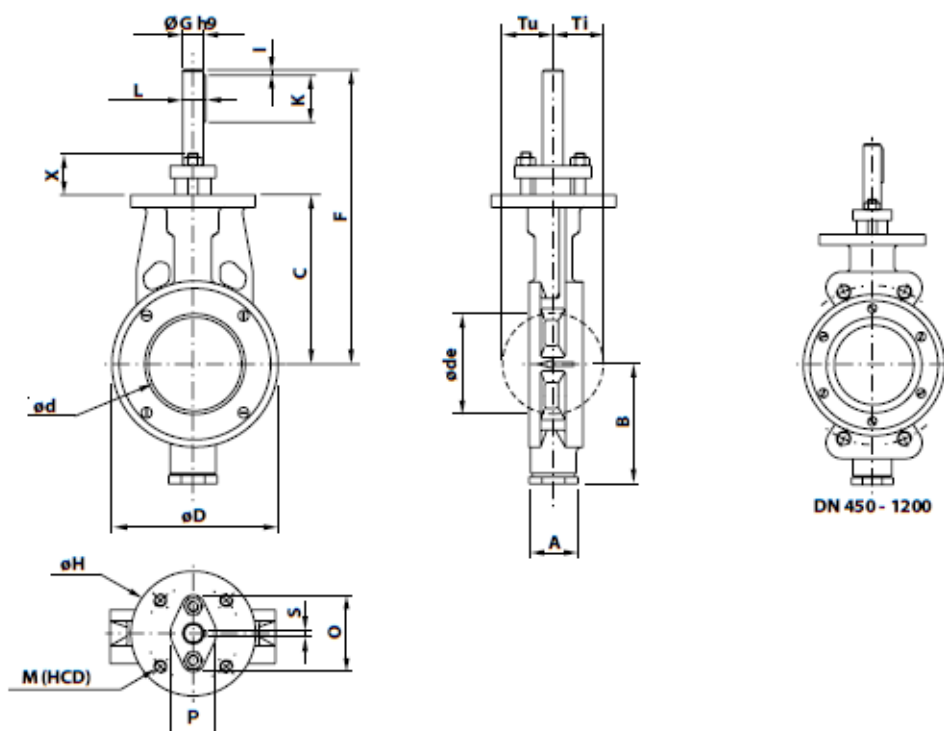
Butterfly valve type VSS

DN	A	B	C	ød	øde	øD	F	øG	øH	I	K	L	M	(HCD)	O	P	S	X	Tu	Ti	weight
80	50	120	150	70	60	133	270	20	120	5	45	22.5	M12	90	74	44	6	40	41	37	7
100	52	120	163	90	86	160	283	20	120	5	45	22.5	M12	90	74	44	6	40	52	48	9
125	56	135	175	116	110	190	295	20	120	5	45	22.5	M12	90	74	44	6	40	64	60	11
150	56	155	195	140	138	215	315	25	120	5	45	28	M12	90	78	50	8	404	77	73	14
200	60	180	235	187	186	270	355	25	120	5	45	28	M12	90	78	50	8	50	100	96	19
250	68	205	275	236	235	324	410	30	150	5	60	33	M12	120	92	58	8	50	124	120	30
300	78	240	290	285	285	375	425	35	150	5	50	38	M12	120	100	64	10	50	149	145	43
350	78	320	315	331	330	435	450	40	150	5	50	43	M12	120	108	70	12	50	172	167	56
400	102	360	340	382	380	490	550	50	150	10	80	53.8	M12	120	124	82	14	50	199	194	85
450	114	385	370	429	425	535	580	50	150	10	80	53.8	M12	120	124	82	14	50	223	217	109
500	127	415	400	479	475	59	610	60	200	10	90	64	M16	160	147	96	18	60	249	242	150
600	154	475	450	579	575	695	675	70	200	10	110	74.5	M16	160	162	112	20	60	300	292	221
650	154	525.6	515	620		780	740	70	200	10	110	75	M16	160	162	112	20	60			
700	165	530	515	674	675	800	730	70	200	10	110	74.5	M16	160	162	112	20	60	343	343	300
800	190	600	580	774	775	910	825	80	200	10	120	64	M16	160	183	120	22	76	393	393	420

Flange standard

SOMAS butterfly valve type VSS in this data sheet is of wafer type for mounting between flanges PN 10-25.

For other standards consult SOMAS.

The valve can also be delivered in lugged design.

The valve can be ordered in other flange standards.

When ordering, please always state the type and rating of the counter flanges. See the valve specifiction system on page 8, code 11.

Seat design

The valves with a nominal size between DN80 - DN 800 have a Y-shaped metal seat according to code D.

Also check the valve specification system (code 6) to find further seat alternatives.

Further technical information

Technical data for the materials used in the SOMAS valves. flange standard. steam data. etc. can be found in section 6 of the SOMAS catalogue.

Actuators and accessories

The valves can be fitted with SOMAS manual. on/off or control actuators in accordance with the selection table. The valves will then be delivered as tested units ready for installation.

Check sections 4 and 5 of the SOMAS catalogue. where positioners. limit switches and solenoid valves are also presented.

We can also fit other types of actuators and accessories in accordance with your specification.

Supplemental information

Note: Use gaskets with the correct inside diameter to ensure that pressure is applied on the cover plate

Valve DN	Gaskets according to EN 15414-1				Valve DN	Gaskets according to ASME B16.21 RF	
	Max Inside dia di (mm)	Outside dia. (dy) (mm)				Max Inside dia di (mm)	Outside dia. (dy) (mm)
		PN 10	PN 16	PN 25			Class 150
80	89	142	142	142	80	89	136
100	115	162	162	168	100	114	174
125	141	192	192	194	125	141	196
150	169	218	218	224	150	168	222
200	220	273	273	284	200	219	279
250	273	328	329	340	250	273	340
300	324	378	384	400	300	324	410
350	356	438	444	457	350	356	451
400	407	489	495	514	400	406	515
450	458	539	555	564	450	457	550
500	508	594	617	624	500	508	606
600	610	695	734	731	600	610	720
650	*	*	*	*	650	660	775
700	712	810	804	833	700	711	831
800	813	917	911	942	800	813	940

I.4 SOMAS Pneumatic Actuator Specifications

Mounting

The standard actuator mounting is perpendicular to the pipeline as shown in position A (see Fig.1).

Position B, C or D is available on request (specify when ordering).

Always specify mounting position when ordering.

The actuator is mounted in position A if the position is not stated.
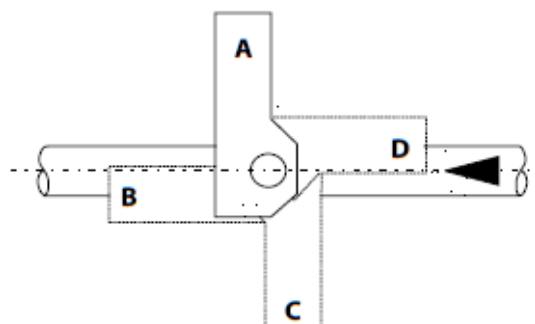
Fig.1   Mounting

Torque

The linear motion from the piston in converted into a rotary motion via a linkage mechanism. The curve shows the output torque from the actuator as a function of the actuator shaft angle (see Fig.2).

Maximum torque is achieved in the closed position which corresponds to the demand of ball segment valves, ball valves and metal seated butterfly valves.

For butterfly valves, the dynamic torque can be high in case of high differential pressure across the valve. This increased torque demand is normally covered by the actuator selection tables.

The highest specified value for each size, in the tables below, is the upper limit of permitted transfer torque.
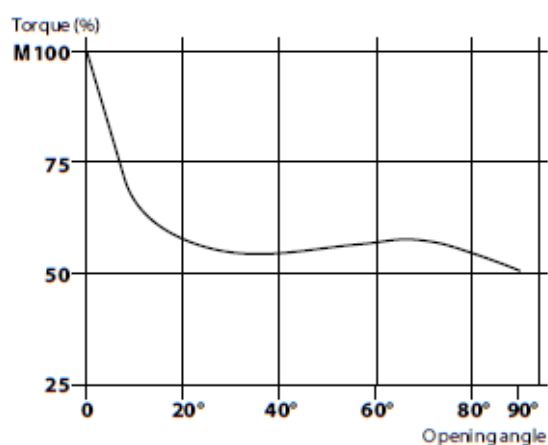
Fig.2   Double acting actuator type A

Type	DA	Closing torque M100 (Nm) at air supply 5,5 bar SC (Spring to close)	SO (Spring to open)	Type	DA	Closing torque M100 (Nm) at air supply 4 bar SC (Spring to close)	SO (Spring to open)	Type	DA	Cylinder volume (litre) SC (Spring to close)	SO (Spring to open)
A11	84			A11	61			A11	0.22		
A13	140	55	55	A13	102	45	45	A13	0.38	0.38	0.38
A21	196			A21	142			A21	0.42		
A22	413			A22	300			A22	0.8		
A23	441	150	150	A23	370	150	150	A23	1.12	1.1	1.1
A24		300	300	A24	528	300	300	A24	1.5	2.2	2.2
A31	761			A31	553			A31	1.74		
A32	1609			A32	1170			A32	3.2		
A33		600	600	A33	1500	600	600	A33	4.7	4.7	4.7
A34		1200	1200	A34	2100	1200	1200	A34	6.2	9.2	9.2
A41	2914			A41	2118			A41	6.5		
A42	6117			A42	4447			A42	12		
A43		2000	2000	A43	5750	2000	2000	A43	17.5	17.5	17.5
A44		4000	4000	A44	8000	4000	4000	A44	23	33.7	33.7
A51	9552			A51	6945			A51	22.1		
A52	19925			A52	14485			A52	40.6		

Measure T and ØD is valid only for Ødi 15-50
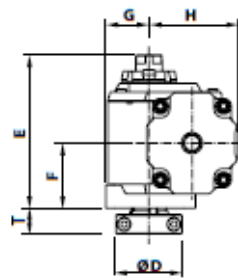
Mounting pattern according to ISO 5211
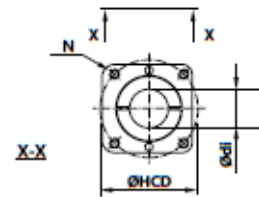
VDI/VDE
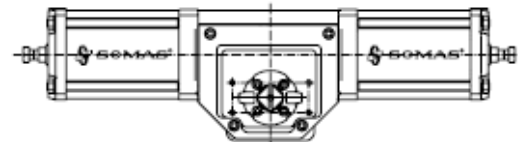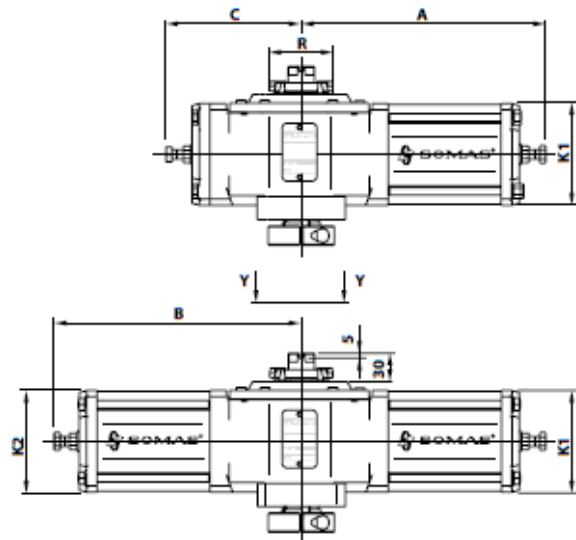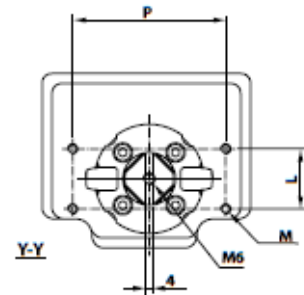
Actuator type A (DA) double acting

Type	A	B	C	Ødi	ØD	E	F	G	H	K1	K2	L	M	N	P	R	T	ØHCD	Air-conn.	Weight
A11-F07	215	–	90	15-20	48	128	50	37	73	84	–	30	M5	M8	80	56	14	70	1/4"	3
A13-F07	250	–	90	15-20	48	128	50	37	83	106	–	30	M5	M8	80	56	14	70	1/4"	5
A21-F10	255	–	140	20-30	69	160	68	45	94	106	–	30	M5	M10	80	66	27	102	1/4"	7,5
A22-F10	255	260	–	20-30	69	160	68	45	94	106	106	30	M5	M10	80	66	27	102	1/4"	9
A23-F10	305	–	140	20-30	69	160	68	45	117	152	–	30	M5	M10	80	66	27	102	1/4"	11
A24-F10	305	310	–	20-30	69	160	68	45	117	152	106	30	M5	M10	80	66	27	102	1/4"	15
A31-F14	380	–	215	30-50	98	225	107,5	69	144	152	–	30	M5	M16	130	66	40	140	1/4"	23
A32-F14	380	395	–	30-50	98	225	107,5	69	144	152	152	30	M5	M16	130	66	40	140	1/4"	29
A33-F14	470	–	215	30-50	98	225	107,5	69	183	228	–	30	M5	M16	130	66	40	140	3/8"	36
A34-F14	470	485	–	30-50	98	225	107,5	69	183	228	152	30	M5	M16	130	66	40	140	1/4"+3/8"	53
A41-F16	550	–	315	40-80	98	309	153	97	211	228	–	50	M6	M20	200	66	40	165	3/8"	70
A42-F16	545	560	–	40-80	98	309	153	97	211	228	228	50	M6	M20	200	66	40	165	3/8"	85
A43-F16	680	–	315	40-80	98	309	153	97	279	354	–	50	M6	M20	200	66	40	165	1/2"	142
A44-F16	680	695	–	40-80	98	309	153	97	279	354	228	50	M6	M20	200	66	40	165	3/8"+1/2"	157
A51-F30	745	–	370	70-100	–	412	198	130	314	354	–	50	M6	M20	200	66	–	298	1/2"	198
A52-F30	745	760	–	70-100	–	412	198	130	314	354	354	50	M6	M20	200	66	–	298	1/2"	234

Actuator type A (SC/SO) single acting

Type	A	B	C	Ødi	ØD	E	F	G	H	K1	K2	L	M	N	P	R	T	ØHCD	Air-conn.	Weight
A13-F07	325	–	90	15-20	48	128	50	37	83	106	–	30	M5	M8	80	56	14	70	1/4"	7
A23-F10	415	–	140	20-30	69	160	68	45	117	152	–	30	M5	M10	80	66	27	102	1/4"	15
A24-F10	415	420	–	20-30	69	160	68	45	117	152	152	30	M5	M10	80	66	27	102	1/4"	24,5
A33-F14	660	–	215	30-50	98	225	107,5	69	183	228	–	30	M5	M16	130	66	40	140	3/8"	56
A34-F14	665	680	–	30-50	98	225	107,5	69	183	228	228	30	M5	M16	130	66	40	140	3/8"	84
A43-F16	920	–	315	40-80	98	309	153	97	279	354	–	50	M6	M20	200	66	40	165	1/2"	156
A44-F16	925	935	–	40-80	98	309	153	97	279	354	354	50	M6	M20	200	66	40	165	1/2"	210

Weight = Weight for actuator without mounting kit

Ordering example

Pneumatic double acting actuator type A 32-DA. Mounting position A.

When ordering actuators separately, please specify also the mounting kit you require for the actual valve type.

Material specification

Housing, cover, end cover:	Aluminium (Duasolid painted)
Cylinder:	Aluminium (Duasolid painted)
Tie rod:	EN 1.4305
Piston seal:	Carbon filled PTFE + O-ring made of cold-resistant nitrile rubber
Screws/nuts:	Acidproof steel
Connection: (between actuator and accessories)	Plastic tubing (standard) Acidproof steel tubing (option)

Technical specification

Air supply:	4 - 8 bar
Rotary motion:	Max 95° adjustable travel stops
Ambient temperature:	− 40 to + 90 °C (standard) (+ 120 °C Option O-ring made of Viton)

I.5 SIPART PS2 Electropneumatic Positioner Specifications

Technical specifications all versions

Technical specifications

SIPART PS2 (all versions)

General data

Travel range (linear actuators)	3 ... 130 mm (0.12 ... 5.12 inch) (angle of feedback shaft 16 ... 90°)
Angle of rotation (part-turn actuators)	30 ... 100°
Installation	
• On linear actuators	Using attachment set 6DR4004-8V and where necessary with an additional lever arm 6DR4004-8L on actuators according to IEC 534-6 (NAMUR) with ribs, bars or flat face
• On part-turn actuators	Using attachment set 6DR4004-8D on actuators with mounting plane according to VDI/VDE 3845 and DIN 3337: The required mounting console has to be provided on the actuator side; shaft with groove and female thread M6
Controller	
• Five-point switch	Self-adjusting
• Dead zone	
- dEbA = Auto	Self-adjusting or can be set as fixed value
- dEbA = 0.1 ... 10%	Self-adjusting or can be set as fixed value
A/D converter	
• Scan time	10 ms
• Resolution	≤ 0.05%
• Transmission error	≤ 0.2%
• Temperature effect	≤ 0.1%/10 K (≤ 0.1%/18 °F)
Cycle time	
• 20 mA/HART device	20 ms
• PA device	60 ms
• FF device	60 ms (min. loop time)
Binary input BE1 (terminals 9/10; electrically connected to the basic device)	Suitable only for floating contact; max. contact load < 5 mA with 3 V
Degree of protection	IP66 to EN 60 529/NEMA 4x
CE marking	Conformity as regards EMC Directive 89/336 EC in accordance with the following standards
EMC requirements	EN 61326/A1 Appendix A.1 and NAMUR NE21 August 98
Material	
• Housing	
- 6DR5..0-... (plastic)	Glass-fiber-reinforced Macrolon
- 6DR5..1-... (metal)	GD AlSi12
- 6DR5..2-... (stainless steel)	Austenitic stainless steel mat. No. 1.4581
- 6DR5..5-... (metal, pressure-proof)	GK AlSi12
• Pressure gauge block	Aluminium AlMgSi, anodized
Vibration resistance	
• Harmonic oscillations (sine-wave) according to DIN EN 60062-2-6/05.96	3.5 mm (0.14 inch), 2 ... 27 Hz 3 cycles/axis 98.1 m/s² (321.84 ft/s²), 27 ...300 Hz, 3 cycles/axis
• Bumping (half-sine) to DIN EN 60068-2-29/03.95	150 m/s² (492 ft/s²), 6 ms, 1000 shocks/axis

• Noise (digitally controlled) to DIN EN 60068-2-64/08.95	10 ... 200 Hz; 1 (m/s²)²/Hz (3.28 (ft/s²)²/Hz)
	200 ... 500 Hz; 0.3 (m/s²)²/Hz (0.98 (ft/s²)²/Hz)
	4 hours/axis
• Recommended continuous duty range of the complete fitting	≤ 30 m/s² (≤ 98.4 ft/s²) without resonance sharpness
Weight, basic device	
• Plastic casing	Approx. 0.9 kg (1.98 lb)
• Metal casing, aluminium	Approx. 1.3 kg (2.86 lb)
• Metal casing, stainless steel	Approx. 3.9 kg (8.58 lb)
• Metal casing EEx d version	Approx. 5.2 kg (11.46 lb)
Dimensions	See "Dimensional drawings"
Climate class 4	To DIN EN 60721-3-4
• Storage[1]	1K5, but -40 ... +80 °C (1K5, but -40 ... +176 °F)
• Transport[1]	2K4, but -40 ... +80 °C (2K4, but -40 ... +176 °F)
• Operation[2]	4K3, but -30 ... +80 °C[3] (4K3, but -22 ... +176 °F)

Certificate and approvals

Classification according to pressure equipment directive (DRGL 97/23/EC)	For gases of fluid group 1, complies with requirements of article 3, paragraph 3 (sound engineering practice SEP)

Pneumatic data

Power supply	Compressed air, nitrogen or cleaned natural gas
• Pressure	1.4 ... 7 bar (20.3 ... 101.5 psi): Sufficiently greater than max. drive pressure (actuating pressure)
Air quality to ISO 8573-1	
• Solid particle size and density	Class 2
• Pressure dew point	Class 2 (min. 20 K (36 °F) below ambient temperature)
• Oil content	Class 2
Unthrottled flow	
• Inlet air valve (ventilate actuator)[4]	
- 2 bar (29 psi)	4.1 Nm³/h (18.1 USgpm)
- 4 bar (58 psi)	7.1 Nm³/h (31.3 USgpm)
- 6 bar (87 psi)	9.8 Nm³/h (43.1 USgpm)
• Outlet air valve (exhaust actuator)[4]	
- 2 bar (29 psi)	8.2 Nm³/h (36.1 USgpm)
- 4 bar (58 psi)	13.7 Nm³/h (60.3 USgpm)
- 6 bar (87 psi)	19.2 Nm³/h (84.5 USgpm)
Valve leakage	< 6·10⁻⁴ Nm³/h (0.0026 USgpm)
Throttle ratio	Adjustable up to ∞ : 1
Power consumption in the controlled state	< 3.6·10⁻² Nm³/h (0.158 USgpm)
Types of actuators	
• In casing	Single-action and double-action
• In aluminium casing	Single-action
• In flameproof casing	Single-action and double-action
• In stainless steel casing	Single-action and double-action

[1] During commissioning at ≤ 0 °C (≤ 32 °F) make sure that the valves are flushed long enough with the dry medium.
[2] At ≤ -10 °C (14 °F) the display refresh rate of the LCD is limited. Only T4 is permissible when using I_y module.
[3] -25 ... +75 °C (-13 ... +167 °F) for 6DR55.-0G..., 6DR56.-0G..., 6DR55.-0D... and 6DR56..-0D...
[4] With EEx d version (6DR5..5-...) the values are reduced by approx. 20%.

Technical specifications

SIPART PS2	Basic device without Ex protection	Basic device with Ex d protection (flameproof casing)	Basic device with Ex ia/ib protection	Basic device with Ex n/dust protection
Explosion protection to ATEX	Without	Ex d II 2 G Ex d II C T6	Ex ia/ib II 2 G Ex ia/ib II C T6	Ex n II 3 G Ex nA nL[nL] IIC T6 Dust II 3 D Ex tD A22 IP66 T100°C
Mounting location		Zone 1	Zone 1	Zone 2/22
Permissible ambient temperature for operation At ≤ -10 °C (+14 °F) the display refresh rate of the LCD is limited. (for basic devices with EEx ia/ib and EEx n protection the following applies: Only T4 is permissible when using I_y module.)	-30 ... +60 °C (-22 ... +176 °F)	T4: -30 ... +60 °C (-22 ... +176 °F) T5: -30 ... +65 °C (-22 ... +149 °F) T6: -30 ... +50 °C (-22 ... +122 °F)		

Electrical data

Input

2-wire connection (terminals 6/8)

Rated signal range	4 ... 20 mA	4 ... 20 mA	4 ... 20 mA	4 ... 20 mA
Current to maintain the power supply	≥ 3.6 mA	≥ 3.6 mA	≥ 3.6 mA	≥ 3.6 mA
Required load voltage U_B (corresponds to Ω at 20 mA)				
• Without HART (6DR50..)				
- Typical	6.36 V (corresponds to 318 Ω)	6.36 V (corresponds to 318 Ω)	7.8 V (corresponds to 390 Ω)	7.8 V (corresponds to 390 Ω)
- Max.	6.48 V (corresponds to 324 Ω)	6.48 V (corresponds to 324 Ω)	8.3 V (corresponds to 415 Ω)	8.3 V (corresponds to 415 Ω)
• Without HART (6DR53..)				
- Typical	7.9 V (corresponds to 395 Ω)	–	–	–
- Max.	8.4 V (corresponds to 420 Ω)	–	–	–
• With HART (6DR51..)				
- Typical	6.6 V (corresponds to 330 Ω)	6.6 V (corresponds to 330 Ω)	–	–
- Max.	6.72 V (corresponds to 336 Ω)	6.72 V (corresponds to 336 Ω)	–	–
• With HART (6DR52..)				
- Typical	–	8.4 V (corresponds to 420 Ω)	8.4 V (corresponds to 420 Ω)	8.4 V (corresponds to 420 Ω)
- Max.	–	8.8 V (corresponds to 440 Ω)	8.8 V (corresponds to 440 Ω)	8.8 V (corresponds to 440 Ω)
• Static destruction limit	± 40 mA		–	–
Internal capacitance C_i				
• Without HART	–	–	22 nF	22 nF (at "nL")
• With HART	–	–	7 nF	7 nF (at "nL")
Internal inductance L_i				
• Without HART	–	–	0.12 mH	0.12 mH (at "nL")
• With HART	–	–	= 0.24 mH	0.24 mH (at "nL")
For connection to power circuits with the following max. ratings	–	–	intrinsically safe U_i = 30 V DC I_i = 100 mA P_i = 1 W	at "nA" and "tD": U_n = 30 V DC I_n = 100 mA at "nL": U_i = 30 V DC I_i = 100 mA

Technical specifications

Option modules	Without Ex protection (EEx d also)	With Ex protection Ex ia/ib	With Ex n/dust protection
Ex protection to ATEX	–	II 2G Ex ia/ib II C T4/T5/T6 (only in conjunction with)	Ex n II 3 G Ex nA nL[nL] II C T6 Dust II 3 D Ex tD A22 IP66 T100°C
Mounting location	–	Zone 1	Zone 2/22
Permissible ambient temperature for operation (For devices with Ex protection: Only in conjunction with the basic device 6DR5... -.E.... Only T4 is permissible when using I_y module)	-30 ... +80 °C (-22 ... +176 °F)	T4: -30 ... +80 °C (-22 ... +176 °F)[1] T5: -30 ... +65 °C (-22 ... +149 °F)[1] T6: -30 ... +50 °C (-22 ... +122 °F)[1]	
Alarm module	6DR4004-8A (without Ex protection)	6DR4004-6A (with Ex protection)	6DR4004-6A (with Ex protection)
Binary alarm outputs A1, A2 and alarm output			
Signal status High (not responded) Signal status Low* (responded) (* Low is also the status when the basic device is faulty or has not electric power supply)	Active, R = 1 kΩ, +3/-1%* Disabled, I_R < 60 µA (* When used in the flameproof casing the current consumption is limited to 10 mA per output.)	≥ 2.1 mA ≤ 1.2 mA (Switching threshold with supply to EN 60947-5-6: U_H = 8.2 V, R_i = 1kΩ)	≥ 2.1 mA ≤ 1.2 mA (Switching threshold with supply to EN 60947-5-6: U_H = 8.2 V, R_i = 1kΩ)
Internal capacitance C_i	–	5.2 nF	5.2 nF (at "nL")
Internal inductance L_i	–	Negligible	Negligible
Power supply U_H	≤ 35 V	–	–
Connection to power circuits with with the following max. ratings	–	intrinsically safe switching amplifier EN 60947-5-6 U_o =15.5 V DC I_k = 25 mA, P = 64 mW	at "nA" and "tD": Un = 15.5 V DC at "nL": Ui = 15.5 V DC Ii = 25 mA
Binary input BE2			
• Electrically connected to the basic device			
- Signal status 0	Floating contact, open	Floating contact, open	Floating contact, open
- Signal status 1	Floating contact, closed	Floating contact, closed	Floating contact, closed
- Contact load	3 V, 5 µA	3 V, 5 µA	3 V, 5 µA
• Electrically isolated from the basic device			
- Signal status 0	≤ 4.5 V or open	≤ 4.5 V or open	≤ 4.5 V or open
- Signal status 1	≥ 13 V	≥ 13 V	≥ 13 V
- Natural resistance	≥ 25 kΩ	≥ 25 kΩ	≥ 25 kΩ
Static destruction limit	± 35 V	–	–
Internal inductance and capacitance	–	Negligible	Negligible
Connection to power circuits with the following max. ratings	–	Intrinsically safe Ui = 25.2 V	at "nA" and "tD": Un = 25.2 V DC at "nL": Ui = 25.2 V DC
Electrical isolation	The 3 outputs, the input BE2 and the basic device are electrically isolated from each other.		
Test voltage	840 V DC, 1 s	840 V DC, 1 s	840 V DC, 1 s

[1] Only in conjunction with the basic device 6DR5...-E..... With ly module only T4 permitted.

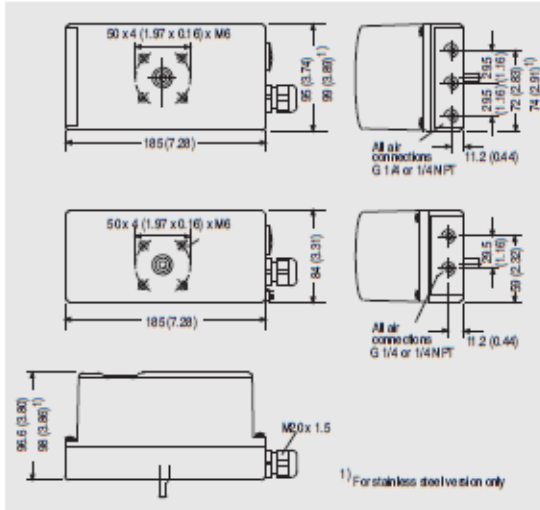| Option modules	Without Ex protection	With Ex protection EEx ia/ib	With Ex n/dust protection
SIA module **Limit switches with slot-type initiators and alarm output**	6DR4004-8G (without Ex protection) (not for Ex-d version)	6DR4004-6G (with Ex protection)	6DR4004-6G (with Ex protection)
Limit switches A1, A2	2-wire connection	2-wire connection	2-wire connection
Ex protection	Without	II 2 G EEx ia/ib IIC T6	II 3 G EEx nA L [L] IIC T6
Connection	2-wire system to EN 60947-5-6 (NAMUR), for switching amplifier to be connected on load side		
2 slot-type initiators	Type SJ2-SN	Type SJ2-SN	Type SJ2-SN
Function	NC (normally closed)	NC (normally closed)	NC (normally closed)
Connection to power circuits with the following max. ratings	nominal voltage 8 V Current consumption: $\geq$ 3 mA (limit value not responded) $\leq$ 1 mA (limit value responded)	intrinsically safe switching amplifier EN 60947-5-6 $U_i = 15.5$ V DC $I_i = 25$ mA, P $i = 64$ mW	at "nA" and "tD": $U_n = 15.5$ V DC $P_n = 64$ mW at "nL": $U_i = 15.5$ V DC $I_i = 25$ mA
Internal capacitance	–	41 nF	41 nF (at "nL")
Internal inductance	–	100 mH	100 mH (at "nL")
Electrical isolation	The 3 outputs are electrically isolated from the basic device.		
Test voltage	840 V DC, 1 s	840 V DC, 1 s	840 V DC, 1 s
Alarm output			
Connection	2-wire system to EN 60947-5-6 (NAMUR), for switching amplifier to be connected on load side $U_H = 8.2$ V, $R_i = 1$ kΩ		
Signal status High (not active)	$R = 1.1$ kΩ	≥ 2.1 mA	≥ 2.1 mA
Signal status Low (active)	$R_i = 10$ kΩ	≤ 1.2 mA	≤ 1.2 mA
Internal capacitance C_i	–	5.2 nF	5.2 nF (bei „nL")
Internal Inductance L_i	–	Negligible	Negligible
Power supply U_H	$U_H \leq 35$ V DC, $I \leq 20$ mA	–	–
For connection to power with the following max. ratings	–	intrinsically safe switching amplifier EN 60947-5-6 $U_i = 15.5$ V DC $I_i = 25$ mA $P_i = 64$ mW	at „nA" and „tD": $U_n = 15.5$ V DC at „nL": $U_i = $ DC 15.5 V $I_i = 25$ mA
Limit value contact module **Limit switches with mechanical ground contact and alarm output**	6DR4004-8K (not for EEx d version)	6DR4004-6K	6DR4004-6K
Limit switches A1, A2			
Ex protection	without	II 2 G Ex ia/ib IIC T6	II 3 G Ex nL [nL] IIC T6 (in progress)
Max. switching current AC/DC	4 A	Connection to intrinsically safe circuit with maximum values: $U_i = 30$ V, $I_i = 100$ mA, $P_i = 750$ mW	Connection to circuits with maximum values: at "nL": $U_i = 30$ V $I_i = 100$ mA,
Max. switching voltage AC/DC	250 V / 24 V	30 V DC	
Internal capacitance C_i	–	Negligible	Negligible
Internal inductance L_i	–	Negligible	Negligible
Electrical isolation	The 3 outputs are electrically isolated from the basic device.		
Test voltage	3150 V DC, 2s	3150 V DC, 2 s	3150 V DC, 2 s
Alarm output			
Connection	2-wire system to EN 60947-5-6 (NAMUR), for switching amplifier to be connected on load side $U_H = 8.2$ V, $R_i = 1$ kΩ		
Signal status High (not active)	$R = 1.1$ kΩ	≥ 2.1 mA	≥ 2.1 mA
Signal status Low (active)	$R_i = 10$ kΩ	≤ 1.2 mA	≤ 1.2 mA
Internal capacitance C_i	–	5.2 nF	5.2 nF (bei „nL")
Internal Inductance L_i	–	Negligible	Negligible
Power supply U_H	$U_H \leq 35$ V DC, $I \leq 20$ mA	–	–
For connection to power with the following max. ratings	–	Intrinsically safe switching amplifier EN 60947-5-6 $U_i = 15.5$ V DC $I_i = 25$ mA $P_i = 64$ mW	at „nL": $U_i = 15.5$ V DC $I_i = 25$ mA

| Option modules	Without Ex protection	With Ex protection EEx ia/ib	With Ex n/dust protection
I_y module	6DR4004-8J (without Ex protection)	6DR4004-6J (with Ex protection)	6DR4004-6J (with Ex protection)
DC output for position feedback	2-wire connection	2-wire connection	2-wire connection
Nominal signal range	4 ... 20 mA, short-circuit-proof	4 ... 20 mA, short-circuit-proof	4 ... 20 mA, short-circuit-proof
Total operating range	3.6 ... 20.5 mA	3.6 ... 20.5 mA	3.6 ... 20.5 mA
Power supply U_H	+12 ... +35 V	+12 ... +30 V	+12 ... +30 V
External load R_B [kΩ]	≤ (U_H [V] - 12 V) /i [mA]	≤ (U_H [V] - 12 V) /i [mA]	≤ (U_H [V] - 12 V) /i [mA]
Transmission error	≤ 0.3%	≤ 0.3%	≤ 0.3%
Temperature effect	≤ 0.1%/10 K (≤ 0.1%/18 °F)	≤ 0.1%/10 K (≤ 0.1%/18 °F)	≤ 0.1%/10 K (≤ 0.1%/18 °F)
Resolution	≤ 0.1%	≤ 0.1%	≤ 0.1%
Residual ripple	≤ 1%	≤ 1%	≤ 1%
Internal capacitance C_i	–	11 nF	11 nF (at "nL")
Internal inductance L_i	–	Negligible	Negligible
For connection to power circuits with the following max. ratings		Intrinsically safe: Ui = 30 V DC Ii = 100 mA Pi = 1 W (only T4)	at "nA" and "tD" Un = 30 V DC In = 100 mA Pn = 1 W (only T4) at "nL": Ui = 30 V DC Ii = 100 mA
Electrical isolation	Electrically isolated from the basic device	Electrically isolated from the basic device	Electrically isolated from the basic device
Test voltage	840 V DC, 1 s	840 V DC, 1 s	840 V DC, 1 s
NCS sensor			
(not for EEx d version)			
Position range			
• Linear actuator	3 ... 130 mm (0.12 ... 5.12 inch), to 200 mm (7.87 inch) on request	3 ... 130 mm (0.12 ... 5.12 inch), to 200 mm (7.87 inch) on request	
• Part-turn actuator	30° ... 100°	30° ... 100°	
Linearity (after correction by SIPART PS2) • Linear actuator	± 1%	± 1%	
• Part-turn actuator	± 1%	± 1%	
Hysteresis	± 0.2%	± 0.2%	
Continuous working temperature	-40 ... +85 °C (-40 ... +185 °F), extended temperature range on request	-40 ... +85 °C (-40 ... +185 °F), extended temperature range on request	
For connection to power circuits with the following max. ratings		Intrinsically safe Ui = 5 V DC	at "nL": Ui = 5 V DC
Internal capacitance Ci	-	10 nF	10 nF (at "nL")
Internal inductance Li	-	240 mH	240 mH (at "nL")
Degree of protection of casing	IP68/NEMA 4X	IP68/NEMA 4X	

Dimensional drawings

Plastic and stainless steel casing (top), aluminium casing (center), plastic and metal casing (bottom), dimensions in mm (inch)
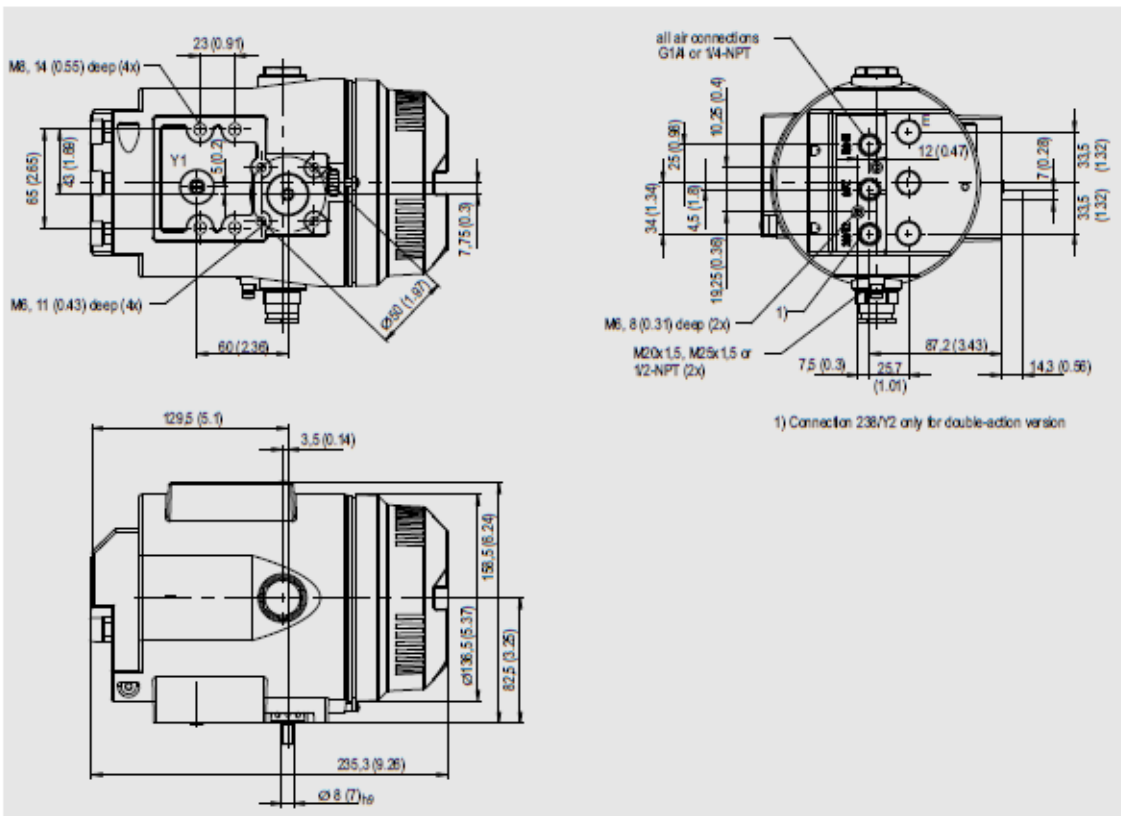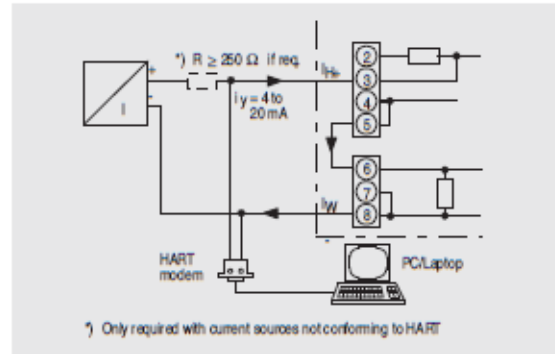
Flameproof casing left, dimensions in mm (inch)

Mounting onto part-turn actuators; mounting plate (scope of delivery of actuator manufacturer), extract from VDI/VDE 3845, dimensions in mm (inch)

Schematics

Electric connection of 2-wire devices (6DR50.. and 6DR51..)

Devices of types 6DR50.. and 6DR51.. are operated in a 2-wire system.
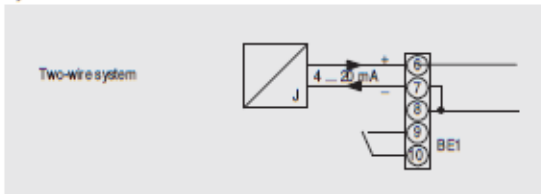
SIPART PS2 electropneumatic positioner, input circuit for 6DR50.. and 6DR51..

Electric connection of PROFIBUS PA device (6DR55..) and FOUNDATION Fieldbus devices (6DR56..)

*) Input for safety shutdown (activated using coding jumper)
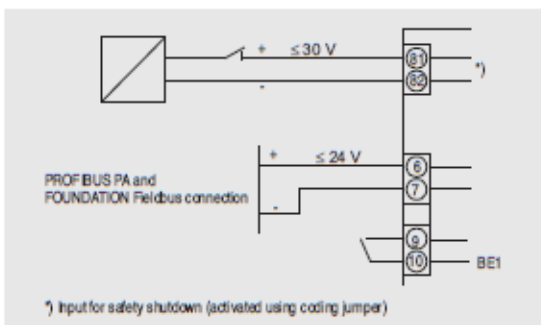
SIPART PS2 PA and SIPART PS2 FF electropneumatic positioner, input circuit for 6DR55.. and 6DR56..

Electric connection of 2-, 3- and 4-wire device (6DR52.. and 6DR53..)

Devices of types 6DR52.. and 6DR53.. can be operated in a 2-, 3- and 4-wire system.

*) Only required with current sources not conforming to HART

SIPART PS2 electropneumatic positioner, example of connection for communication through HART for 6DR52..

*) Jumper between 5 and 7 only for three-wire system
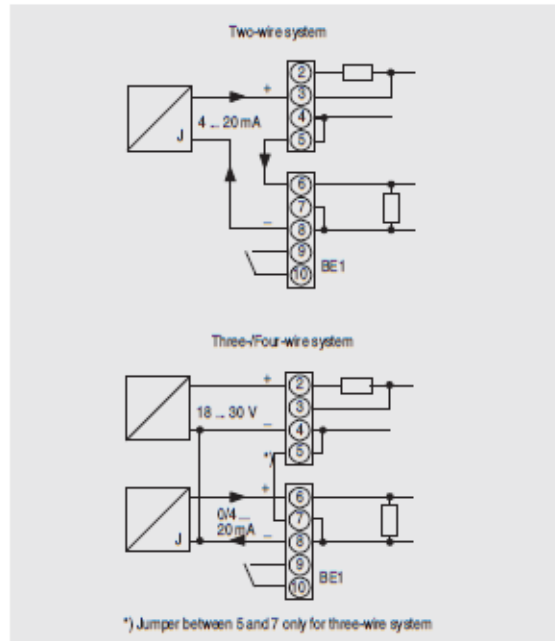
SIPART PS2 electropneumatic positioner, input circuits for 6DR52..

131

I.6 Flow Sensor ZS25 UFA Specifications

**Flow measurement with sensors ZS25
at working temperatures up to +500 °C
optional with integrated and configurable transducer UFA**

Drawing 4

Measurable variable
- standard flow velocity v [m/s] in air/gases

Measuring range
- 0.4 ... 120 m/s

Functional principle
- vane wheel flow sensor
- scanning the vane rotation; non-contact inductive proximity switch

Advantages
- low starting value
- large measuring range span
- maximum fatigue strength thanks to vane wheel which is easy on the bearings
- corrosion resistant
- sterilisable
- high working temperature and pressure ranges
- operates to a large extent irrespective of density and composition of the gas
- low pressure drop
- easy adjustment to process parameter

Vane wheel flow sensor ZS25
(see Page 3 for dimensions)

Design
- insertion probe with AS80 housing

Medium
- air, gas mixtures and clean gases

Range and examples of application
- flow rate measuring, e.g. of air, exhaust gas, process gas
- monitoring laminar flow
- monitoring flow in pharmaceutic works

Humidity in the gas
- relative gas humidity of less than 100 % does not affect the measurement uncertainty

Model designation (example)							
ZS25/25	-350	G	E	350	p10	Ex	ZG4
(1)	(2)	(3)	(4)	(5)	(6)	(7)	(8)

Basic types

Type	Transducer/ Outuput	Article No.
'100 °C' / integrated UFA		
ZS25/25-**250**GE/100/p10/ZG4	UFA-int / 4-20 mA	b002/190-ufa
ZS25/25-**350**GE/100/p10/ZG4	UFA-int / 4-20 mA	b002/191-ufa
ZS25/25-**450**GE/100/p10/ZG4	UFA-int / 4-20 mA	b002/192-ufa
ZS25/25-**550**GE/100/p10/ZG4	UFA-int / 4-20 mA	b002/193-ufa
ZS25/25-**650**GE/100/p10/ZG4	UFA-int / 4-20 mA	b002/194-ufa
'260 °C' / integrated UFA		
ZS25/25-**250**GE/260/p10/ZG4	UFA-int / 4-20 mA	b002/195-ufa
ZS25/25-**350**GE/260/p10/ZG4	UFA-int / 4-20 mA	b002/196-ufa
ZS25/25-**450**GE/260/p10/ZG4	UFA-int / 4-20 mA	b002/197-ufa
ZS25/25-**550**GE/260/p10/ZG4	UFA-int / 4-20 mA	b002/198-ufa
ZS25/25-**650**GE/260/p10/ZG4	UFA-int / 4-20 mA	b002/199-ufa
'370 °C' / integrated UFA		
ZS25/25-**250**GE/370/p10/ZG4	UFA-int / 4-20 mA	b002/200-ufa
ZS25/25-**350**GE/370/p10/ZG4	UFA-int / 4-20 mA	b002/201-ufa
ZS25/25-**450**GE/370/p10/ZG4	UFA-int / 4-20 mA	b002/202-ufa
ZS25/25-**550**GE/370/p10/ZG4	UFA-int / 4-20 mA	b002/203-ufa
ZS25/25-**650**GE/370/p10/ZG4	UFA-int / 4-20 mA	b002/204-ufa
'500 °C' / integrated UFA		
ZS25/25-**250**GE/500/p10/ZG4	UFA-int / 4-20 mA	b002/205-ufa
ZS25/25-**350**GE/500/p10/ZG4	UFA-int / 4-20 mA	b002/206-ufa
ZS25/25-**450**GE/500/p10/ZG4	UFA-int / 4-20 mA	b002/207-ufa
ZS25/25-**550**GE/500/p10/ZG4	UFA-int / 4-20 mA	b002/208-ufa
ZS25/25-**650**GE/500/p10/ZG4	UFA-int / 4-20 mA	b002/209-ufa
'100 °C'/ separate evaluation unit		
ZS25/25-**250**GE/100/p10/ZG4	sep. eval. unit / v/FA	b002/190
ZS25/25-**350**GE/100/p10/ZG4	sep. eval. unit / v/FA	b002/191
ZS25/25-**450**GE/100/p10/ZG4	sep. eval. unit / v/FA	b002/192
ZS25/25-**550**GE/100/p10/ZG4	sep. eval. unit / v/FA	b002/193
ZS25/25-**650**GE/100/p10/ZG4	sep. eval. unit / v/FA	b002/194
'260 °C'/ separate evaluation unit		
ZS25/25-**250**GE/260/p10/ZG4	sep. eval. unit / v/FA	b002/195
ZS25/25-**350**GE/260/p10/ZG4	sep. eval. unit / v/FA	b002/196
ZS25/25-**450**GE/260/p10/ZG4	sep. eval. unit / v/FA	b002/197
ZS25/25-**550**GE/260/p10/ZG4	sep. eval. unit. / v/FA	b002/198
ZS25/25-**650**GE/260/p10/ZG4	sep. eval. unit / v/FA	b002/199

Basic types (cont.)

Type	Transducer/ output	Article no.
'370 °C' / separate evaluation unit		
ZS25/25-**250**GE/370/p10/ZG4	sep. eval. unit / v/FA	b002/200
ZS25/25-**350**GE/370/p10/ZG4	sep. eval. unit / v/FA	b002/201
ZS25/25-**450**GE/370/p10/ZG4	sep. eval. unit / v/FA	b002/202
ZS25/25-**550**GE/370/p10/ZG4	sep. eval. unit / v/FA	b002/203
ZS25/25-**650**GE/370/p10/ZG4	sep. eval. unit / v/FA	b002/204
'500 °C' / separate evaluation unit		
ZS25/25-**250**GE/500/p10/ZG4	sep. eval. unit / v/FA	b002/205
ZS25/25-**350**GE/500/p10/ZG4	sep. eval. unit / v/FA	b002/206
ZS25/25-**450**GE/500/p10/ZG4	sep. eval. unit / v/FA	b002/207
ZS25/25-**550**GE/500/p10/ZG4	sep. eval. unit / v/FA	b002/208
ZS25/25-**650**GE/500/p10/ZG4	sep. eval. unit / v/FA	b002/209

(1) Sensor type / Sensor diameter

Vane wheel flow sensor ZS25 with sensor Ø 25 mm and shaft Ø 25 mm

(2) Sensor length dimension C (see Drawing 4, Page 1)

250 / 350 / 450 / 550 / 650 mm

(3) Medium

... G ...	air / gases

(4) Materials in contact with the medium

Design	Material
... E ...	stainless steel 1.4404 / AISI 316L, ceramics Al_2O_3 99.9 %
'100 °C' and '260 °C'	PTFE seal
'370 °C' and '500 °C'	pure graphite seal

(5) Permissible temperature of the medium

Design	Temperature of the medium	
... 100 ...	-20 ... +100 °C (continuous)	
... 260 ...	-40 ... +260 °C (continuous) -40 ... +300 °C (short-time)	
... 370 ...	-40 ... +370 °C (continuous) -40 ... +400 °C (short-time)	
... 500 ...	-40 ... +500 °C (continuous) -40 ... +550 °C (short-time)	
ambience	-40 ... +80 °C	with separate evaluation unit
	-40 ... +80 °C	with integrated transducer UFA-int
	-5 ... +50 °C	with optional 'LCD display'

(6) Max. working pressure / Type of protection for sensor

up to 10 bar / 1 MPa kPa above atmospheric	
protection class IP68	

(7) Option 'Ex'

Type of protection	Art. No.	Comment
Ex nA IIC T6 Gas-Ex: Category 3G (Zone 2) Ex tc IIIC TX Dust-Ex: Category 3D (Zone 22)	faex2	only in connection with: • evaluation unit or • flowtherm NT
Ex ia IIC T6 Gas-Ex: Category 2G (Zone 1)	faex1	only in connection with: • isolation/supply unit LDX2 <u>and</u> 'non-Ex evaluation unit or • compatible separate evaluation unit with Ex-output

(8) Design

as in Drawing 4 (Page 1)						
dimensions	A	Ø 25 mm	B	13.9 mm	C	250/350/450/550/650 mm
	D	60 mm	E	80 mm	F	130 mm

Measurement range (with a gas density of approx. 1.2 kg/m³) / vane wheel type

Measurement range	Vane wheel type	Art. No.
0.4 ... 20 m/s	mn 20 E	v_mn20GE
0.5 ... 40 m/s	mn 40 E	v_mn40GE
1.0 ... 80 m/s	mn 80 E	v_mn80GE
1.4 ... 120 m/s	mn 120 E	v_mn120GE
measurement uncertainty	< 1.5 % of measured value + 0.5 % of terminal value	
repeatability	±(0.05 % of terminal value + 0.02 m/s)	

Connection housing AS80

dimensions	80 / 80 / 60 mm (L / W / H)
connection	connector GO 070 with terminal screws
terminal assignment	see Page 6
protection class	IP65

Output / transducer (see Pages 2 & 3, 'Basic types')

ouput 4-20 mA / integrated UFA	UFA integrated in the housing (see Page 6)
ouptut sensor v/FA / separate evaluation unit necessary	Höntzsch evaluation unit with v/FA input necessary for signal evaluation
output sensor v/FA-Ex, sensor with option 'Ex' for use in Category 2G (Zone1) / sep. eval. unit necessary	Höntzsch evaluation unit with intrinsically safe v/FA-Ex signal input or with v/FA input in conjunction with a series connected isolation/supply unit necessary for signal evaluation

Transducer UFA-int, integrated in the sensor connection housing

|	
analog output/resistance	4 ... 20 mA = 0 ... ___ m/s, resistance max. 400 Ohm
output 'limit value' or 'quantity pulse'	Open Collector / max. 50 mA / max. 27 V DC, pulse duration 0.5 s
PC interface	RS232
	output signals electrically isolated from the power supply
self-monitoring	parameter settings, sensor interface; in case of error: analog output less than 3.6 mA
connection	connector GO 070 with terminal screws
power supply	24 V DC (20 ... 27 V DC)
power consumption	less than 3 W
working temp. range	-40 ... +80 °C
housing	sensor connection housing AS80
EMC	EN 61 000-6-2
setting parameter	analog output, profile factor/coefficient, pipe inside diameter, time constant, sensor type, measurement range, medium, limit value or quantity pulse (valency adjustable), switching actual/standard flow with setting parameters, 'actual pressure' and 'actual temperature' ...
setting parameter with PC software UCOM and programming adapter (see below) changeable	

Accessories (cont.) / options

	Description	Art. No.
LCD display in housing cover	2 x 16 digit, numerals 3 mm high, working temperature range -5...+50 °C	a010/007
PC software UCOM	for configuring the UFA/int via RS232	a010/052
programming adapter G0 070 / RS232	for software UCOM, connection PC Sub-D 9-pin, power plug 230VAC/24VDC	a010/004
interface converter USB / RS232	PC connection : USB plug type A on instrument : Sub-D 9-pin	a010/100

optional LCD display in the housing cover
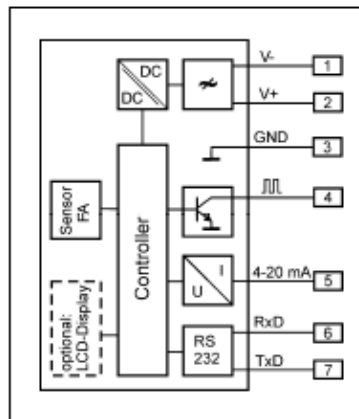
Wiring diagram with integrated UFA
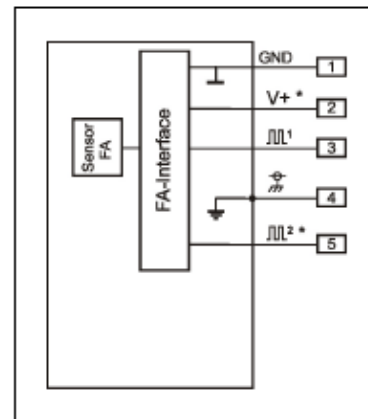
Wiring diagram sensor for separate evaluation unit (* optional)

I.7 TR10-C RTD Specifications

Sensor

The sensor is located in the measuring insert. This is replaceable and spring-loaded.

Sensor connection method
- 2-wire
- 3-wire
- 4-wire

Tolerance value of the sensor to DIN EN 60751
- Class B
- Class A
- Class AA

The combinations of a 2-wire connection with class A or class AA are not permissible.

For detailed specifications for Pt100 sensors, see Technical Information IN 00.17 at www.wika.com.

Measuring insert

The measuring insert is made of a vibration-resistant, sheathed, mineral-insulated cable (MI cable).
The diameter of the measuring insert should be approx. 1 mm smaller than the bore diameter of the thermowell.
Gaps of more than 0.5 mm between thermowell and the measuring insert will have a negative effect on the heat transfer, and they will result in unfavourable response behaviour from the thermometer.

In order to ensure that the measuring insert is firmly pressed down onto the bottom of the thermowell, the insert must be spring-loaded (spring travel: max. 10 mm).

The standard material used for the measuring insert sheath is stainless steel. Other materials are available on request.

Standard measuring insert lengths

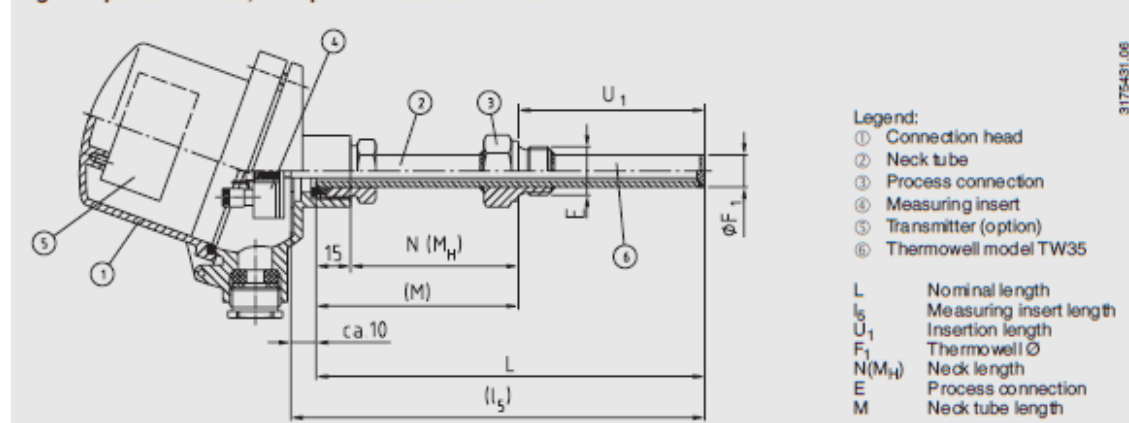| Measuring insert Ø in mm	Standard measuring insert lengths in mm										
3	275	315		375		435					
6	275	315	345	375	405	435	525	555	585	655	735
8	275	315	345	375	405	435	525	555	585	655	735

The lengths specified in this table correspond to the standard lengths. Intermediate lengths or greater lengths are possible without any difficulty.

Possible combinations of measuring insert diameter, number of sensors and sensor connection method

Measuring insert Ø in mm	Sensor, connection method 1 x Pt100			Sensor, connection method 2 x Pt100		
	2-wire	3-wire	4-wire	2-wire	3-wire	4-wire
3	x	x	x	x	x	-
6	x	x	x	x	x	x
8	x	x	x	x	x	x

Components model TR10-C

Fig. with parallel thread, for tapered thread see "Dimensions in mm"

Legend:
① Connection head
② Neck tube
③ Process connection
④ Measuring insert
⑤ Transmitter (option)
⑥ Thermowell model TW35

L	Nominal length
l_5	Measuring insert length
U_1	Insertion length
F_1	Thermowell Ø
$N(M_H)$	Neck length
E	Process connection
M	Neck tube length

Connection head

| BS | BSZ / BSZ-K | BSZ-H / BSZ-HK | BSS | BSS-H | BVS |
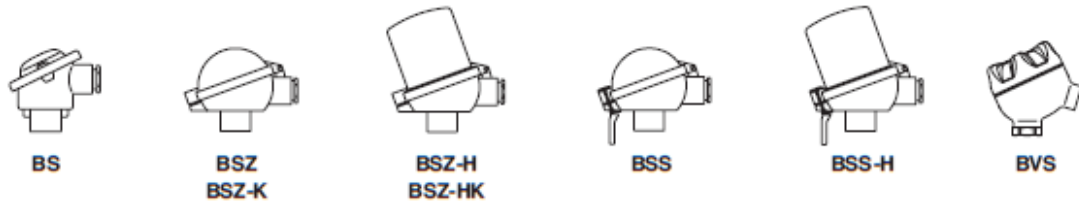
Model	Material	Cable entry	Ingress protection	Cap	Surface finish
BS	Aluminium	M20 x 1.5 [1]	IP 65	Cap with 2 screws	Blue, painted [2]
BSZ	Aluminium	M20 x 1.5 [1]	IP 65	Hinged cover with cylinder head screw	Blue, painted [2]
BSZ-K	Plastic	M20 x 1.5 [1]	IP 65	Hinged cover with cylinder head screw	Black
BSZ-H	Aluminium	M20 x 1.5 [1]	IP 65	Hinged cover with cylinder head screw	Blue, painted [2]
BSZ-HK	Plastic	M20 x 1.5 [1]	IP 65	Hinged cover with cylinder head screw	Black
BSS	Aluminium	M20 x 1.5 [1]	IP 65	Hinged cover with clip	Blue, painted [2]
BSS-H	Aluminium	M20 x 1.5 [1]	IP 65	Hinged cover with clip	Blue, painted [2]
BVS	Stainless steel	M20 x 1.5 [1]	IP 65	Screw cover	Precision casting, electropolished

1) Standard
2) RAL 5022

Connection head with digital indicator (option)

As an alternative to the standard connection head the thermometer can be fitted with an optional DIH10 digital indicator. The connection head used for this is similar to the model BSZ-H head. For operation, a 4 ... 20 mA transmitter is needed, which is mounted to the measuring insert. The indication range is configured identically to the measuring range of the transmitter.

Designs with ignition protection type "intrinsically safe", Ex i, are also available.

Connection head with digital indicator, model DIH10

Transmitter (option)

Depending on the connection head used, a transmitter can be mounted within the thermometer.

O Mounted instead of terminal block
● Mounted within the cap of the connection head
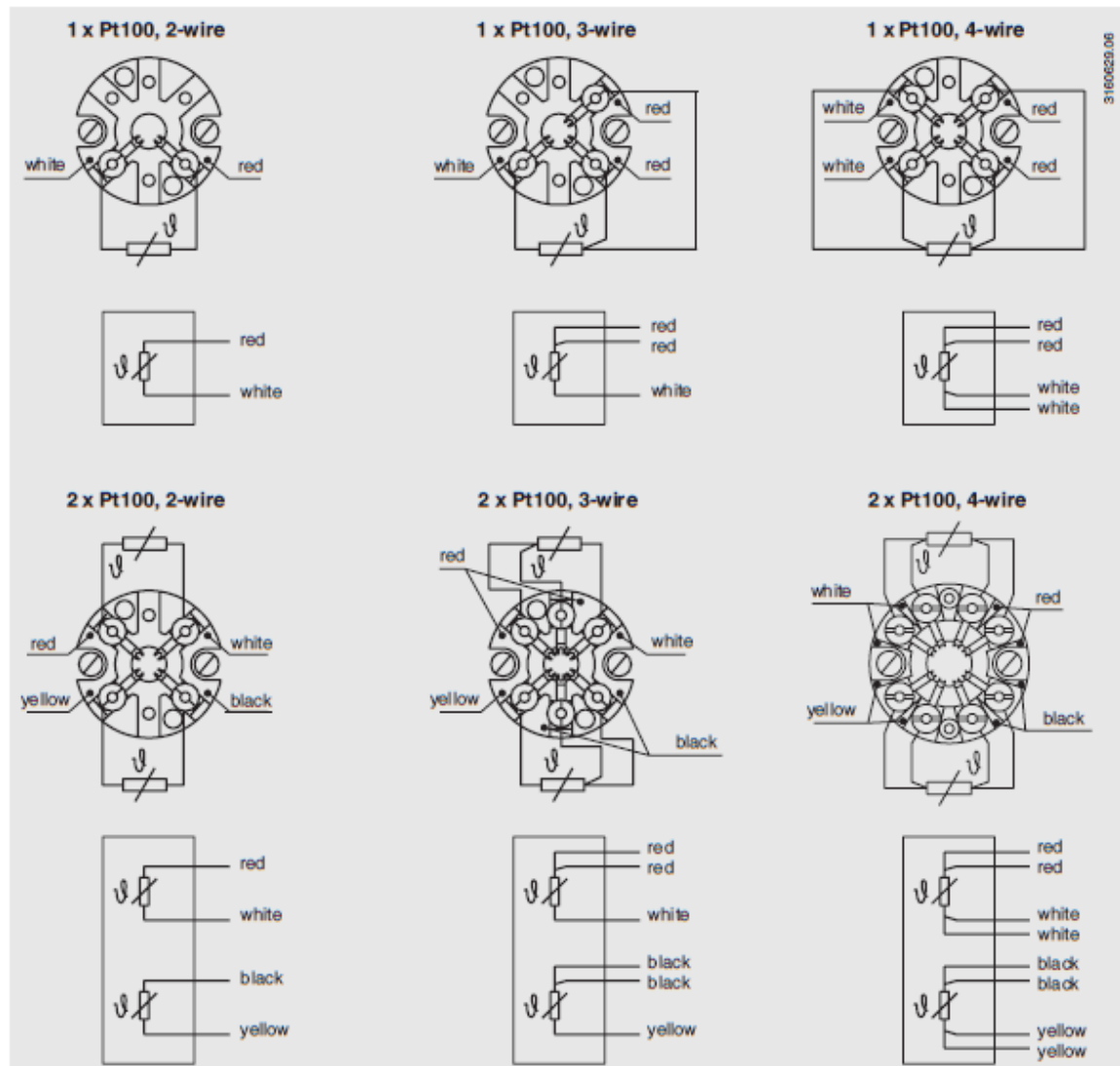– Mounting not possible

Mounting of two transmitters on request.

Connection head	Transmitter model				
	T12	T19	T24	T32	T53
BS	-	O	O	-	O
BSZ / BSZ-K	O	O	O	O	O
BSZ-H / BSZ-HK	●	●	●	●	●
BSS	O	O	O	O	O
BSS-H	●	●	●	●	●
BVS	O	O	O	O	O

Model	Description	Explosion protection	Data sheet
T19	Analogue transmitter, configurable	Without	TE 19.03
T24	Analogue transmitter, PC configurable	Optional	TE 24.01
T12	Digital transmitter, PC configurable	Optional	TE 12.03
T32	Digital transmitter, HART® protocol	Optional	TE 32.04
T53	Digital transmitter FOUNDATION™ Fieldbus and PROFIBUS® PA	Standard	TE 53.01

Electrical connection

(Colour code per EN/IEC 60751)

1 x Pt100, 2-wire — white, red

1 x Pt100, 3-wire — white, red, red

1 x Pt100, 4-wire — white, white, red, red

2 x Pt100, 2-wire — red, white, yellow, black

2 x Pt100, 3-wire — red, white, yellow, black

2 x Pt100, 4-wire — white, red, yellow, black

For the electrical connections of built-in temperature transmitters see the corresponding data sheets or operating instructions.

I.8 T19 Analogue Transmitter Specifications

Specifications		Models T19.10 and T19.30		
		1P01	1P02	1P03
Input		1 x Pt100 per IEC 60584 (α = 0.00385) *		
		2- or 3-wire		
■ Not configured		not factory configured / the measuring range can be configured via solder jumpers, within the limits specified below		
■ Standard [1]	°C	-50 ... +50	-50 ... +200	-30 ... +30
	°C	0 ... 50	0 ... 200	-30 ... +50
	°C	0 ... 100	0 ... 250	0 ... 60
	°C	0 ... 120	0 ... 300	0 ... 80
	°C	0 ... 150	0 ... 350	0 ... 100
	°C	0 ... 200	0 ... 400	0 ... 120
■ Special measuring ranges		factory-configured, permanent, changing the measuring range configuration is no longer possible between -200 ... +850 °C (min. span: 20 K, max. span: 1050 K)		
Adjustment range zero point	°C	approx. ± 10	approx. ± 25	approx. ± 30
Adjustment range span	%	approx. 10		
Sensor measuring current		approx. 0.8 mA		
Max. output resistance		30 Ω per wire, 3-wire symmetric		
Cold junction compensation		-		
Analogue output		4 ... 20 mA, 2-wire design		
Linearisation		proportional to temperature per IEC 60751/DIN 43760		
Output limits				
Sensor burnout	mA	down scale, < 3 [2]		
Sensor short circuit	mA	down scale, < 3 [3]		
Rise time t_{90}	s	< 0.01		
Switch-on time (time to first measured value)	s	< 0.1		
Measuring rate		Permanent (analogue system)		
Power supply U_B [4]		DC 10 ... 30 V from 4 ... 20 mA loop		
Load R_A		$R_A \leq (U_B - 10\,V) / 0.02\,A$ with R_A in Ω and U_B in V		
Measuring deviation per DIN EN 60770, at 23 °C ± 5 K	%	± 0.5 [5]		
Load effect	%/100 Ω	± 0.05 Ω		
Power supply effect	%/V	± 0.025		
Warm-up time		5 minutes to reach data sheet specifications		
Linearity error	%	± 0.1 [6]		
Amplification error	%	-		
Error effect of cold junction compensation		-		
Temperature coefficient T_K of -40 ... 85 °C		ZP: ± 0.1 %/10 K or ± 0.2 K/10 K [7] Span: ± 0.2 K/10 K		
Effect of the supply lead resistances		3-wire: ± 0.2 K / 10 Ω 2-wire: resistance of the supply lead		
Electromagnetic compatibility (EMC)		CE-Conformity per DIN EN 61326-1		
Galvanic isolation between the sensor and output side (4 ... 20 mA)		No		

Specifications in % refer to the measuring span

* Pt1000 and special measuring ranges on request.
1) Further units e.g. °F and K are possible.
2) Up scale, in the event only lead no. 1 open-circuit.
3) Temperature value, in the event of a short between leads no. 2 and no. 3 (operation of Pt100 in 2-wire configuration).
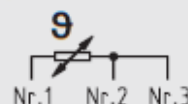4) Input power supply protected from reverse polarity.
5) With factory configured measuring range.
6) ±0.15 % with measuring range: 0 ... 50 °C, 0 ... 300 °C, 0 ... 350 °C
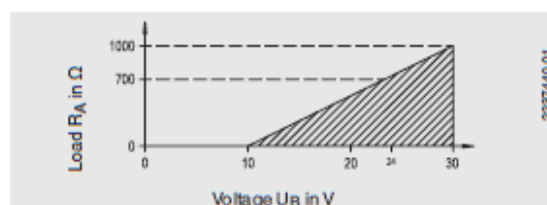7) Whichever is greater.

Legend for lead numbers

Nr.1   Nr.2   Nr.3

Load diagram

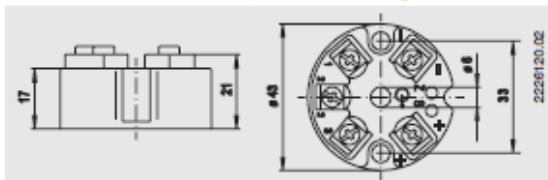The permissible load is dependent upon the loop power supply voltage.

Case

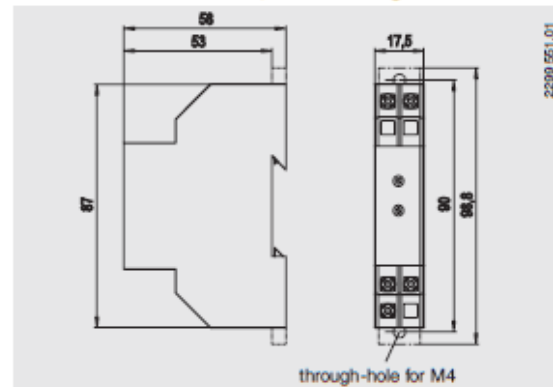| Model	Material	Weight	Ingress protection Case (terminal connection)	Terminal connection (captive screws)
T19.10	plastic, PA, glass-fibre reinforced	approx. 0.03 kg	IP00 (IP40)	0.14 ... 1.5 mm²
T19.30	polyamide, glass-fibre reinforced	0.05 kg	IP10 (IP40)	0.5 ... 1.5 mm²

Ambient conditions

Model	Climate class per DIN IEC 60068-2-30	Ambient / storage temperature	Vibration per DIN IEC 60068-2-6	Shock per DIN IEC 60068-2-27
T19.10	Cx (-40 ... +85 °C, 5 % to 95 % relative humidity)	-40 ... +85 °C	10 ... 2000 Hz; 5g	10 g
T19.30	Bx (-20 ... +70 °C, 5 % to 95 % relative humidity)	-20 ... +70 °C	10 ... 2000 Hz; 5g	10 g

Dimensions in mm

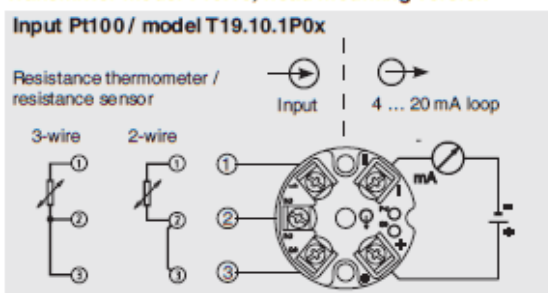**Transmitter model T19.10, head mounting version**

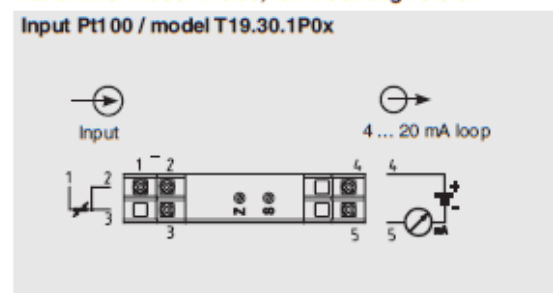**Transmitter model T19.30, rail mounting version**

through-hole for M4

Designation of terminal connectors

Transmitter model T19.10, head mounting version

Input Pt100 / model T19.10.1P0x

Resistance thermometer / resistance sensor

3-wire 2-wire

Input 4 ... 20 mA loop

Transmitter model T19.30, rail mounting version

Input Pt100 / model T19.30.1P0x

Input 4 ... 20 mA loop

Accessories for model T19.10 temperature transmitter, head mounting version (please order separately)	Order No.
Adapter, plastic/stainless steel, dimensions: 60 x 20 x 41.6 mm Suitable for TS 35 per DIN EN 60715 (DIN EN 50022 or TS 32 per DIN EN 50036)	3593789
Adapter, tinned steel, dimensions: 49 x 8 x 14 mm Suitable for TS 35 per DIN EN 60715 (DIN EN 50022)	3619851
Field case, plastic (ABS), ingress protection IP 65, dimensions: 82 x 80 x 55 mm (B x L x H) For head mounting of transmitter, permissible ambient temperature: -40 ... +80 °C, with two M16 x 1.5 cable glands	3301732

I.9 MINI MCR-SL-I-U-4 Specifications

Ambient conditions

Ambient temperature (operation)	-20 °C ... 65 °C
Ambient temperature (storage/transport)	-40 °C ... 85 °C
Degree of protection	IP20

Input data

Configurable/programmable	No
Current input signal	4 mA ... 20 mA
Max. input current	50 mA
Input resistance current input	approx. 50 Ω

Output data

Configurable/programmable	No
Voltage output signal	0 V ... 10 V
Max. output voltage	12.5 V
Short-circuit current	approx. 2 mA
Load/output load voltage output	≥ 10 kΩ

Power supply

Nominal supply voltage	24 V DC
Supply voltage range	19.2 V DC ... 30 V DC (The T connector (ME 6,2 TBUS-2 1,5/5-ST-3,81 GN, Order No. 2869728) can be used to bridge the supply voltage. It can be snapped onto a 35 mm DIN rail according to EN 60715))
Max. current consumption	< 9 mA
Power consumption	< 200 mW

Connection data

|	
Connection method	Screw connection
Conductor cross section solid min.	0.2 mm²
Conductor cross section solid max.	2.5 mm²
Conductor cross section stranded min.	0.2 mm²
Conductor cross section stranded max.	2.5 mm²
Conductor cross section AWG/kcmil min.	26
Conductor cross section AWG/kcmil max	12
Stripping length	12 mm
Screw thread	M3

General

Maximum transmission error	≤ 0.1 % (of final value)
Maximum temperature coefficient	< 0.01 %/K
Temperature coefficient, typical	< 0.002 %/K
Limit frequency (3 dB)	approx. 100 Hz
Step response (10-90%)	approx. 3.5 ms
Electrical isolation	Basic insulation according to EN 61010
Surge voltage category	II
Pollution degree	2
Rated insulation voltage	50 V AC/DC
Test voltage, input/output/supply	1.5 kV (50 Hz, 1 min.)
Electromagnetic compatibility	Conformance with EMC Directive 2004/108/EC
Noise emission	EN 61000-6-4
Noise immunity	EN 61000-6-2 When being exposed to interference, there may be minimal deviations.
Color	green
Housing material	PBT
Mounting position	any
Assembly instructions	The T connector can be used to bridge the supply voltage. It can be snapped onto a 35 mm DIN rail according to EN 60715.
Conformance	CE-compliant
ATEX	Ex II 3 G Ex nA IIC T4 Gc X
UL, USA / Canada	UL 508 Recognized
	Class I, Div. 2, Groups A, B, C, D T5 applied for
GL	GL EMC 2 D

Drawings

Block diagram
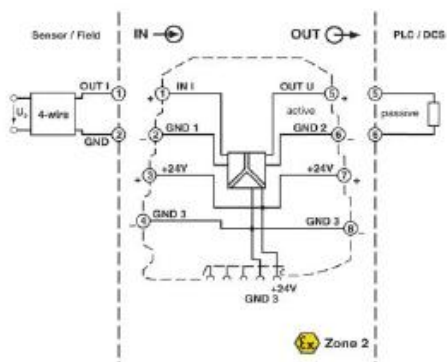
Dimensioned drawing
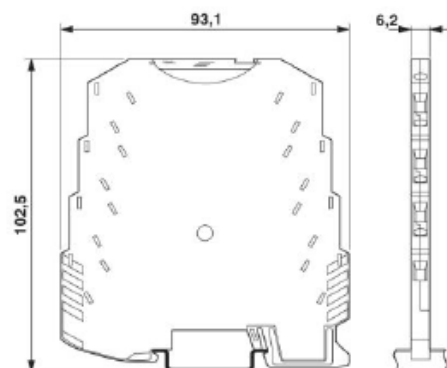
I.10 MINI MCR-SL-UI-UI-NC Specifications

Ambient conditions

Ambient temperature (operation)	-20 °C ... 65 °C
Ambient temperature (storage/transport)	-40 °C ... 85 °C
Degree of protection	IP20

Input data

Configurable/programmable	Yes, unconfigured
Voltage input signal	0 V ... 10 V
	0 V ... 5 V
	1 V ... 5 V
	2 V ... 10 V
Current input signal	0 mA ... 20 mA
	4 mA ... 20 mA
Max. input voltage	30 V
Max. input current	50 mA
Input resistance of voltage input	approx. 100 kΩ
Input resistance current input	approx. 50 Ω

Output data

Configurable/programmable	Yes, unconfigured
Voltage output signal	0 V ... 10 V
	0 V ... 5 V
	1 V ... 5 V
	2 V ... 10 V
Current output signal	0 mA ... 20 mA (please indicate if different setting when ordering)
	4 mA ... 20 mA
Max. output voltage	approx. 12.5 V
Max. output current	28 mA
Short-circuit current	approx. 22 mA
Load/output load voltage output	≥ 10 kΩ
Load/output load current output	< 500 Ω (at 20 mA)

Power supply

Nominal supply voltage	24 V DC
Supply voltage range	19.2 V DC ... 30 V DC (The T connector (ME 6,2 TBUS-2 1,5/5-ST-3,81 GN, Order No. 2869728) can be used to bridge the supply voltage. It can be snapped onto a 35 mm DIN rail according to EN 60715))

Max. current consumption	< 19 mA (Current output, at 24 V DC incl. load)
	< 9 mA (Voltage output, at 24 V DC incl. load)
Power consumption	< 450 mW (Current output)
	< 200 mW (Voltage output)

Connection data

Connection method	Screw connection
Conductor cross section solid min.	0.2 mm²
Conductor cross section solid max.	2.5 mm²
Conductor cross section stranded min.	0.2 mm²
Conductor cross section stranded max.	2.5 mm²
Conductor cross section AWG/kcmil min.	26
Conductor cross section AWG/kcmil max	12
Stripping length	12 mm
Screw thread	M3

General

| No. of channels	1
Maximum transmission error	≤ 0.1 % (of final value)
	< 0.4 % (Without adjustment)
Maximum temperature coefficient	< 0.01 %/K
Temperature coefficient, typical	< 0.002 %/K
Limit frequency (3 dB)	approx. 100 Hz
Step response (10-90%)	approx. 3.2 ms
Protective circuit	Transient protection
Electrical isolation	Basic insulation according to EN 61010
Surge voltage category	II
Pollution degree	2
Rated insulation voltage	50 V AC/DC
Test voltage, input/output/supply	1.5 kV (50 Hz, 1 min.)
Electromagnetic compatibility	Conformance with EMC Directive 2004/108/EC
Noise emission	EN 61000-6-4
Noise immunity	EN 61000-6-2 When being exposed to interference, there may be minimal deviations.
Color	green
Housing material	PBT
Mounting position	any

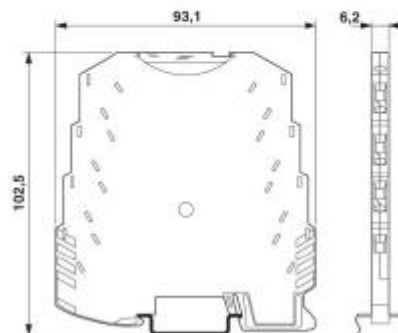| Assembly instructions	The T connector can be used to bridge the supply voltage. It can be snapped onto a 35 mm DIN rail according to EN 60715.
Conformance	CE-compliant
ATEX	Ex II 3 G Ex nA IIC T4 Gc X
UL, USA / Canada	UL 508 Recognized
	Class I, Div. 2, Groups A, B, C, D T5
GL	GL EMC 2 D

Drawings

Application drawing
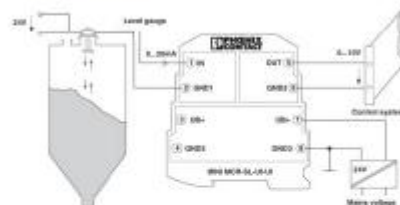
Block diagram
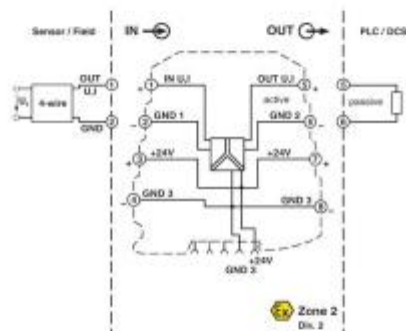
Dimensioned drawing

I.11 DS1103 PPC Controller Board Specifications

Technical Details

Parameter		Specification
Processor	PowerPC Type	■ PPC 750GX
	CPU clock	■ 1 GHz
	Cache	■ 32 KB level 1 (L1) instruction cache ■ 32 KB level 1 (L1) data cache ■ 1 MB level 2 (L2)
	Bus frequency	■ 133 MHz
	Temperature sensor	■ Reads actual temperature at the PPC
Memory	Local memory	■ 32 MB application SDRAM as program memory, cached
	Global memory	■ 96 MB communication SDRAM for data storage and data exchange with host
Timer	2 general-purpose timers	■ One 32-bit down counter ■ Reload by software ■ 15-ns resolution ■ One 32-bit up counter with compare register ■ Reload by software ■ 30-ns resolution
	1 sampling rate timer (decrementer)	■ 32-bit down counter ■ Reload by software ■ 30-ns resolution
	1 time base counter	■ 64-bit up counter ■ 30-ns resolution
Interrupt controller		■ 3 timer interrupts ■ 7 incremental encoder index line interrupts ■ 1 UART (universal asynchronous receiver and transmitter) interrupt ■ 1 CAN interrupt ■ 1 slave DSP interrupt ■ 2 slave DSP PWM interrupts ■ 1 host interrupt ■ 4 external interrupts (user interrupts)
A/D converter	Channels	■ 16 multiplexed channels equipped with 4 sample & hold A/D converters (4 channels belong to one A/D converter. 4 consecutive samplings are necessary to sample all channels belonging to one A/D converter.) ■ 4 parallel channels each equipped with one sample & hold A/D converter ■ Note: 8 A/D converter channels (4 multiplexed and 4 parallel) can be sampled simultaneously.
	Resolution	■ 16-bit
	Input voltage range	■ ±10 V
	Overvoltage protection	■ ±15 V
	Conversion time	■ Multiplexed channels: 1 μs[1] ■ Parallel channels: 800 ns[1]
	Offset error	■ ±5 mV
	Gain error	■ ±0.25%
	Offset drift	■ 40 μV/K
	Gain drift	■ 50 ppm/K
	Signal-to-noise ratio	■ >83 dB
D/A converter	Channels	■ 8 channels
	Resolution	■ 16-bit
	Output range	■ ±10 V
	Settling time	■ 5 μs (14-bit)
	Offset error	■ ±1 mV
	Gain error	■ ±0.5%
	Offset drift	■ 30 μV/K
	Gain drift	■ 25 ppm/K

[1] Speed and timing specifications describe the capabilities of the hardware components and circuits of our products. Depending on the software complexity, the attainable overall performance figures can deviate significantly from the hardware specifications.

Parameter		Specification
D/A converter	Signal-to-noise ratio	■ >83 dB
	I_{max}	■ ±5 mA
	Cl_{max}	■ 10 nF
Digital I/O	Channels	■ 32-bit parallel I/O ■ Organized in four 8-bit groups ■ Each 8-bit group can be set to input or output (programmable by software)
	Voltage range	■ TTL input/output levels
	$I_{out, max}$	■ ±10 mA
Digital incremental encoder interface	Channels	■ 6 independent channels ■ Single-ended (TTL) or differential (RS422) input (software programmable for each channel)
	Position counters	■ 24-bit resolution ■ Max. 1.65 MHz input frequency, i.e., fourfold pulse count up to 6.6 MHz ■ Counter reset or reload via software
	Encoder supply voltage	■ 5 V/1.5 A ■ Shared with analog incremental encoder interface
Analog incremental encoder interface	Channels	■ 1 channel ■ Sinusoidal signals: 1 Vpp differential or 11 µApp differential (software programmable)
	Position counters	■ < 5° resolution ■ 32-bit loadable position counter ■ Max. 0.6 MHz input frequency, i.e., fourfold pulse count up to 2.4 MHz
	A/D converter performance	■ 6-bit resolution ■ 10 MSPS
	Encoder supply voltage	■ 5 V/1.5 A ■ Shared with digital incremental encoder interface
CAN interface	Configuration	■ 1 channel based on SAB 80C164 microcontroller ■ ISO DIS 11898-2 CAN high-speed standard
	Baud rate	■ Max. 1 Mbit/s
Serial interface	Configuration	■ TL6C550C single UART with FIFO ■ PLL-driven UART for accurate baud rate selection ■ RS232/RS422 compatibility
	Baud rate	■ Up to 115.2 kBd (RS232) ■ Up to 1 Mbd (RS422)
Slave DSP	Type	■ Texas Instruments TMS320F240 DSP
	Clock rate	■ 20 MHz
	Memory	■ 64Kx16 external code memory ■ 28Kx16 external data memory ■ 4Kx16 dual-port memory for communication ■ 32 KB flash memory
	I/O channels	■ 16 A/D converter inputs ■ 10 PWM outputs ■ 4 capture inputs ■ 2 serial ports
	Input voltage range	■ TTL input/output level ■ A/D converter inputs: 0 … 5 V
	Output current	■ Max. ±13 mA
Host interface		■ Plug & Play support ■ Requires a full-size 16-bit ISA slot
Physical characteristics	Physical size	■ 340 x 125 x 45 mm (13.4 x 4.9 x 1.77 in)
	Ambient temperature	■ 0 … 50 °C (32 … 122 °F)
	Cooling	■ Passive cooling
	Power supply	■ +5 V ±5%, 4 A ■ +12 V ±5%, 0.75A ■ -12 V ±5%, 0.25A

Appendix II: Drawings

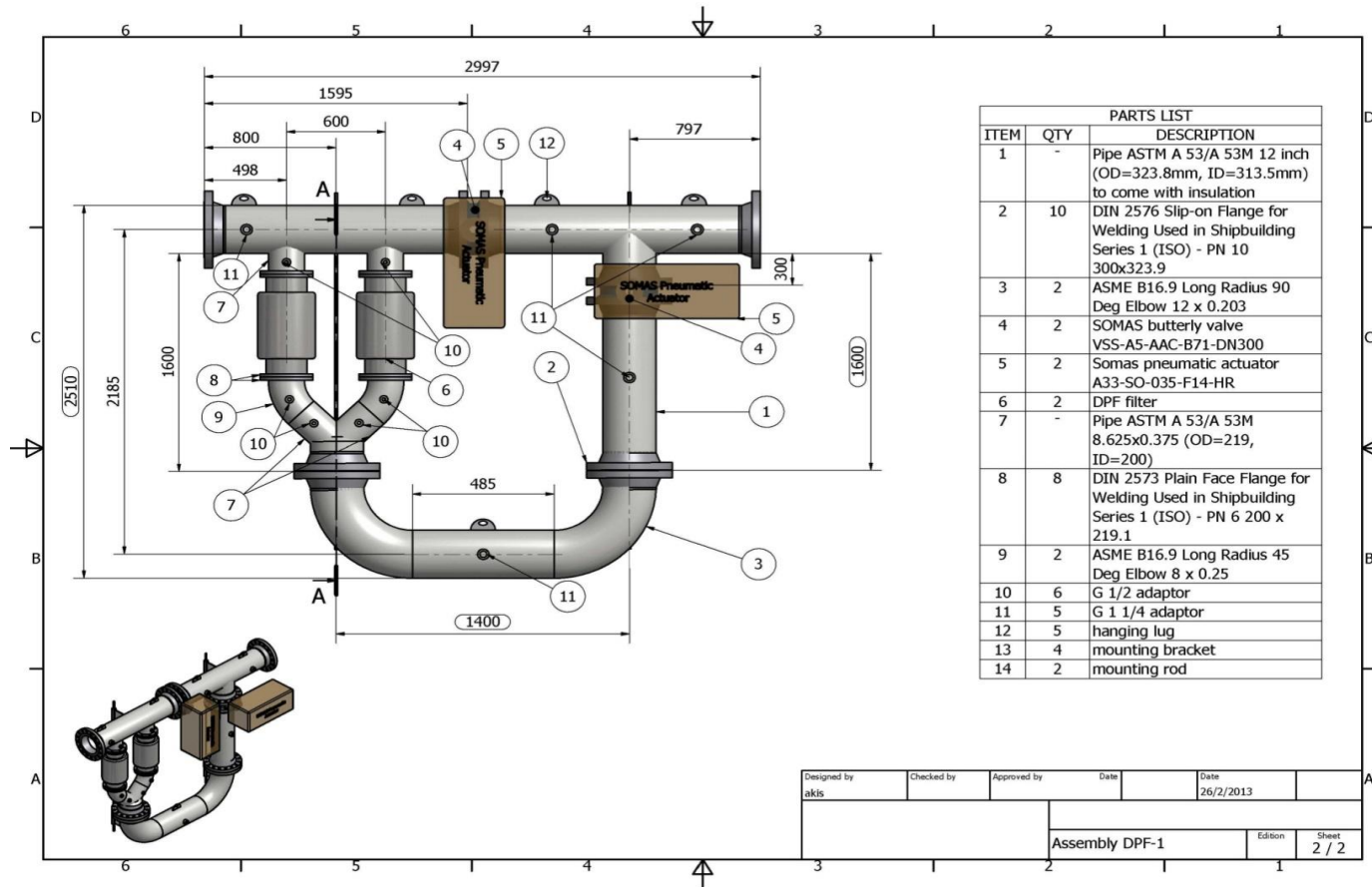**Figure A.II 1: Exhaust bypass system initial assembly design**

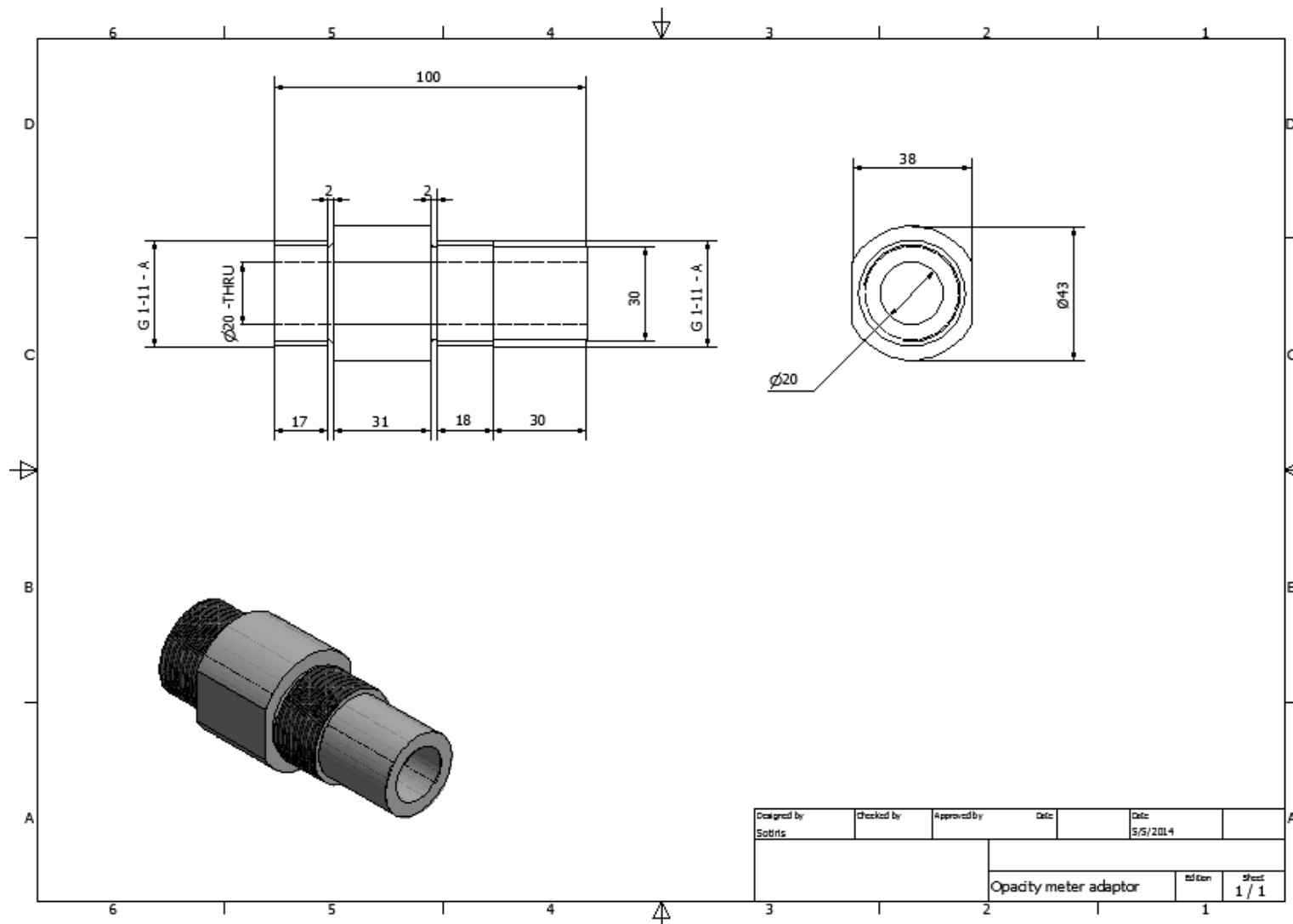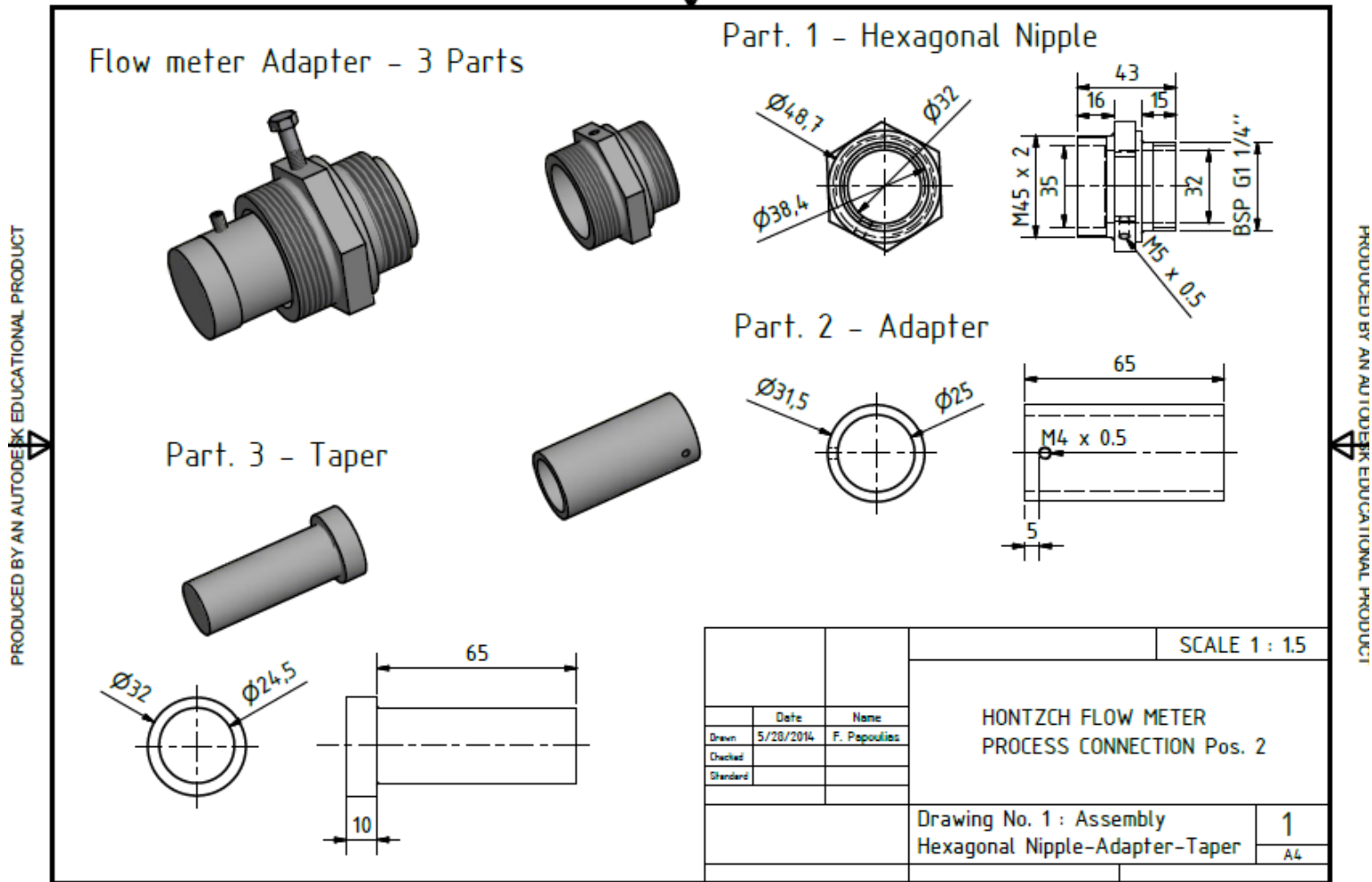**Figure A.II 2: Socket pipes design**

Flow meter Adapter – 3 Parts

Part. 1 – Hexagonal Nipple

Ø48,7 Ø32 Ø38,4

43 16 15

M45 x 2 35 32 BSP G1 1/4"

M5 x 0,5

Part. 2 – Adapter

Part. 3 – Taper

Ø31,5 Ø25

65

M4 x 0,5

5

Ø32 Ø24,5

65

10

	Date	Name		SCALE 1 : 1,5
Drawn	5/28/2014	F. Papoulias		HONTZCH FLOW METER PROCESS CONNECTION Pos. 2
Checked				
Standard				

Drawing No. 1 : Assembly
Hexagonal Nipple-Adapter-Taper

1

A4

Figure A.II 3: Flow meter adaptor design

Room I.13

Panel A1
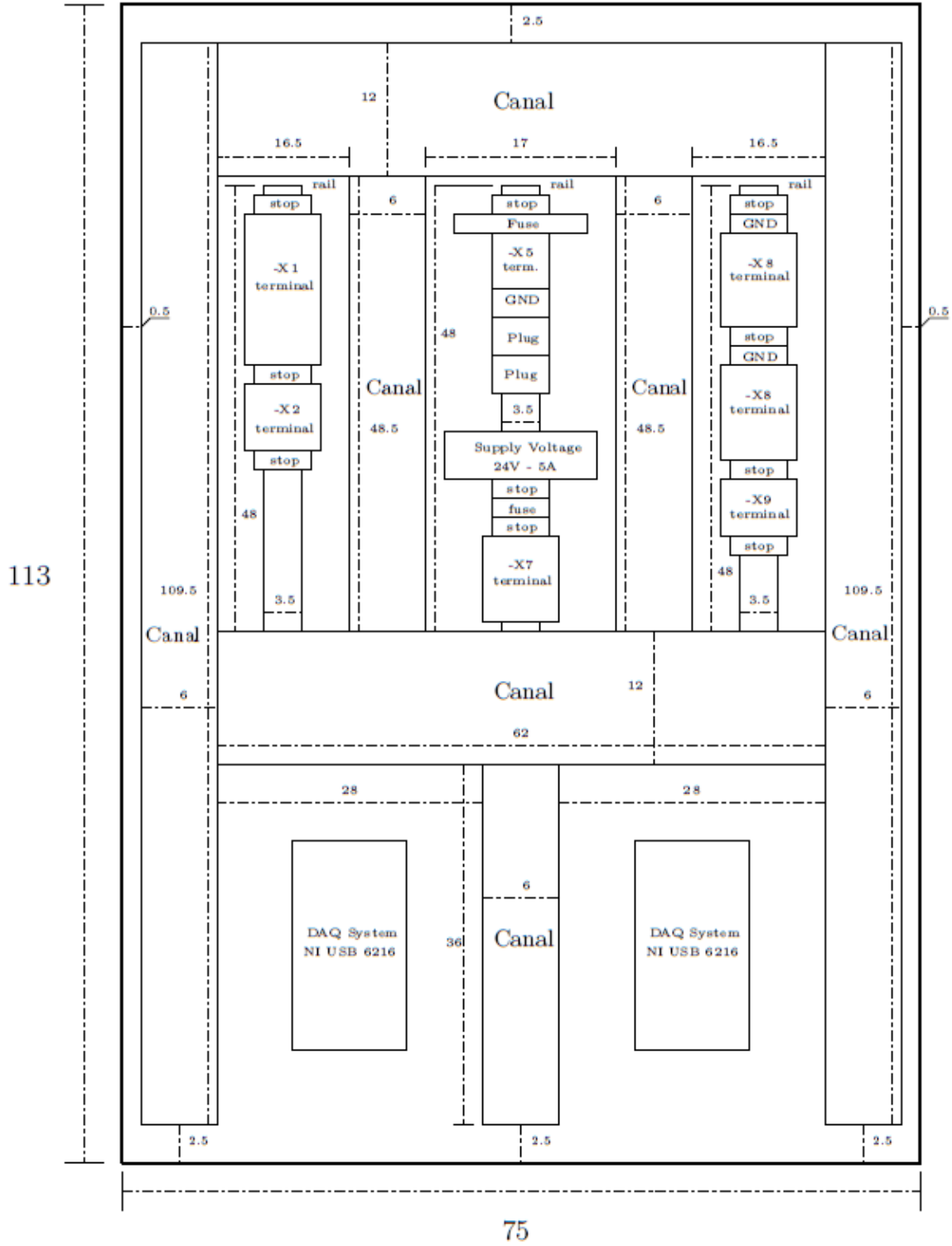
Figure A.II 4: Panel A1 initial design (it features two NI USB 6216 DAQ modules for local control).
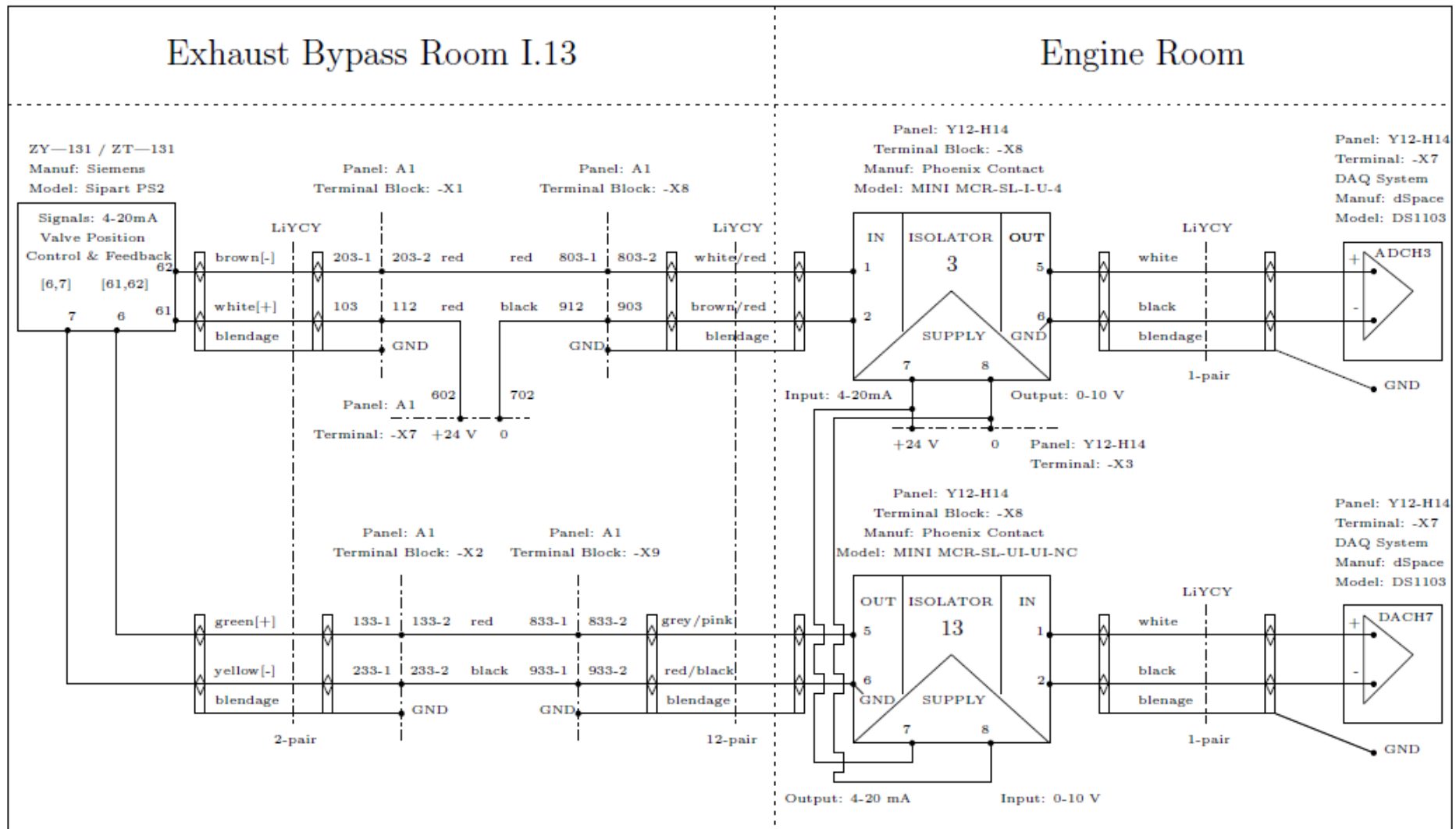
Figure A.II 5: Electrical connection of butterfly valve positioner 1
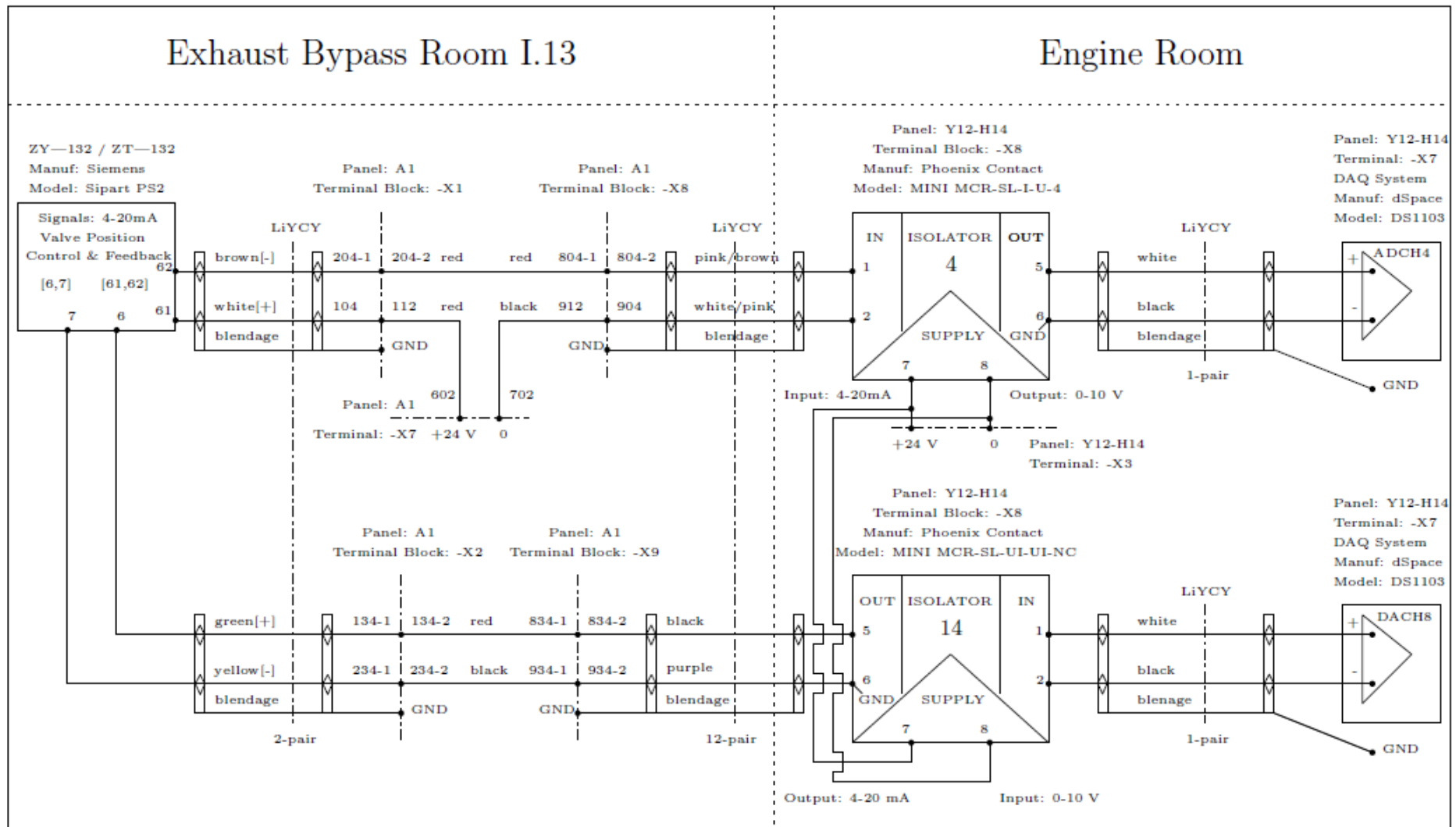
Figure A.II 6: Electrical Connection of butterfly valve positioner 2
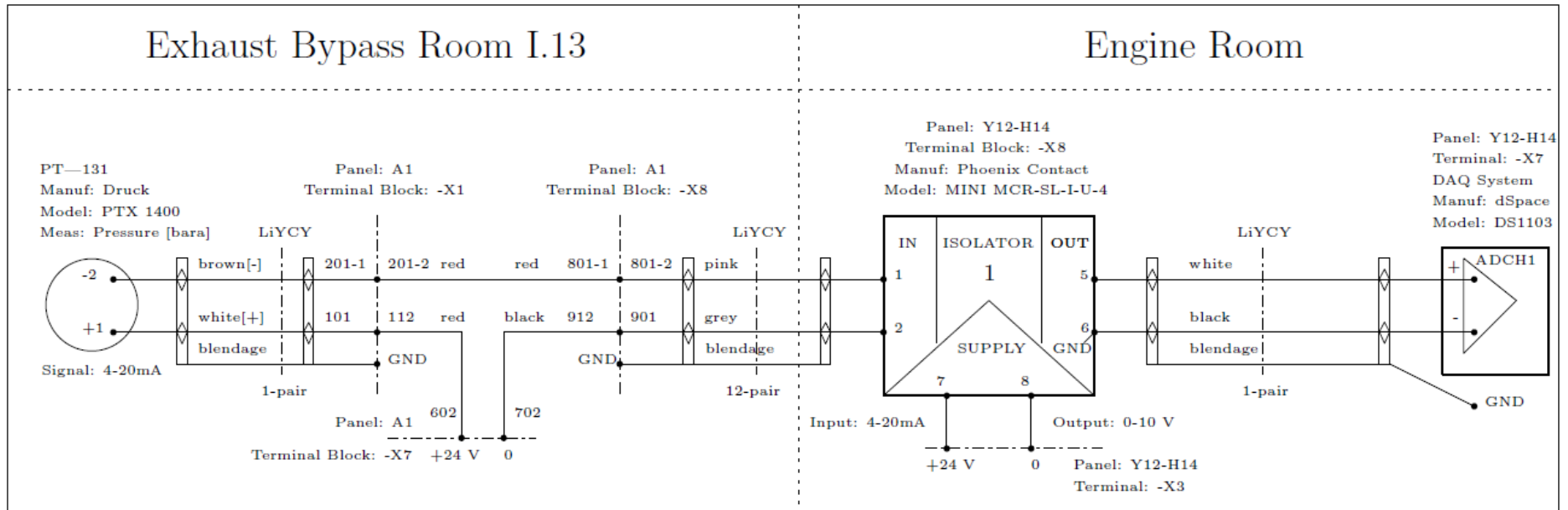
Figure A.II 7: Electrical connection of PTX 1400 pressure transmitter
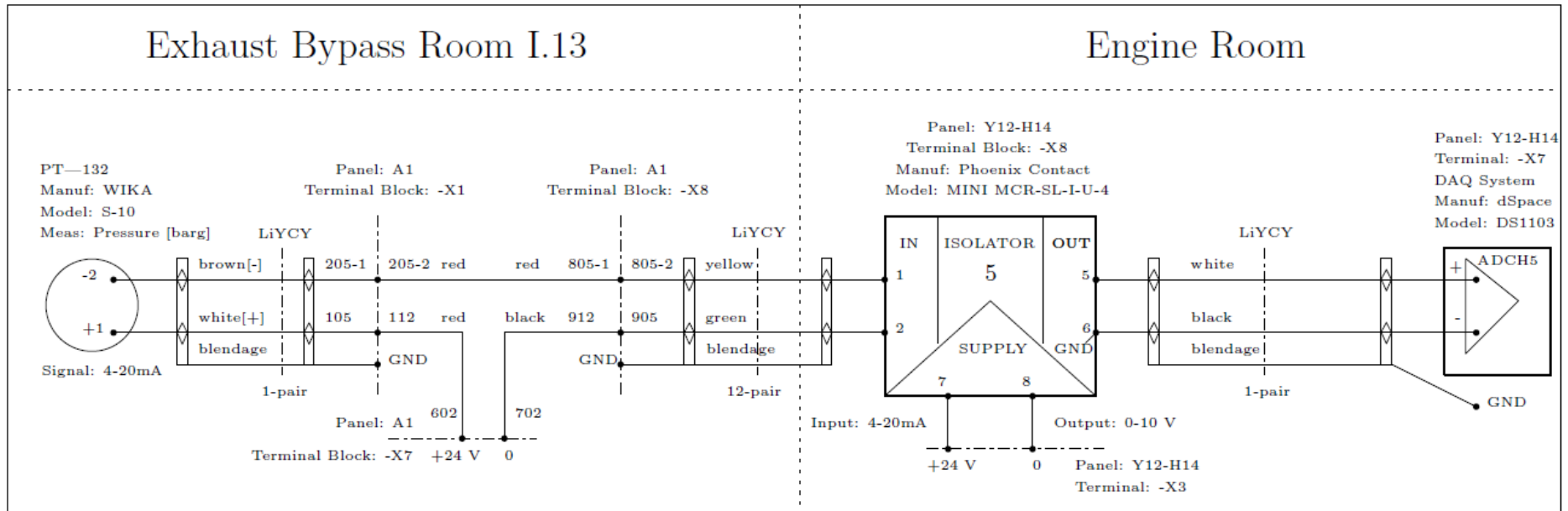
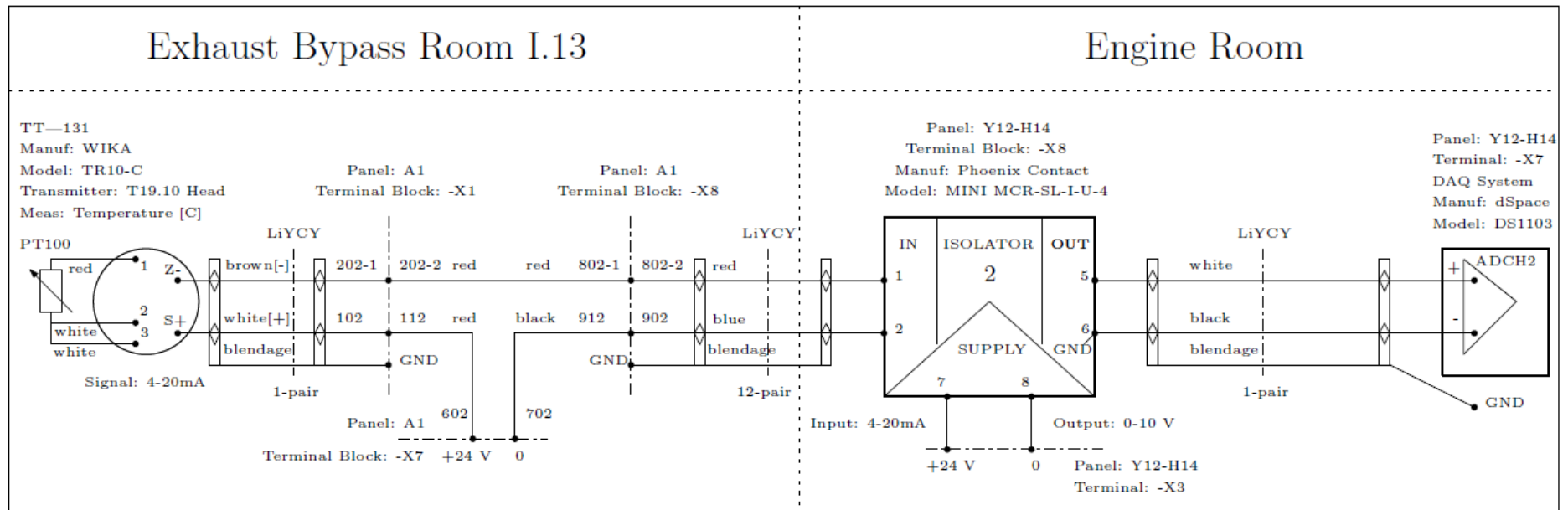**Figure A.II 8: Electrical connection of S-10 pressure transmitter 1**
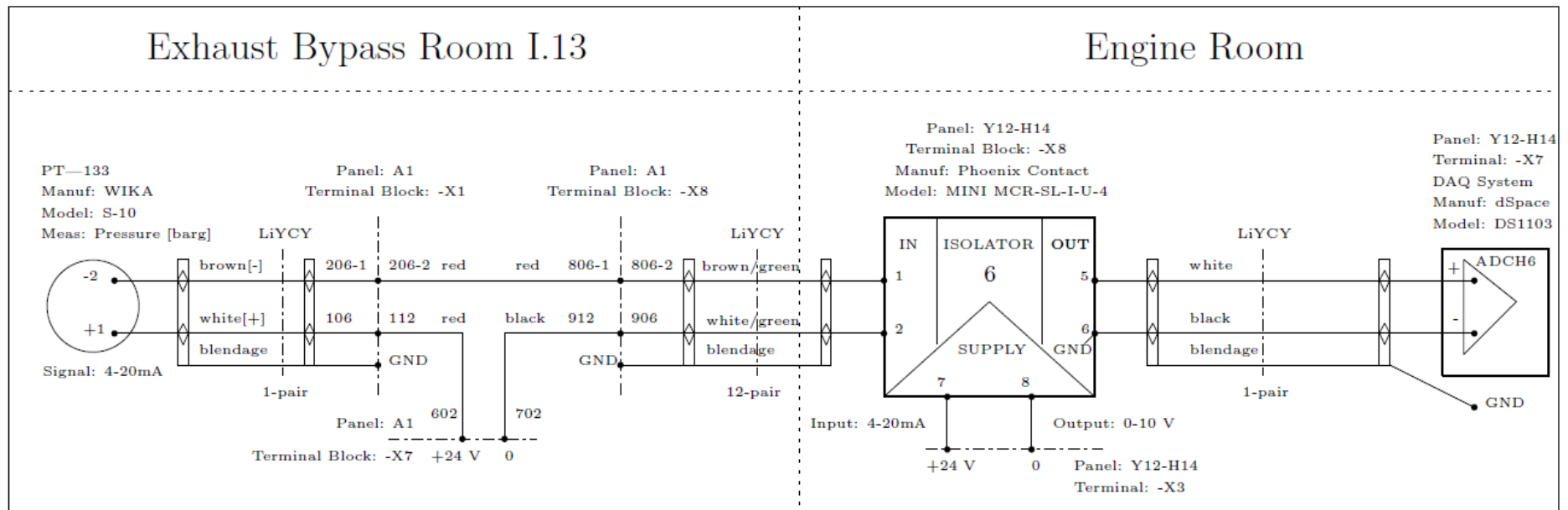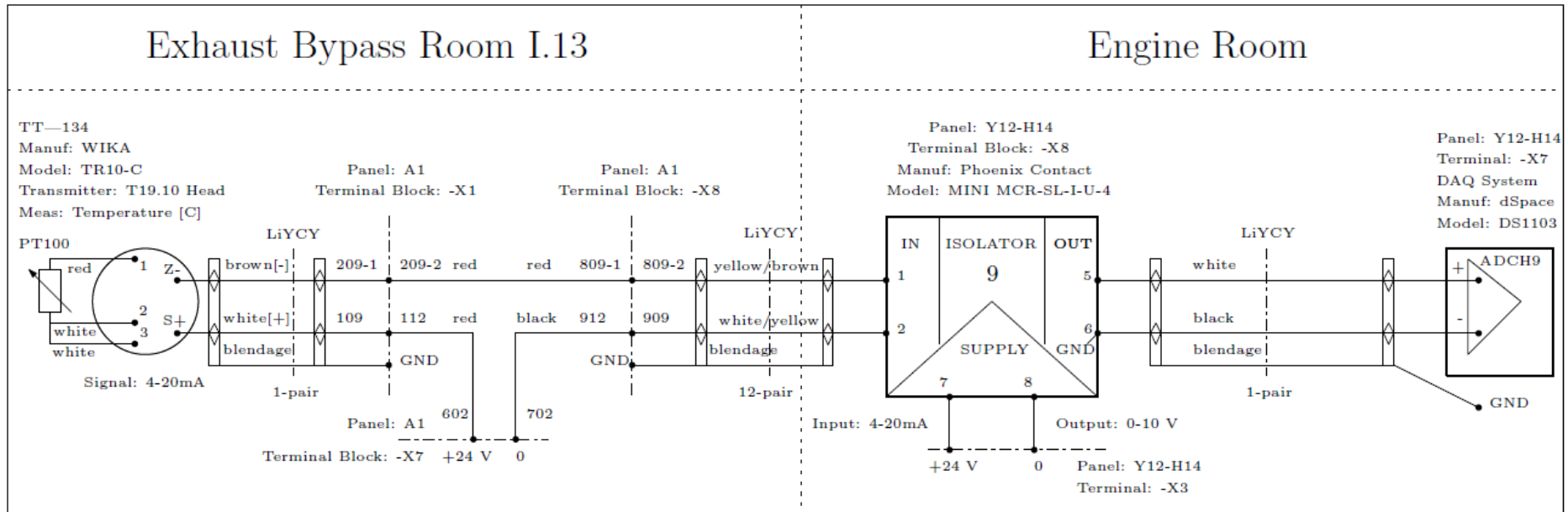
Figure A.II 9: Electrical connection of S-10 pressure transmitter 2
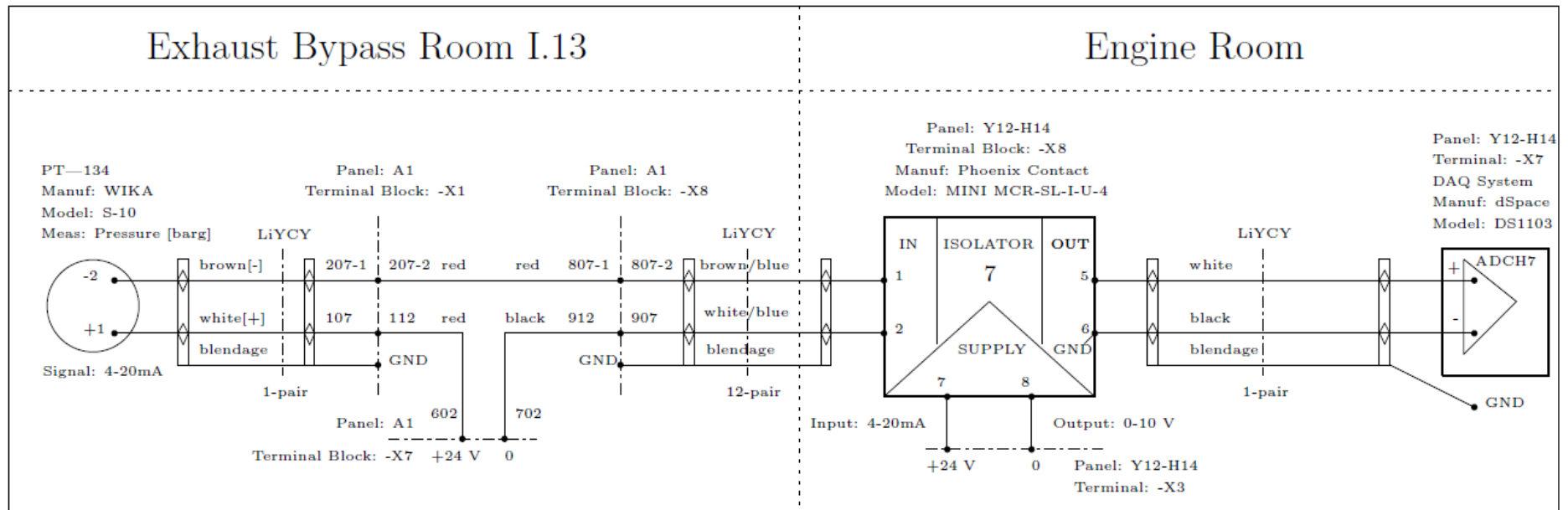
Figure A.II 10: Electrical connection of S-10 pressure transmitter 3
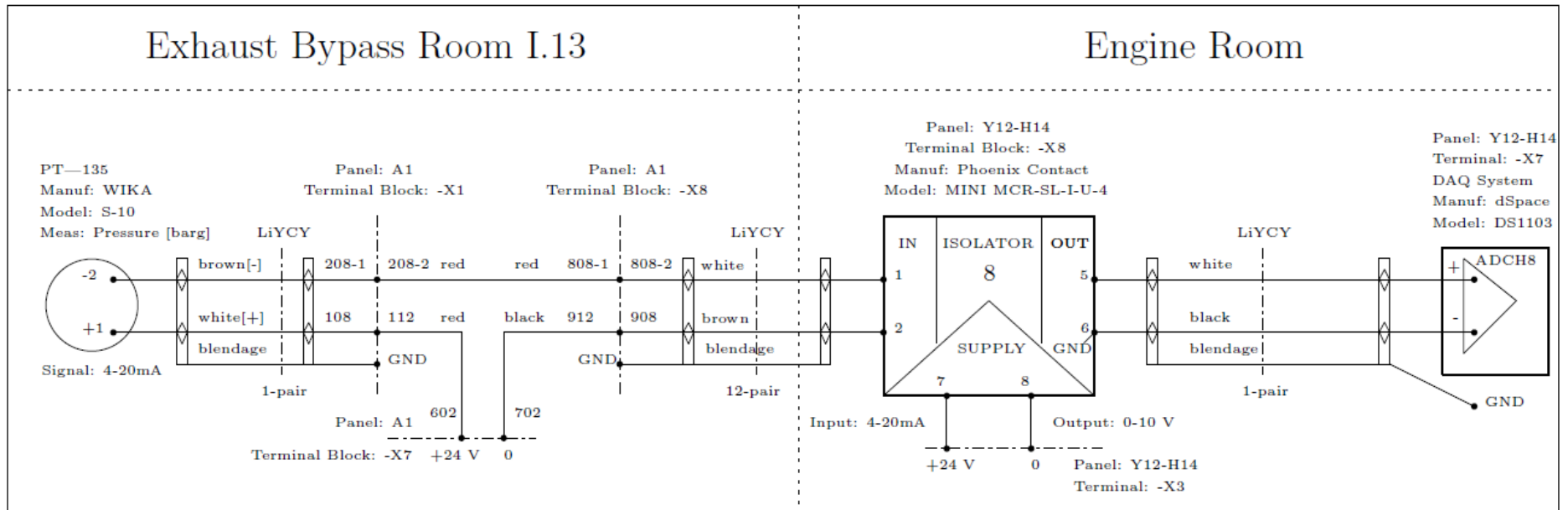
Figure A.II 11: Electrical connection of S-10 pressure transmitter 4

Figure A.II 12: Electrical connection of TR10C - T19 transmitter 1

Figure A.II 13: Electrical connection of the TR10C - T19 transmitter 2
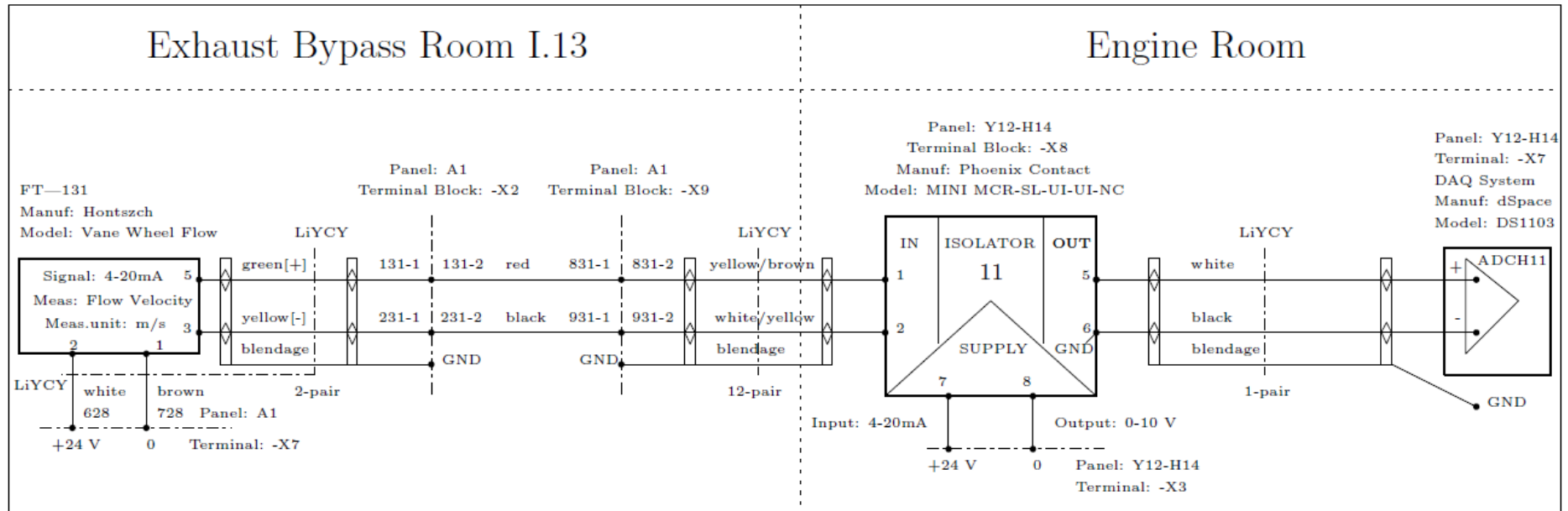
Figure A.II 14: Electrical connection of TR10C - T19 transmitter 3
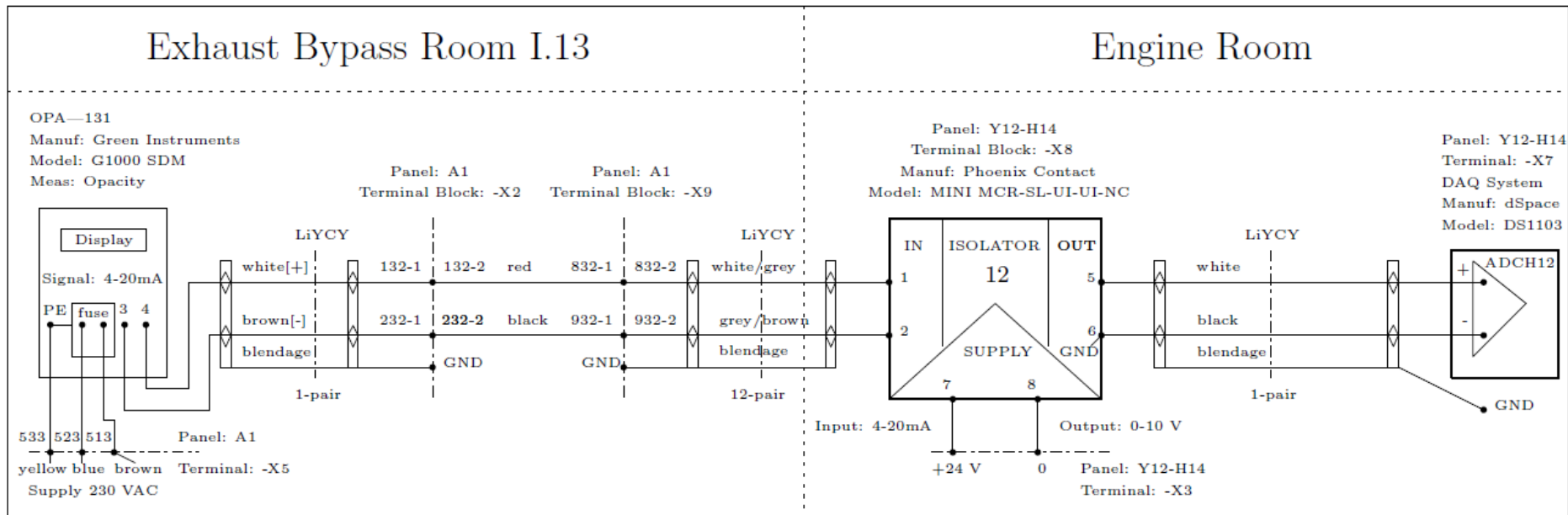
Figure A.II 15: Electrical connection of G1000 SDM

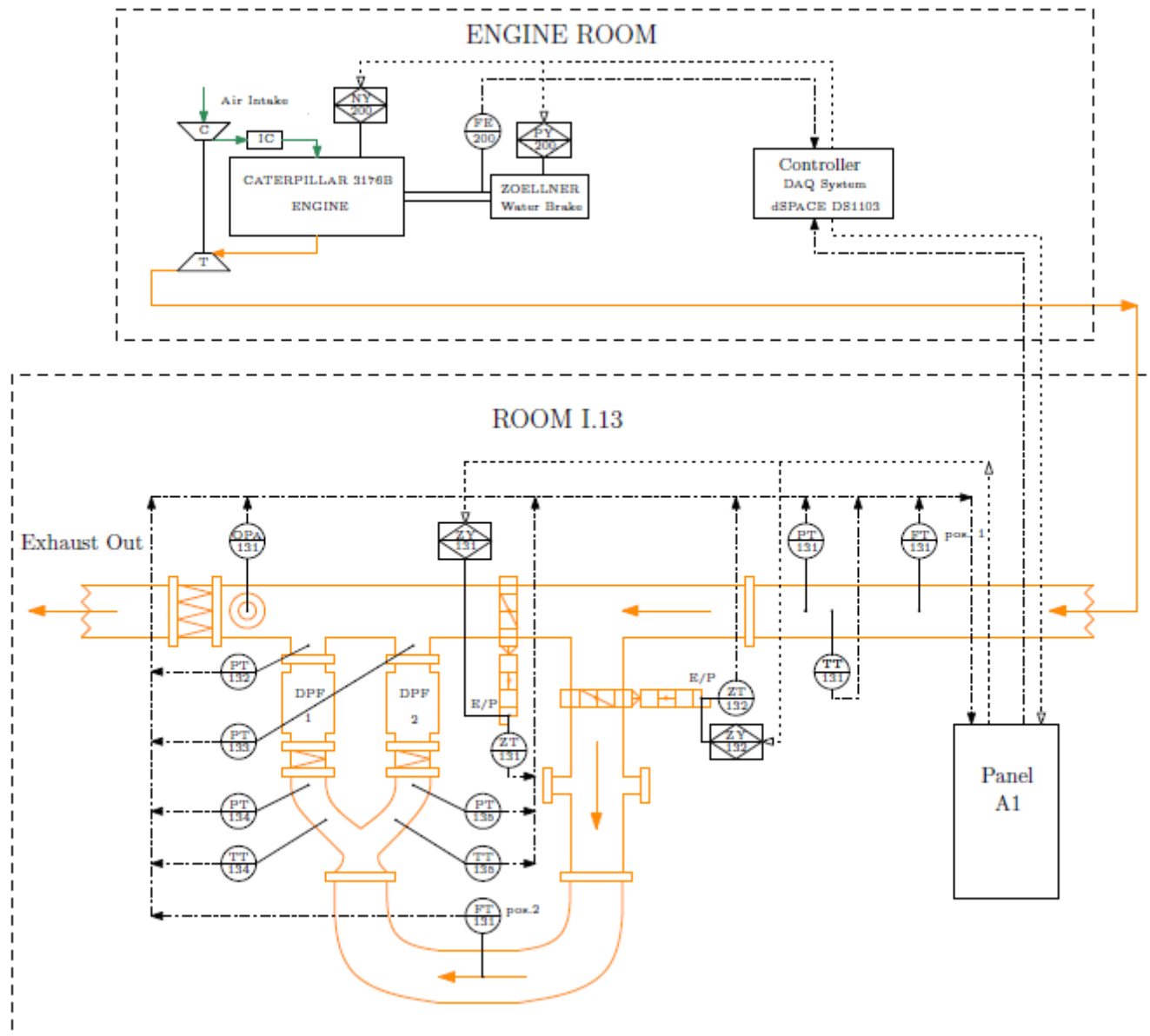**Figure A.II 16: Electrical connection of vane wheel flow sensor**

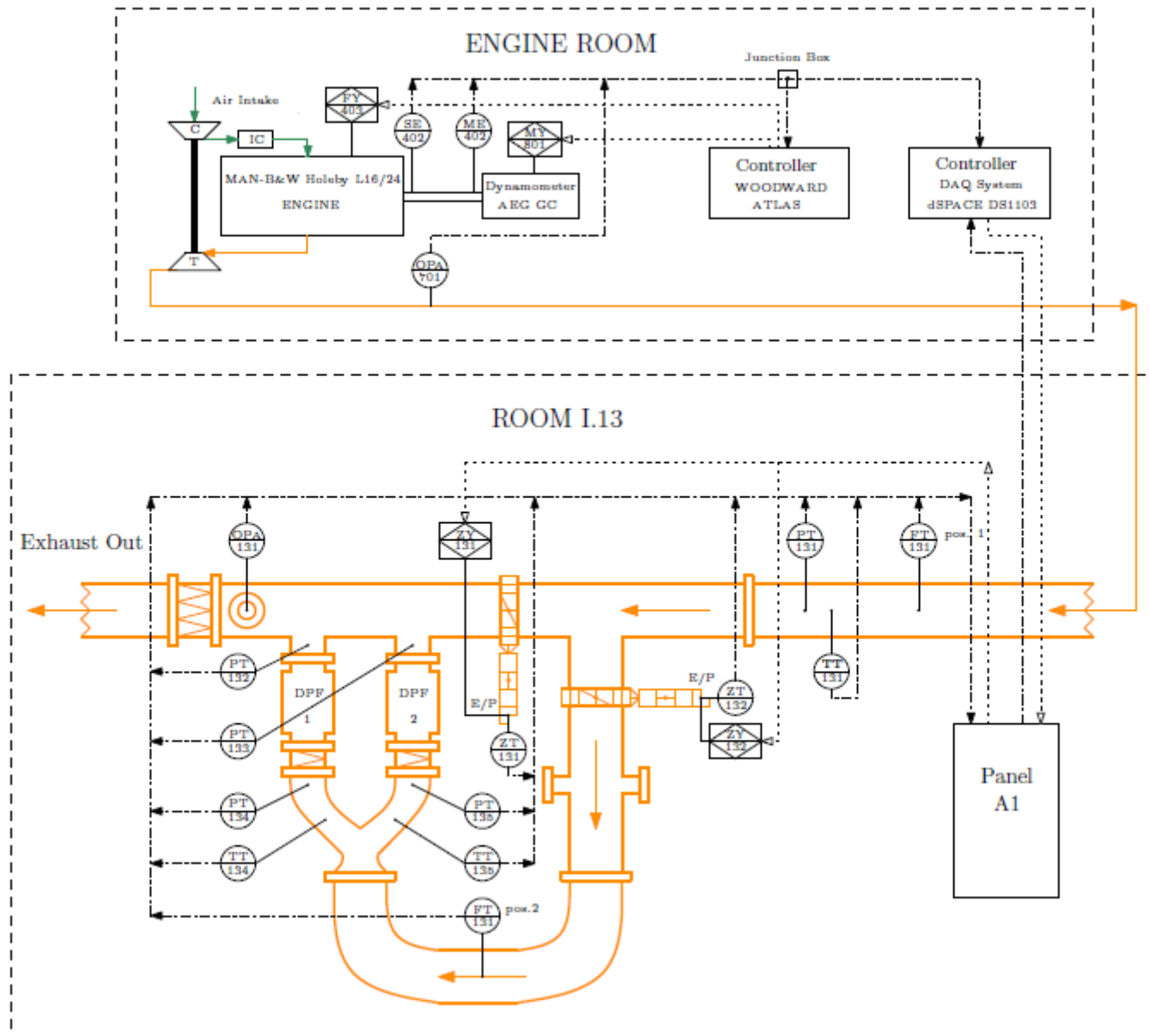Figure A.II 17: Wiring design of EBS for Caterpillar 3176b engine

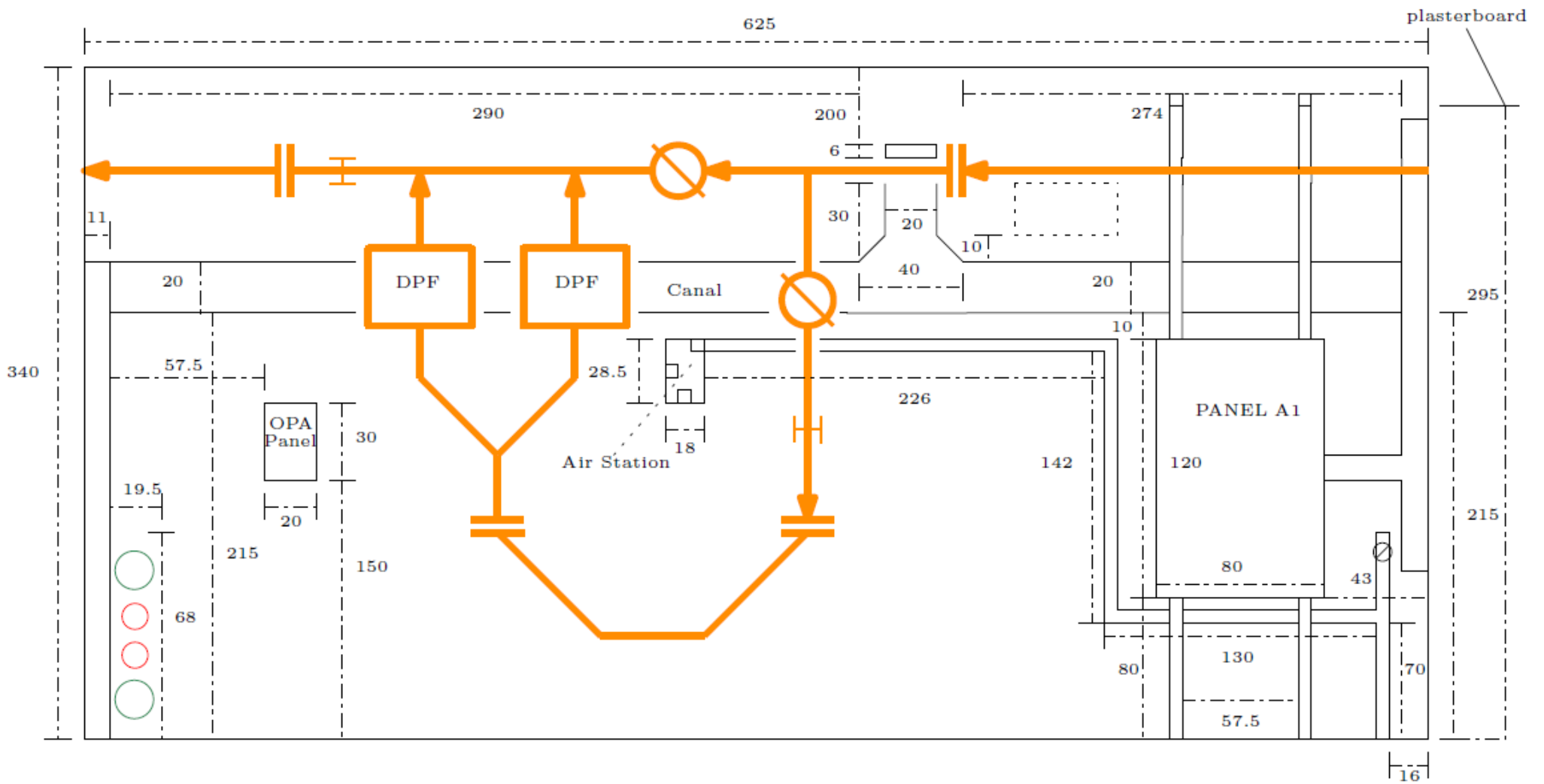Figure A.II 18: Wiring design of EBS for MAN B&W Holeby L16/24 engine

Figure A.II 19: Draft of room I.13 front view